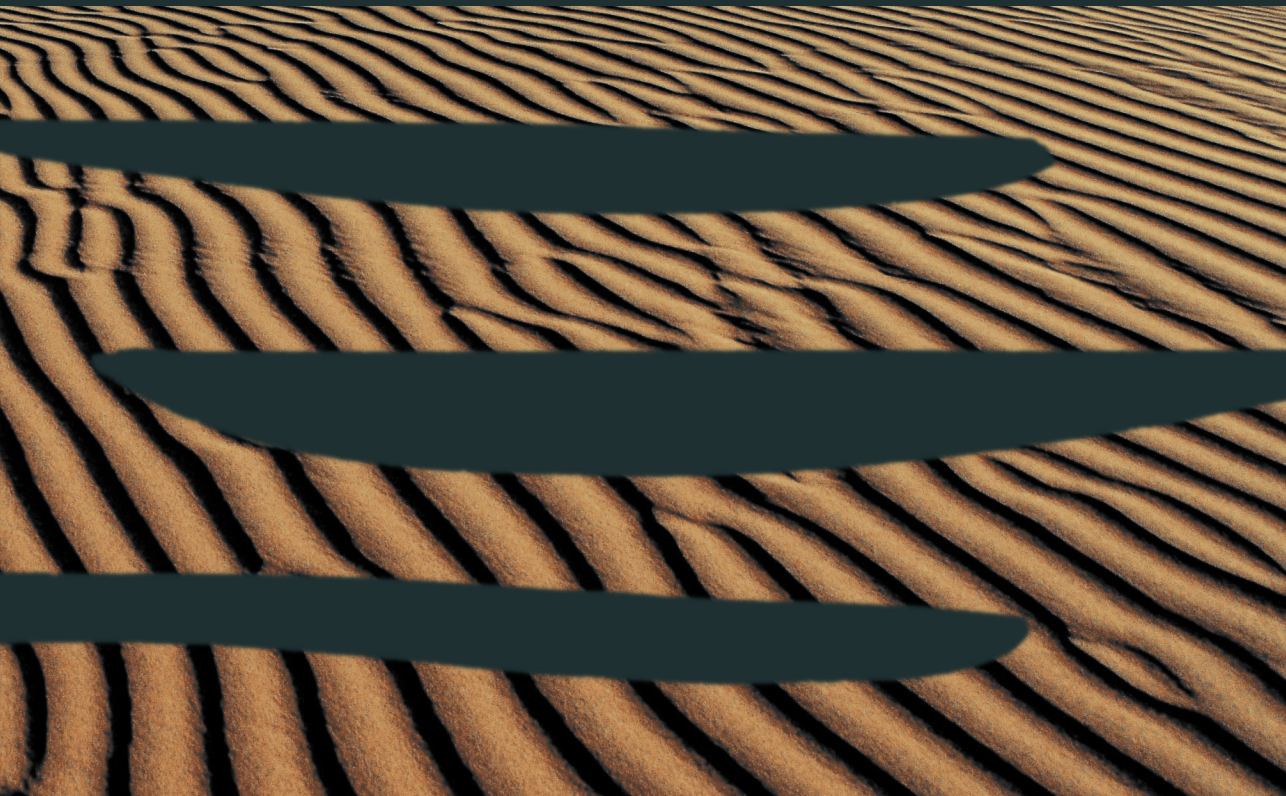


# Granular flows: effects of grain shape, surface friction and grain elasticity



*Bo Fan*

## **Propositions**

1. The quality of granular materials is derived from their quantity.  
(this thesis)
2. Everyday materials hide interesting science.  
(this thesis)
3. Machine learning is just another research tool, like experiment or simulation.
4. Science would benefit if profit-oriented publishers paid for the contents.
5. Many doctors perform experiments on their patients.
6. Homeless people need psychological help as much as food and shelter.

Propositions belonging to the thesis, entitled

Granular flows: effects of grain shape, surface friction and grain elasticity

Bo Fan

Wageningen, 14 November 2023

# **Granular flows: effects of grain shape, surface friction and grain elasticity**

*Bo Fan*

## **Thesis committee**

### **Promotor**

Jasper van der Gucht  
Professor of Physical Chemistry and Soft Matter  
Wageningen University & Research

### **Co-promotors**

Tamás Börzsönyi  
Scientific Advisor of Institute for Solid State Physics and Optics  
Wigner Research Centre for Physics, Budapest, Hungary

Joshua Dijkman  
Associate Professor of Van der Waals-Zeeman Institute  
University of Amsterdam  
Associate Professor of Physical Chemistry and Soft Matter  
Wageningen University & Research

### **Other members**

Prof. Dr. Erik van der Linden, Wageningen University & Research  
Prof. Dr. Miklós Vincze, Eötvös Loránd University, Budapest, Hungary  
Prof. Dr. Devaraj van der Meer, University of Twente  
Dr. Mazi Jalaal, University of Amsterdam

This research was conducted under the auspices of VLAG Graduate School  
(Biobased, Biomolecular, Chemical, Food and Nutrition Sciences)

# **Granular flows: effects of grain shape, surface friction and grain elasticity**

*Bo Fan*

## **Thesis**

submitted in fulfillment of the requirements for the degree of doctor  
at Wageningen University  
by the authority of the Rector Magnificus,  
Prof. Dr A.P.J. Mol,  
in the presence of the  
Thesis Committee appointed by the Academic Board  
to be defended in public  
on Tuesday 14 November 2023  
at 1.30 p.m. in the Omnia Auditorium.

Bo Fan  
Granular flows: effects of grain shape, surface friction and grain  
elasticity,  
148 pages.

PhD thesis, Wageningen University, Wageningen, The Netherlands  
(2023)  
with references, with summary in English

ISBN: 978-94-6447-846-4

DOI: <https://doi.org/10.18174/636929>



---

# CONTENTS

<b>1</b>	<b>General Introduction</b>	<b>1</b>
1.1	Basic features of granular flow in a silo . . . . .	3
1.2	Influences of particle properties on granular flow . . . . .	7
1.3	Outline . . . . .	16
<b>2</b>	<b>Elongated grains discharged from a narrow 3D silo</b>	<b>23</b>
2.1	Introduction . . . . .	24
2.2	Experimental setup . . . . .	25
2.3	Results and discussion . . . . .	27
2.4	Summary . . . . .	36
<b>3</b>	<b>From rice to lentil: the effect of different ellipsoidal shapes on the hourglass flow</b>	<b>41</b>
3.1	Introduction . . . . .	42
3.2	Experimental setup . . . . .	43
3.3	Results and discussion . . . . .	45
3.4	Summary . . . . .	48
<b>4</b>	<b>Asymmetric grains in a 3D silo and shear flow</b>	<b>53</b>
4.1	Introduction . . . . .	54
4.2	Experimental system . . . . .	54
4.3	Results and Discussion . . . . .	56
4.4	Conclusion . . . . .	63



---

<b>5</b>	<b>Elliptical grains in a two-dimensional silo discharged with a conveyor belt</b>	<b>69</b>
5.1	Introduction . . . . .	70
5.2	Experimental setup . . . . .	71
5.3	Results and discussion . . . . .	71
5.4	Summary . . . . .	83
<b>6</b>	<b>Mixtures of hydrogel and airsoft beads in a 2D silo</b>	<b>89</b>
6.1	Introduction . . . . .	90
6.2	Experimental methods and materials . . . . .	91
6.3	Results and Discussion . . . . .	93
6.4	Discussion . . . . .	100
6.5	Summary . . . . .	101
<b>7</b>	<b>Mixtures of hydrogel and airsoft beads in a 3D silo and a shear cell</b>	<b>107</b>
7.1	Introduction . . . . .	108
7.2	Experimental procedures . . . . .	109
7.3	Results and Discussion . . . . .	111
7.4	Summary . . . . .	117
7.5	Appendix . . . . .	118
<b>8</b>	<b>General discussion</b>	<b>123</b>
8.1	Introduction . . . . .	123
8.2	Shape effects on granular flow . . . . .	124
8.3	Influences of friction and elasticity of mixed ensembles on granular flow . . . . .	130
8.4	Conclusions and outlook . . . . .	132
	<b>Summary</b>	<b>139</b>
	<b>List of publications</b>	<b>141</b>
	<b>Acknowledgements</b>	<b>143</b>
	<b>About the author</b>	<b>145</b>
	<b>Overview of completed training activities</b>	<b>147</b>

## General Introduction

*Granular materials are present in many aspects of our life. For instance, the harvested grains from the field and the powders and granulates used in different manufacturing processes are all granular materials. In this chapter, the introduction to such materials and the scientific description of the factors influencing the flow formed by them are presented.*

From sand dunes on the Earth to the planetary rings of Saturn [1], granular media are ubiquitous, and can present in different forms (granular solid, granular liquid and granular gas) [2]. They are a collection of particles which can interact with each other through contact forces. If external forces are exerted on a granulate, the granular system can respond with flow, which can be seen in many natural and industrial processes as shown in Fig. 1.1, such as the flow of sand driven by gravity in an hourglass, some disasters like avalanches and landslides, and powder flow in pharmaceutical industry or food manufacturing. Therefore, research on granular flows is an important area with wide applications. However, the mechanisms behind the granular flow are not well understood despite the long history of applications (e.g. the hourglass) and its ubiquity in daily life, due to the unrecognized effects of some particles' properties on the flow and the complexity of the combination of different factors such as elasticity, friction and shape.

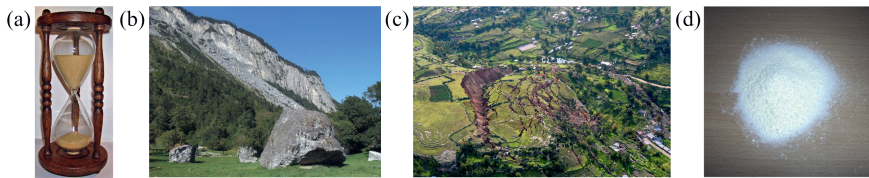


**Figure 1.1:** (a) Sand flow driven by gravity in a hourglass (*Wooden hourglass* by S Sepp. Copyright license: CC BY-SA 3.0). (b) A rock avalanche (*Rock avalanches* by Kecko. Copyright license: CC BY 2.0). (c) A landslide (*A landslide near Cusco, Peru, in 2018.* by Galeria del Ministerio de Defensa del Perú. Copyright license: CC BY 2.0). (d) Powdered milk (*Powdered milk* by Lorian. Copyright license: CC BY-SA 3.0).

Inside a granular flow, complex interactions between grains take place, such as friction and inelastic collisions which are the most important ones for dry granulates consisting of large enough grains. For powders cohesive van der Waals forces become important and for systems containing moisture capillary forces can become significant. Focusing on friction and collisions, the friction between grains can be described by Coulomb's friction law  $F_t = \mu F$  where  $F_t$  is the friction force,  $\mu$  is the friction coefficient, and  $F$  is the normal force between two contact surfaces; and the inelastic collisions can be characterized by the coefficient of restitution  $e = v_2/v_1$  where  $v_1$  and  $v_2$  are the relative velocities before and after collision, respectively. The calculation of friction force can be complicated due to the shape and surface condition, and the inelastic collisions lead to great energy dissipation [3], which constitute the basic features of granular media.

In a liquid flow, we describe the internal frictional force using the concept of

viscosity, which is defined as  $\eta = \sigma/\dot{\gamma}$  where  $\dot{\gamma}$  is the shear rate and  $\sigma$  is the shear stress, which is typically independent of pressure. In a granular flow, the effective friction coefficient is employed to quantify the frictional force, which is defined as  $\mu_{\text{eff}} = \sigma/p$  where  $\sigma$  is the shear stress and  $p$  is the pressure, signifying that the shear stress increases linearly with pressure [4].

Besides the mechanical analysis, granular flow can behave very differently under different conditions from a macroscopic perspective. In order to have a comprehensive image of granular flow in different scenarios, the basic features of a granulate in a silo, the influence of particle properties on granular flow such as the effect of particle shape or elasticity, and the effect of an external disturbance, e.g. controlling the outflow rate with a conveyor belt below the container, will be introduced in the following.

### 1.1 Basic features of granular flow in a silo

When a granular material is stored in a silo, it behaves differently from a liquid. One interesting phenomenon is called the Janssen effect [5, 6]: the pressure at the silo bottom saturates with increasing filling height of the granulate, as part of the weight of the granulate is transferred to the silo walls through the particle contacts. The other interesting feature is that the flow rate during discharge is constant (independent of fill height) [7, 8], and it increases with the orifice diameter as a power law function, which is called the Beverloo law [9]. In addition to these two phenomena, clogs can form if the grains pass through a narrow aperture [10–12], where an arch (or dome) forms over the aperture, and then the flow is arrested. In the following, Sections 1.1.1, 1.1.2 and 1.1.3 will present these phenomena, respectively.

#### 1.1.1 Janssen effect

Despite the fact that this effect is named after Janssen [5, 6], the observation of pressure saturation with height in a granular material in a silo was first reported in Huber-Burnand's work in 1829 qualitatively [13], and then studied more in detail in the work of Hagen in 1852 [7, 8].

Janssen deduced this peculiar behavior of granular media from simple experiments with corn seeds. The experimental device is shown in Fig. 1.2 (a). The bottom is detached from the side walls of the cuboid silo, and it is connected to a balance to measure the weight exerted on the bottom. The side walls are fixed onto the base. In Fig. 1.2 (b), we can see that the bottom pressure first increases with corn amount, and afterwards it saturates to a finite value. The remaining weight of the granulate is transmitted onto the side walls and balanced with the frictional force between the granulate and the walls.

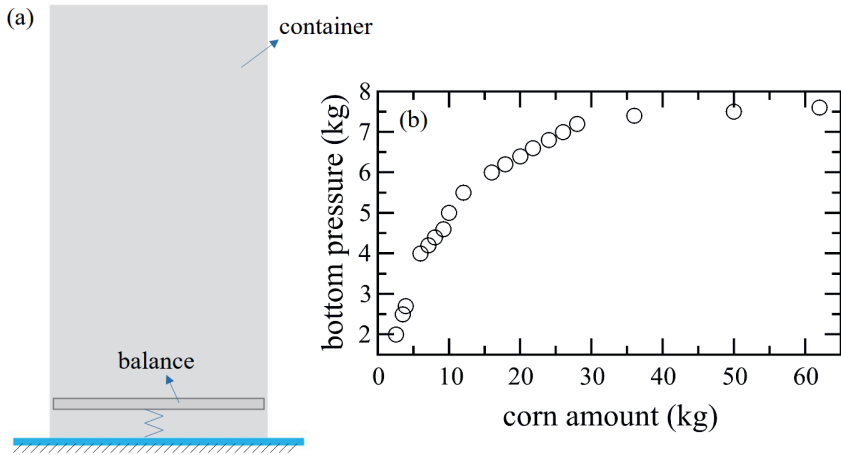


**Figure 1.2:** Janssen effect. (a) Experimental device with corns. (b) bottom pressure as a function of corn amount filled in the silo (redrawn from Ref. [6]).

The bottom pressure deduced from the analysis is shown in Equation 1.1, where  $K$  is defined as the ratio of the horizontal pressure  $p_s$  of the granulate on the side walls, and the bottom pressure  $p$ ,  $s$  is the side length of the quadratic cell profile,  $x$  is the filling height of the granulate in the cell,  $\gamma$  is the specific weight of the granulate, and  $e$  is the base of the natural logarithm. The parameter  $K$  can be determined by experiments.

$$p = \frac{s\gamma}{4K}(1 - e^{-4K\frac{x}{s}}) \quad (1.1)$$

However, there are several objections to Janssen's original model, as pointed out in Ref. [6]. These issues are solved in a later work by Nedderman et al. in 1992 with more refined continuum theories [14]. Therefore, Equation 1.1 still holds after some appropriate changes.

### 1.1.2 Beverloo law

Beverloo law [9] reveals the relation between the discharge rate  $W$  of granular materials out of a silo and the geometrical parameters of the system such as the orifice size  $D$  at the silo bottom, the particle diameter  $d$  and the bulk density  $\rho_b$ . Beverloo derived the equation by dimensional analysis of the quantities involved in silo discharge. The result is shown below:

$$W = C\rho_b\sqrt{g}(D - kd)^{n+\frac{1}{2}} \quad (1.2)$$

where  $n = 1$  and  $n = 2$  correspond to two-dimensional (2D) and three-dimensional (3D) silos respectively;  $k$  is a dimensionless constant, and  $D - kd$  represents the effective size of the outlet;  $C$  is also a dimensionless constant, related to the properties of the granular material.

Prior to Beverloo's work on the study of discharge rate of a granular material out of a silo, Hagen [7, 8] also studied the mass flow rate and suggested an equation. Moreover, he introduced the assumption of a paraboloid surface above the orifice from where the particles experience free fall. In Janda et al.'s work in 2012 [15], the authors provided solid experimental evidence and developed a new expression for mass flow rate to explain the mechanism of the particles flowing through an orifice during silo discharge. Furthermore, they also confirmed the existence of a parabolic region from where the particles accelerate, and by analyzing the velocity profiles of the particles passing through the orifice they found that the height of this parabolic arch is approximately equal to the radius of the orifice.

In addition, the assumption of the existence of a free fall region above the orifice also accounts for the constant flow rate of a granular material passing through an orifice during silo discharge. Particles which are higher than the free-fall region have negligible velocities while the ones below that region fall under gravity. However, no direct experimental evidences such as force-chain analysis in a two-dimensional silo [16] and investigation of density patterns in a cylindrical silo [17] could prove the existence of such a free-fall region. Recently, Rubio-Largo et al. [18] clarified the paradox of the existence of the free-fall arch with an experimental and numerical study. They pointed out that no discontinuities in the stress field were identified. Nevertheless, decomposing the stress tensor into contact and kinetic components, they found that kinetic pressure grows and has a maximum as a function of the distance measured from the top surface of the granulate towards the orifice, and the maximum in kinetic pressure field corresponds to a parabolic dome. The parabolic profiles obtained for different orifice sizes can be collapsed by scaling with the orifice radius. The contact pressure was found to monotonically increase with increasing vertical distance from the orifice. Therefore, kinetic pressure is dominant in this region due to the weakening contact pressure, and the parabolic dome in the kinetic pressure field scaling with

orifice radius explains why the free-fall arch assumption has been an approximation to depict the mechanism of the particles flowing through the orifice during silo discharge.

### 1.1.3 Clogging

When granular materials flow through a bottleneck or small apertures, clogging can happen [10, 11, 19] due to the formation of an arch (or dome) above the aperture [20, 21]. In Fig. 1.3, a sketch of a typical clog structure of spheres is shown. Clogging occurs spontaneously, and the relation between the clogging probability and the opening size raised a lot of interest [11, 12, 22–25].

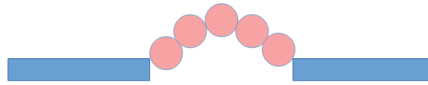


**Figure 1.3:** A clog structure

Zuriguel et al. [12] fitted the data of avalanche sizes (the amount of grains flowing out between two consecutive clogs) vs. opening size with a power-law function. Such fits yield a critical opening size  $R_c$ , at which the avalanche size diverges, i.e. above which the clogging probability becomes zero. The mean avalanche size between two consecutive clogs for a finite normalized opening size  $R$  (opening radius divided by the grain radius) is written as:  $\langle s \rangle = A/(R_c - R)^\gamma$ , where  $s$  is the mean avalanche size and  $A$  is a constant. The curve fitting the experimental data yielded  $\gamma = 6.9 \pm 0.2$  and  $R_c = 4.94 \pm 0.03$ , which means that if the opening size of the silo is at least about 5 times the grain diameter, then clogging can be avoided. Later, Thomas et al. [25] fitted the data of avalanche sizes with an exponential curve, based on the assumption that the clogging process having a Poisson character can be formulated as:  $F = \exp(-\ln(V_1/V_{pc})(D/d)^\alpha)$ , where  $F$  is the fraction of flowing configurations that precede a clog,  $V_1$  is the number of single-grain microstates,  $V_{pc}$  is the number of the single-grain microstates preceding a clog,  $D$  is the diameter of the orifice,  $d$  is the grain diameter and  $\alpha$  depends on the dimensionality. In this approach we do not get a critical opening size, since the exponential function does not diverge at any finite  $R_c$ . In Fig. 1.4, we can see both the green dashed lines (power law) and the blue solid lines (exponential) fit the data well. Therefore, the power law fit and the resulting critical opening size remains a convenient method to characterize the clogging process.

## 1.2. Influences of particle properties on granular flow

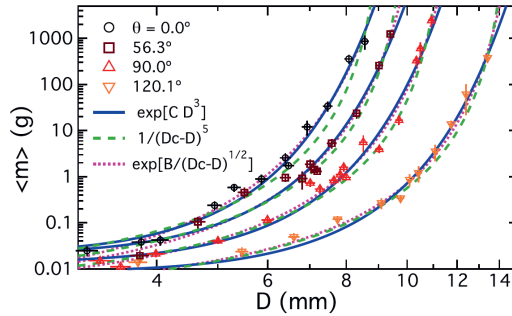


**Figure 1.4:** Average mass  $\langle m \rangle$  discharged before a clog forms, illustrated as a function of hole diameter  $D$ . (Adapted from Fig. 1 in Ref. [25])

## 1.2 Influences of particle properties on granular flow

Particle properties play an important role in the behavior of granular flow. The shape can affect the way in which grains interact with each other. For instance, elongated particles tend to align with the flow direction [26, 27]. Besides, grain elasticity and friction affect the collective behavior of a granulate significantly. For low-friction soft particles, the clogging behavior [28] and the nature of silo discharge [29] differ a lot from the case of hard grains. Adjusting the friction coefficient can also alter the nature of the flow rate curve obtained during a discharge process [30].

### 1.2.1 Shape effects

In natural environment or industrial practices where granular materials are concerned, grains with a spherical shape are usually the exception. Thus, it becomes important to understand how non-spherical grain shapes affect the nature of granular flow. Different shapes of grains can cause different modes of interactions of particles, able to change the flow resistance of the granulate as well as the structures inside the granular flow. There are various grain shapes. Nevertheless, I will focus on the simple elongated (or flat) shapes such as rod-like and ellipsoidal particles rather than the ones with more complex shapes, since good understanding of simple shapes is the foundation for potential further investigation of the behavior of grains with more complex shapes. In the following, the characteristics of elongated grains in shear flow, silo flow and flow-rate-controlled silo flow will be presented.



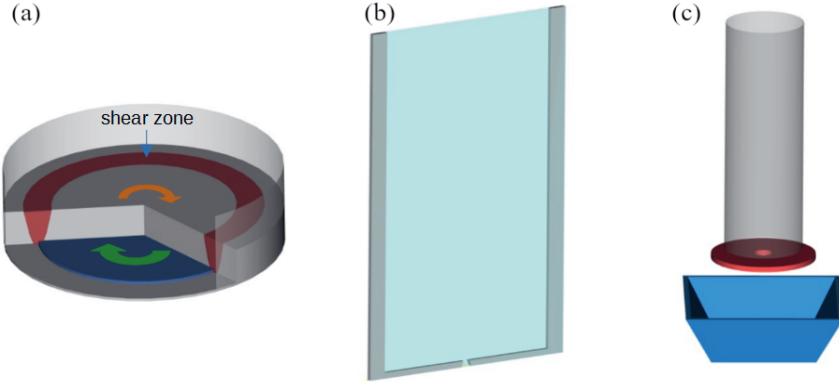


**Figure 1.5:** Experimental setups used for granular flow experiments. (a) Split-bottom shear cell (the red region is the shear zone), (b) 2D silo, and (c) cylindrical silo.

### Shear flow

One conspicuous feature in shear flow of elongated grains is that the average orientation of the long axes of the grains becomes nearly parallel with the flow direction [26, 27]. This is a result of their irregular rotation as dictated by the global shear flow and the actual interaction with the neighbors [27]. On average, they rotate slower when they are nearly parallel to the flow direction and rotate faster when they are perpendicular to it. Thus, during their rotation they spend most of the time nearly parallel to the flow, which leads to the above-described average orientation. But as they rotate, neighboring particles actually get into conflict and hinder each other's motion.

The angle  $\theta$  to the streamline is defined as the angle between the long axis of the elongated particle and the streamline where the particle is located. Particle rotation is quantified by the normalized angular velocity  $\omega/\dot{\gamma}$  ( $\omega$  is the angular velocity, and  $\dot{\gamma}$  is the local average shear rate). The illustration of the quantities is shown in Fig. 1.6. In order to describe the particle alignment quantitatively, the average angle  $\theta_{av}$  to the streamline and the order parameter  $S$  are used. The order parameter is an assessment of the extent of alignment of the particles with the average angle in a certain region [27, 31, 32]. For a perfectly aligned system with all particles parallel  $S = 1$ , while for a system with random particle orientations  $S = 0$ . For a perfectly aligned system  $\langle \cos^2(\theta - \theta_{av}) \rangle = 1$  for both 2D and 3D systems. For a system with random particle orientations the value of  $\langle \cos^2(\theta - \theta_{av}) \rangle$  becomes 1/2 in 2D and 1/3 in 3D. Therefore, the order parameter is formulated as  $S = \frac{1}{N} \sum (2 \cos^2(\theta_{av} - \theta) - 1)$  for two-dimensional

## 1.2. Influences of particle properties on granular flow

(2D) or  $S = \frac{1}{N} \Sigma ((3 \cos^2(\theta_{av} - \theta) - 1)/2)$  for three-dimensional (3D) scenarios. It is the largest eigenvalue of the symmetric traceless order tensor  $T$ , which for a 3D system has the following form:

$$T_{ij} = \frac{3}{2N} \sum_{n=1}^N [l_i^{(n)} l_j^{(n)} - \frac{1}{3} \delta_{ij}] \quad (1.3)$$

where  $\vec{l}^{(n)}$  is a unit vector along the long axis of particle  $n$ , and the sum is over all  $N$  detected particles.

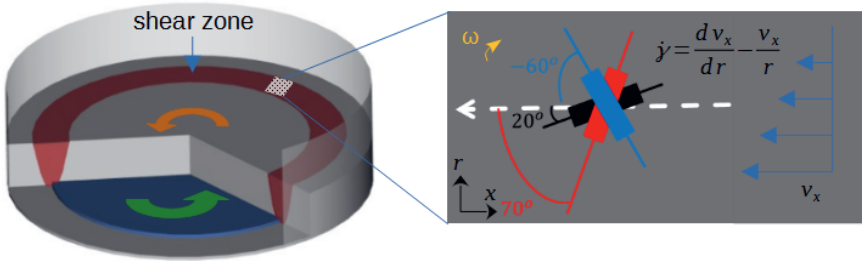


**Figure 1.6:** Illustration of the particle orientation in shear flow. Left side: sketch of the cylindrical split-bottom shear cell, right side: an elongated particle placed in a flow with flow direction along  $x$  and velocity gradient along  $y$  rotates with angle dependent angular velocity  $\omega$ .

A convenient setup to obtain stationary shear flow experimentally is the so called cylindrical split-bottom shear cell, which is shown in Fig. 1.5 (a). Here a layer of granular material is placed in a cylinder and the middle section of the granulate is rotated by a rotating plate below it. The shear flow is established in the so called shear zone, which is the section between the rotating inner part and the stationary outer part. Shearing a freshly prepared sample results in the dilation of the material (so called Reynolds dilation). At the same time the particles quickly get ordered in the shear flow, leading to an increase of packing fraction which typically can not fully compensate for the Reynolds dilation [33]. During the ordering process a decrease of the effective friction is observed until the granulate reaches the steady state in the shear flow [26].

In the work of Börzsönyi et al. [26, 27], the authors found that in relatively slow granular flows the average angle and order parameter of elongated particles are not sensitive to the change of shear rate, which is similar to the case of flow aligning nematic liquid crystals. The shear alignment angle is related to the geometrical parameters of the particles, it decreases with increasing the aspect ratio. Besides, the order parameter

increases with decreasing average angle, indicating that the width of the orientation distribution is smaller. When the particles get more elongated, the entangling among particles is stronger, which hinders particles' rotation. Thus, the angular fluctuation is smaller, leading to a smaller width of the orientation distribution and smaller average angle.

In chapter 4, we investigate the shear induced alignment process in a new class of materials which have an asymmetric elongated shape. We study the orientation of such grains in the shear zone in a split bottom shear cell as well as in a 3D silo with the help of x-ray Computed Tomography (CT), focusing on the statistics of the orientation of the sharpened heads of the pegs.

### **Silo flow**

Various particle shapes have been studied in silo flow, including sphero-disc [34], sphero-cylinder [35], ellipsoidal [36], and rod-like, lentil-like or rice-like [37, 38] shapes. These anisotropic shapes can influence the silo flow in terms of the flow patterns, clogging, packing and alignment. The setups used for the silo discharge experiment are shown in Fig. 1.5 (b) and (c).

Langston et al. [35] in 2004 reported that in Discrete Element Method (DEM) simulations the aspect ratio of frictionless sphero-cylinder particles with no friction affected the discharge rate in 2D simulations significantly while having little effect on the discharge rate in 3D rectangular silos. They explained that the difference might come from the frictionless nature of the grains. Li et al. [34] carried out a comparison between a 3D experiment and a DEM simulation in 3D. They claimed that the results of packing analysis, flow rate and flow behavior of sphero-disc and spherical particles in experiments were in good agreement with the ones obtained in DEM simulations. In their simulations, they declared that the sphero-disc particles flowed faster than spherical ones due to an easier flow path over each other than the bumpy ride that the spheres had.

Liu et al. [36] studied the flow features such as flow pattern, velocity, force distribution, and discharge rate of ellipsoidal particles in a cylindrical silo with DEM simulations, and an experiment in a 2D rectangular silo was used to validate the numerical results. The four flow zones (plug flow zone: the upper part of the silo where particles move nearly uniformly; converging flow zone: the part near the silo outlet where particles move towards this outlet at a high speed; stagnant zone: around the corner of the silo bottom where the particles nearly keep still; transition flow zone: the zone between plug flow zone and converging flow zone) are also observed for these ellipsoids with different aspect ratios, which have also been observed before for spherical particles (see Fig. 1.7). The wall effect, which leads to the formation of

## 1.2. Influences of particle properties on granular flow

---

mixed region near the wall for spheres (a considerable velocity gradient presents in this narrow shear zone near the side wall of the silo), disappears for ellipsoids due to their stronger inter-particle locking. In addition, the stagnant zone is smaller for spheres than ellipsoids. Regarding the force network analysis in the silo, the force arch for ellipsoids is stronger than it is for spheres, and may expand from bottom to top. Wall stress for spheres is the largest while all the ellipsoids experience smaller wall stress as a result of their ordered structure near the wall and horizontal direction to the wall. Finally, based on the DEM results on discharge rate for ellipsoids, they modified the Beverloo equation 1.2 by formulating the parameters  $C$  and  $k$  as a function of aspect ratio. Since the DEM simulation is a very effective tool for quantitative comparison with experimental data, the DEM tool is applied in some of our work in chapters 2 and 3 as well in order to carry out some analysis in microscopic characteristics or dynamics for explaining the macroscopic behavior observed in the experiments.

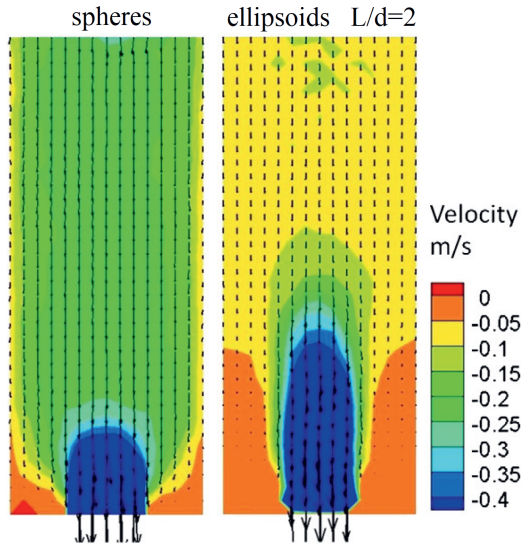


**Figure 1.7:** Time-averaged velocity distribution at the central slice of the cylindrical hopper from the DEM simulations for spheres and ellipsoids with elongation  $L/d = 2$ . (Adapted from Fig. 6 in Ref. [36])

Recently, Börzsönyi et al. [37] investigated the features of packing and alignment of some anisotropic grains such as rod-like, lentil-like and pea (approximately spherical) in a 3D silo experiment with x-ray tomography. They analyzed the particles' orientation,

packing density and the shape of the dome formed above the orifice of the silo in the clogged states for the mentioned grains. The elongated particles get aligned with the streamlines in the flowing zone in the silo but with a larger angle to the streamlines and a smaller order parameter compared to the case of simple shear flow, because the particles' orientation distribution in most parts of the silo did not reach the stationary one due to the limited amount of shear deformation. The order parameter grows with particles moving downwards in the silo as the local shear deformation increases. In the stagnant zone the packing is less dense for longer particles (aspect ratio of 5) than for shorter ones (aspect ratio of 2). In the flowing region the packing is less dense due to the Reynolds dilation, where the difference in the packing between long and short grains diminishes. As the shear induced ordering develops, the related increase in packing fraction is stronger for longer grains. They also observed that the packing density along the central vertical line in the silo decreased all the way from top to bottom. As for the clog dome which inhibits further flow, the height of the dome measured from the orifice level to the top of the dome decreases with increasing aspect ratio of rods up to 5.

Ashour et al. [38] studied the role of size and aspect ratio of elongated particles in the avalanche statistics and mean flow rate in a 3D silo setup with small apertures. They also investigated the clogged configurations by means of x-ray computed tomography. The elongated particles get ordered as they move towards the outlet, and their long axes point to the orifice center. Thus, the number of grains to form a dome is higher than for spheres with a comparable volume. The clogging probability increases with particle aspect ratio (at least up to 8). Moreover, the critical radius of orifice to obtain free flow for elongated grains is much higher than that for spheres. When the aspect ratio exceeds 6, the equations in references [11, 24, 25] for predicting the avalanche size are not suitable anymore, which is related to the change of dome structure. For elongated particles the size of the first avalanche is normally small, and the avalanche size converges towards a stationary distribution after some amount of grains has been discharged, which was not observed for spheres and became more pronounced with increasing the aspect ratio. In terms of discharge rate, the results show no strong dependence on particle aspect ratio when the particles are moderately elongated (aspect ratio smaller than 4), while the rate becomes smaller when the aspect ratio is larger. For large aspect ratios, only small avalanches are possible to be triggered. Additionally, the dome develops a chimney shape that can reach the surface of the granulate in the silo. In chapters 2 and 3, we investigate the influence of aspect ratio of the cylinders and ellipsoids in silo discharge, and focus on the flow rate in the continuous flow regime. For narrow silos filled with elongated grains we find an interesting flow rate increase (surge) near the end of the discharge process. This is not present for spherical grains where the flow rate is constant in time. For wide enough silos, where the flow rate is constant in time for both spherical and non-spherical grains, we find a non-monotonic change

of the flow rate with aspect ratio of ellipsoids. Slightly flat and slightly elongated grains discharge somewhat faster than spherical particles. Strongly anisotropic grains (very flat or very elongated) discharge slower than spherical particles.

### Flow-rate-controlled silo flow

Free silo discharge under gravity has been studied for many years [39–41]. In some industrial applications a conveyor belt placed below the container is used to extract granular materials at a specific rate. This raises the question about the influence of an external disturbance like a conveyor belt to the behavior of granular flow in the silo either at the exit or in the bulk. Hence, the following part I will focus on the scenario of a conveyor belt below a container as a specific type of external disturbance to silo flow.

The clogging features and discharge analysis of spherical particles extracted with a conveyor belt from a 2D silo (the exit part of the setup is shown in Fig. 1.8) have been thoroughly investigated in a recent work [42, 43] of Gella et al. With the help of the conveyor belt, the grain velocities can be controlled given certain geometrical parameters such as grain size and outlet size. Furthermore, this makes it possible to disentangle the contributions to the silo clogging process originating from geometry and kinematics. As a result, the proposed equation for the clogging probability is written as:  $p_c = (a + bv)^{-(D/d_p)^2}$ , where  $a$  determines the clogging probability when the grain velocity is so small that inertial effects are absent, and  $b$  represents the influence of grain velocity on clogging,  $v$  is the mean vertical velocity at the exit,  $D$  is the orifice size, and  $d_p$  is the particle diameter.  $a$  and  $b$  are fitting parameters which can be obtained from fitting the experimental data. Regarding the discharge features with a conveyor belt below the silo, the flow rate saturates as the conveyor belt speed increases to a certain level. The velocity and packing fraction profiles for different belt speeds at the exit are self-similar for each orifice size like the case of free discharge [15]. Given a certain belt speed, the mean velocity decreases with orifice size and its upper limit is determined by the free discharge case. The packing fraction at the exit increases with orifice size, and seems to have an asymptotic value which is near the closest packing fraction in 2D for spheres  $\frac{\pi\sqrt{3}}{6} = 0.906$ , higher than the asymptotic value for the free discharge case. After a mass conservation analysis (an illustration of the geometry at the exit region is shown in Fig. 1.8) at the region of the outlet and the region where the grains are spreading towards the belt to be carried away, the expression for the mean velocity  $v_z$  at the orifice is formulated as:

$$\langle v_z \rangle = K_\varphi \frac{D + 2\Delta + h_{\text{eff}} \cot \theta}{sD} h_{\text{eff}} v_b \quad (1.4)$$

where  $K_\varphi = \frac{\langle \varphi_2 \rangle}{\langle \varphi_1 \rangle}$ ,  $\varphi_1$  and  $\varphi_2$  are the packing fractions at the exit and in the trapezoid

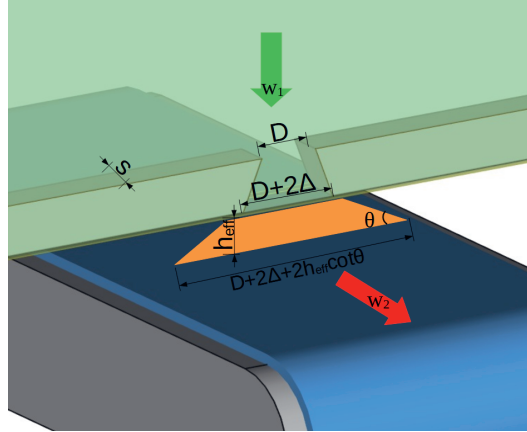


**Figure 1.8:** Mass conservation analysis in the silo discharge with a conveyor belt. (Redrawn from Ref. [43])

pile (orange region in Fig. 1.8), respectively,  $v_b$  is the speed of the conveyor belt, and the rest of the geometric parameters are shown in Fig. 1.8. From this expression, the decreasing tendency of the mean vertical velocity  $v_z$  with increasing orifice size under the condition of a given belt speed can be explained.

In the above summary we described previous investigations on the clogging and flow of spherical grains in the 2D silo discharged with a conveyor belt. However, spheres are usually the exception in industrial and natural process. Grains with anisotropic shapes like elongated ones will bring a new aspect, namely particle orientation, into this setting. In chapter 5, ellipses in such a scenario are used to investigate the effect of particle orientations in this 2D silo geometry.

### 1.2.2 Influence of particle elasticity and friction

Low-friction soft particles present very different behavior when it comes to clogging around a bottleneck geometry or discharging in a silo [28, 29]. Frictional hard particles cause clogs more easily than low-friction soft particles, because the soft particles can deform more easily under load, which can break the clog structure, and cannot sustain long arches. The typical outlet size below which clogging occurs is much smaller for low friction soft particles [28, 44] than it is for frictional hard particles [12, 22, 25], which is illustrated in Fig. 1.9. In the granular systems of hydrogel beads in silos, the combination of its softness and low surface friction leads to the height dependence of

## 1.2. Influences of particle properties on granular flow

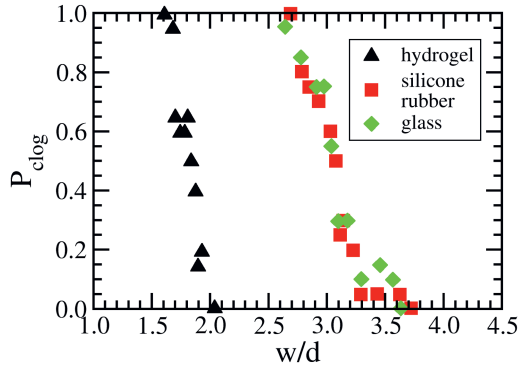


**Figure 1.9:** Experimental probability of clogging as a function of  $w/d$ , the ratio of the hopper exit width  $w$  to the grain diameter  $d$ . (Redrawn from Ref. [44])

clogging characteristics and flow rate [45]. The bottom pressure increases basically linearly with fill height due to the low friction coefficient. Clogs are impermanent and intermittent until the bottom pressure in the silo is low enough during discharge, then permanent clog forms. However, for hard frictional grains the pressure at the bottom saturates with increasing fill height, and the flow rate is height-independent. Moreover, there is no stagnant zone in the container for hydrogels unlike the case of hard frictional particles where the stagnant zone is observed in the corner of the container.

The influence of grain softness and friction on the behavior of silo flow are carefully and systematically examined in the work of Pongó et al. [30]. The evolution of the flow rate and the local pressure in the region above the orifice was correlated in a discharge process. First, as the filling height decreases in the silo, the local pressure above the orifice changes much more for low friction soft grains than for low friction hard grains. Second, the flow rate is much more sensitive to the local pressure above the orifice for low friction soft grains than for low friction hard grains. These two factors both contribute to the fact, that the flow rate decreases with filling height for low friction soft grains (like it does for a liquid) and it is constant for hard grains (basically with any friction coefficient, except frictionless). In view of these recent observations on the flow and clogging of low-friction soft grains in a silo, it is interesting to investigate, how a mixture of low-friction soft grains and frictional hard grains behaves in a silo. This will be the subject of chapters 6 and 7, where mixtures of different compositions of soft low-friction grains and hard frictional grains are studied in a 2D silo and a 3D silo, respectively.



### 1.3 Outline

This thesis focuses on the complex behavior of granular flow in a silo or a shear cell, such as the flow process, orientation-related issues (non-spherical particles), and clogging if the aperture of the silo is small, with special emphasis on the role of particle shape, surface friction or elasticity.

Chapter 2 shows that in a narrow silo filled with rods there is a certain range of the orifice size for which the flow rate is not constant, but there is a surge at the end of the discharge process. For small and large orifices we observe a constant flow rate. The change from the constant flow rate regime to the regime with surge at the end is characterized by a change in the flow field. For the case of constant flow rate there is a larger stagnant zone near the silo wall, while the stagnant zone shrinks in the cases of increasing flow rate.

In chapter 3, we focus on the constant flow rate regime and investigate how the average flow rate changes with aspect ratio of ellipsoids in silo flow. The average flow rate changes with the aspect ratio of ellipsoids non-monotonically. There are two maxima around the aspect ratios of 0.6 (lentil-like) and 1.5 (rice-like). Starting from a spherical shape, the resistance of the granulate against shearing considerably increases for both lentil-like and rice-like particles, which would suggest a decreasing flow rate, which is the opposite of what we observe. The packing fraction shows a slight non-monotonic modulation with grain shape, which partly explains the trend in discharge rate. The other factor is the grain velocity: the slightly non-spherical particles not only form a better packing in the silo but also flow faster through the orifice than spheres.

In chapter 4, we study grain orientations of low symmetry particles (sharpened pegs and wedge shaped corn seeds) in silo flow and shear flow. We find a new type of gravity effect on grain orientation: if the shear gradient has a vertical component, i.e. the particles rotate in a plane which is not exactly horizontal, they spend more time in the configuration with their thicker (heavier) end down. This is detected by the asymmetry of the orientation distributions.

In chapter 5, we performed experiments of ellipses discharged from a 2D silo equipped with a conveyor belt. The conveyor belt - placed directly below the silo outlet - reduces the flow rate, increases the size of the stagnant zone, and it has a very strong influence on the relative velocity fluctuations as they strongly increase everywhere in the silo with decreasing belt speed. In other words, instead of slower but smooth flow, flow reduction by the belt leads to intermittent flow. Interestingly, we show that this intermittency correlates with a strong reduction of the orientational order of the particles at the orifice region. Moreover, we observe that the average orientation of the grains passing through the outlet is modified when they are extracted with the belt, a

feature that becomes more evident for large orifices.

Chapters 6 and 7 are devoted to the study of mixtures of soft low-friction and hard frictional grains in a 2D silo and a 3D silo, respectively, in order to explore the transition from the liquid-like behavior of soft low-friction grains (characterized by hydrostatic pressure conditions and a filling height dependent flow rate) to the classical granular-like behavior of hard frictional particles (characterized by constant flow rate and Janssen screening for the pressure). We find that adding a small proportion of hard frictional grains to a granulate of soft low-friction grains can change the collective features of the sample significantly in terms of height dependence of flow rate and bottom pressure conditions.

Chapter 8 as the final chapter of this thesis, discusses the work done in the previous chapters and some ongoing or future work in investigating more aspects of granular flow.



---

## BIBLIOGRAPHY

- [1] Brilliantov, N. et al. “Size distribution of particles in Saturn’s rings from aggregation and fragmentation”. In: *Proceedings of the National Academy of Sciences* **112** (2015), 9536–9541.
- [2] Andreotti, B., Forterre, Y., and Pouliquen, O. “Introduction”. In: *Granular Media: Between Fluid and Solid*. Cambridge University Press, 2013, pp. 1–14.
- [3] Kollmer, J. E. et al. “Relaxation of a spring with an attached granular damper”. In: *New Journal of Physics* **15** (2013), 093023.
- [4] GDR MiDi. “On dense granular flows”. In: *The European Physical Journal E* **14** (2004), 341–365.
- [5] Janssen, H. A. “Versuche über Getreidedrücke in Silozellen”. In: *Zeitschrift des Vereines Deutscher Ingenieure* **39** (1895), 1045.
- [6] Sperl, M. “Experiments on corn pressure in silo cells – translation and comment of Janssen’s paper from 1895”. In: *Granular Matter* **8** (2006), 59–65.
- [7] Hagen, G. “Bericht über die zur Bekanntmachung geeigneten Verhandlungen der Königlich Preussischen Akademie der Wissenschaften zu Berlin”. In: *Königlich Preussische Akademie der Wissenschaften zu Berlin* (1852), 35–42.
- [8] Tighe, B. P. and Sperl, M. “Pressure and motion of dry sand: translation of Hagen’s paper from 1852”. In: *Granular Matter* **9** (2007), 141–144.
- [9] Beverloo, W., Leniger, H., and van de Velde, J. “The flow of granular solids through orifices”. In: *Chemical Engineering Science* **15** (1961), 260–269.
- [10] To, K., Lai, P., and Pak, H. K. “Jamming of Granular Flow in a Two-Dimensional Hopper”. In: *Physical Review Letters* **86** (2001), 71.

- 
- [11] Zuriguel, I. et al. “Jamming during the discharge of grains from a silo described as a percolating transition”. In: *Physical Review E* **68** (2003), 030301.
- [12] Zuriguel, I. et al. “Jamming during the discharge of granular matter from a silo”. In: *Physical Review E* **71** (2005), 051303.
- [13] Huber-Burnand, P. “Ueber das Ausfliessen und den Druck des Sandes”. In: *Annalen der Physik* **92** (1829), 316–328.
- [14] Nedderman, R. M. and Tuzun, U. *Statics and Kinematics of Granular Materials*. Cambridge University Press, 1992.
- [15] Janda, A., Zuriguel, I., and Maza, D. “Flow rate of particles through apertures obtained from self-similar density and velocity profiles”. In: *Physical Review Letters* **108** (2012), 248001.
- [16] Vivanco, F., Rica, S., and Melo, F. “Dynamical arching in a two dimensional granular flow”. In: *Granular Matter* **14** (2012), 563–576.
- [17] Zuilichem, D. V., Egmond, N. V., and Swart, J. D. “Density behaviour of flowing granular material”. In: *Powder Technology* **10** (1974), 161–169.
- [18] Rubio-Largo, S. M. et al. “Disentangling the Free-Fall Arch Paradox in Silo Discharge”. In: *Physical Review Letters* **114** (2015), 238002.
- [19] Zuriguel, I. et al. “Jamming during the discharge of granular matter from a silo”. In: *Physical Review E* **71** (2005), 051303.
- [20] Brown, R. and Richard, J. “Profile of flow of granules through apertures”. In: *Transactions of the Institution of Chemical Engineers* **38** (1960), 243–256.
- [21] Hong, D. and McLennan, J. “Molecular dynamics simulations of hard sphere granular particles”. In: *Physica A: Statistical Mechanics and its Applications* **187** (1992), 159–171.
- [22] To, K. “Jamming transition in two-dimensional hoppers and silos”. In: *Physical Review E* **71** (2005), 060301.
- [23] Janda, A. et al. “Jamming and critical outlet size in the discharge of a two-dimensional silo”. In: *Europhysics Letters* **84** (2008), 44002.
- [24] Thomas, C. C. and Durian, D. J. “Geometry dependence of the clogging transition in tilted hoppers”. In: *Physical Review E* **87** (2013), 052201.
- [25] Thomas, C. C. and Durian, D. J. “Fraction of clogging configurations sampled by granular hopper flow”. In: *Physical Review Letters* **114** (2015), 178001.
- [26] Börzsönyi, T. et al. “Orientational Order and Alignment of Elongated Particles Induced by Shear”. In: *Physical Review Letters* **108** (2012), 228302.

## Bibliography

---

- [27] Börzsönyi, T. et al. “Shear-induced alignment and dynamics of elongated granular particles”. In: *Physical Review E* **86** (2012), 051304.
- [28] Hong, X., Kohne, M., and Weeks, E. R. “Clogging of soft particles in 2D hoppers”. In: *Physical Review E* **96** (2017), 062605.
- [29] Ashour, A. et al. “Silo outflow of soft frictionless spheres”. In: *Physical Review Fluids* **2** (2017), 123302.
- [30] Pongó, T. et al. “Flow in an hourglass: particle friction and stiffness matter”. In: *New Journal of Physics* **28** (2021), 023001.
- [31] De Gennes, P.-G. and Prost, J. *The physics of liquid crystals*. 83. Oxford university press, 1993.
- [32] Bates, M. A. and Luckhurst, G. R. “Biaxial nematic phases and V-shaped molecules: A Monte Carlo simulation study”. In: *Physical Review E* **72** (2005), 051702.
- [33] Wegner, S. et al. “Effects of grain shape on packing and dilatancy of sheared granular materials”. In: *Soft Matter* **10** (2014), 5157–5167.
- [34] Li, J. et al. “Flow of sphero-disc particles in rectangular hoppers—a DEM and experimental comparison in 3D”. In: *Chemical Engineering Science* **59** (2004), 5917–5929.
- [35] Langston, P. A. et al. “Distinct element modelling of non-spherical frictionless particle flow”. In: *Chemical Engineering Science* **59** (2004), 425–435.
- [36] Liu, S. D. et al. “Flow characteristics and discharge rate of ellipsoidal particles in a flat bottom hopper”. In: *Powder Technology* **253** (2014), 70.
- [37] Börzsönyi, T. et al. “Packing, alignment and flow of shape-anisotropic grains in a 3D silo experiment”. In: *New Journal of Physics* **18** (2016), 093017.
- [38] Ashour, A. et al. “Outflow and clogging of shape-anisotropic grains in hoppers with small apertures”. In: *Soft Matter* **13** (2017), 402–414.
- [39] Nedderman, R. M. et al. “The Flow of Granular Materials I: Discharge Rates from Hoppers”. In: *Chemical Engineering Science* **37** (1982), 1597.
- [40] Mort, P. et al. “Dense granular flow – A collaborative study”. In: *Powder Technology* **284** (2015), 571.
- [41] Savage, S. “Gravity flow of a cohesionless bulk solid in a converging conical channel”. In: *International Journal of Mechanical Sciences* **9** (1967), 651–659.
- [42] Gella, D., Zuriguel, I., and Maza, D. “Decoupling Geometrical and Kinematic Contributions to the Silo Clogging Process”. In: *Physical Review Letters* **121** (2018).

- [43] Gella, D., Maza, D., and Zuriguel, I. “Granular flow in a silo discharged with a conveyor belt”. In: *Powder Technology* **360** (2020), 104–111.
- [44] Tao, R., Wilson, M., and Weeks, E. “Soft particle clogging in two-dimensional hoppers”. In: *Physical Review E* **104** (2021), 044909.
- [45] Harth, K. et al. “Intermittent flow and transient congestions of soft spheres passing narrow orifices”. In: *Soft Matter* **16** (2020), 8013.

---

## Elongated grains discharged from a narrow 3D silo

*This chapter focuses on the time evolution of silo discharge of spherical or elongated grains. We investigate different granular materials in laboratory experiments and with discrete element model (DEM) calculations. For spherical grains, we confirm the widely known typical behavior with constant discharge rate (except for initial and final transients). For elongated particles with aspect ratios between  $2 \leq L/d \leq 6.1$ , we find a peculiar flow rate increase for larger orifices before the end of the discharge process. While the flow field is practically homogeneous for spherical grains, it has strong gradients for elongated particles with a fast-flowing region in the middle of the silo surrounded by a stagnant zone. For large enough orifice sizes, the flow rate increase is connected with a suppression of the stagnant zone, resulting in an increase in both the packing fraction and flow velocity near the silo outlet within a certain parameter range.*

This chapter is published as:

**Tivadar Pongó\***, **Bo Fan\***, **Dariel Hernández-Delfin**, **János Török**, **Ralf Stannarius**, **Raúl Cruz Hidalgo** and **Tamás Börzsönyi**

“The role of the particle aspect ratio in the discharge of a narrow silo”

*New J. Phys.* **24**, 103036 (2022)

*\*shared first authorship*



## 2.1 Introduction

The discharge rate of inelastic granular material out of a container is known to be independent of the filling height, thus constant in time, which is opposed to the case of a liquid where the flow rate decreases with filling height. This feature of granular flow is useful for industrial applications, where controlled constant flow rate of a granulate is required. It enabled humankind to construct the hourglass, a reliable device to measure time, known already in the middle ages. Various aspects of granular discharge have been investigated including the flow rate as a function of the orifice size (Beverloo law [1–5]), clogging phenomena for small orifices [6–9], the geometry of the flow field and possible stagnant zones [10–15], fluctuations in the flow velocity and density [12, 16, 17], resonance phenomena (silo music) [18–20], influences of the particle properties, such as surface friction [21–24], stiffness [24–26] or shape [9, 15, 27–33]. The flow rate of a granulate out of a container however is not always constant in time. Recently, the discharge of soft particles with very low surface friction was shown to be rather similar to the case of a liquid with decreasing flow rate during the process [24].

Small-scale laboratory experiments and numerical modeling are often used to quantify the above-described effects. Exploring the silo discharge, the studies typically use simplified systems, e.g., with spherical particles, 2-dimensional or quasi-2-dimensional geometries, and limited system size. Despite these simplifications, many of the basic features of silo discharge can be captured and quantified, e.g., the dependence of the flow rate on the orifice size [3, 34], the typical stress distribution within the whole silo and especially in the vicinity of the orifice [35–37], etc.

The flow of elongated particles leads to orientational ordering and realignment of the grains in the sheared regions [38–40]. Various studies investigated the effects of grain shape on the clogging properties [9, 41], the geometry of the flow field [10, 12, 15, 30, 32, 42], or discharge rates [9, 27, 28, 31]. Such studies are even more limited for the system size because modeling of elongated grains in numerical investigations is more time-consuming (either for multi-sphere grains, spherocylinders or ellipsoids), and the determination of particle orientations in laboratory experiments requires more effort than only detecting particle positions.

In the present chapter, we show that in a typical laboratory-scale experiment with a narrow silo, the discharge process of elongated grains has a peculiar time-dependent behavior. Namely, the flow rate notably increases near the end of the process. Our findings were reproduced numerically by a 3D model with the same dimensions containing about 100,000 - 400,000 particles. We emphasize that previous work using similar system sizes and grain shapes did not explore this behavior [9, 27–32, 42]. Here, we thoroughly investigate the cause of the increasing flow rate by exploring the spatial structure of the packing fraction and flow velocity inside the silo.

## 2.2 Experimental setup

The granular material is filled in an acrylic cylindrical silo with an inner diameter of  $D_{\text{silo}} = 144 \text{ mm}$ , a height of  $H = 800 \text{ mm}$  and a circular hole at the center of the bottom (see Figure 2.1). The diameter  $D$  of the hole can be adjusted using replaceable inserts. The basal plate of the silo is separated from the silo wall with a gap of

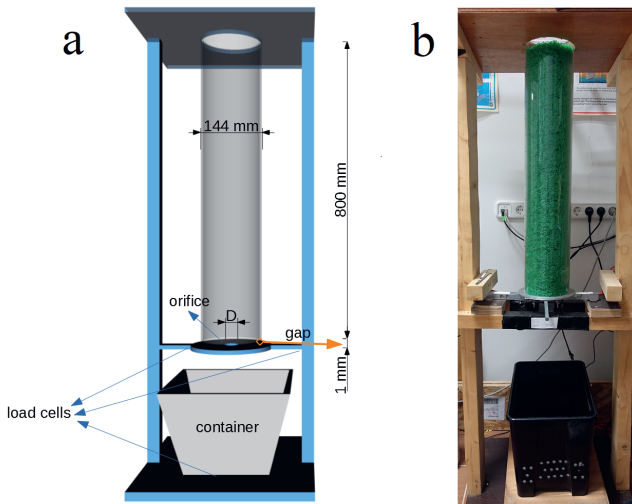







**Figure 2.1:** Experimental setup: (a) sketch; (b) a photo of the silo filled with plastic rods.

approximately 1 mm. The basal plate is supported by two load cells in order to monitor the vertical basal force. The discharged material is collected in a container, while its mass is measured with another load cell.

In the experiments presented in this chapter, five granular samples were used: glass beads (*Sigmund-Lindner GmbH*, Germany) and plastic rods (cylinders with length  $L$  and diameter  $d$ ) with elongations  $L/d = 2, 3, 4.5,$  and  $6$ . The plastic rods were obtained by cutting  $d = 2.4 \text{ mm}$  nylon trimmer lines (*Oregon*) with a cable cutting machine (Model *GlobalCut 100*, *Navia International GmbH*, Germany). Table 2.1 shows photographs, of the particles and also indicates their length  $L$  and diameter  $d$ . The equivalent diameter  $d^*$  is defined as the diameter of a sphere with the same volume as the rod. Table 2.1 also indicates the value of  $d^*$  for each particle.

After filling the silo manually with a filling rate of about  $500 \text{ cm}^3/\text{s}$  directly from

## 2. Elongated grains discharged from a narrow 3D silo

Numerical system							Experimental system			
L (mm)	d (mm)	L/d	d* (mm)	$\mu$	N	L (mm)	d (mm)	L/d	d* (mm)	
	4.5	1	4.5	0.5	150080	4.5	1	4.5		
	2.4	2	3.26	0.3	420000	4.8	2.4	2	3.46	
	2.4	3	3.81	0.3	253760	7.2	2.4	3	3.96	
	2.4	4.5	4.43	0.3	148160	10.8	2.4	4.5	4.54	
	2.4	6.1	4.93	0.3	96640	14.4	2.4	6	4.99	

**Table 2.1:** Pictures of the granular samples (right): glass beads and plastic rods with elongations of  $L/d=2, 3, 4.5,$  and  $6,$  and sketches of the particles used in the DEM simulations (left). The grains are characterized by their length  $L,$  diameter  $d,$  the equivalent diameter  $d^*$  and their surface friction coefficient  $\mu.$  The equivalent diameter is defined as the diameter of a sphere with the volume as the elongated particle. For the numerical system, the number of grains used in the simulations is also indicated.

the top of the silo, the material was discharged, and the evolution of the discharged mass and the silo basal force were continuously recorded during the whole discharge process with a sampling rate of 1 kHz. A typical discharge process lasted for about 50 – 100 s. The data series were smoothed by convolution with a Bartlett (triangle) window of a width of 1 s to reduce noise and fluctuations. The flow rate was obtained by differentiating the curves of the discharged mass and smoothing the result again with the same smoothing procedure. We mention that due to the impact of grains, there is a momentum transfer from the particles to the container. If the flow rate is constant, this effect only causes an offset in the measured mass, thus has no influence on the time derivative, except for an initial and final transient. When the flow rate is changing, the impact momentum is also changing, but in our case its contribution is minor compared to the main effect of the increasing mass in the container. This effect was thus neglected when calculating the flow rate from the load cell data. The value of the flow rate is presented in *grains/s*, using the average unit mass of the individual grains, which was determined by measuring the mass of 200 particles.

## 2.3 Results and discussion

### 2.3.1 Experimental results

In the experiments, the flow rate and the basal force  $F_b$  were measured during the whole discharge process. Fig. 2.2 shows the evolution of these quantities as a function of the mass in the silo for glass beads and plastic rods with elongations  $L/d = 2, 3, 4.5$  and 6. As we see, the nature of the discharge is gradually changing with increasing elongation of the grains: for spherical grains, the flow rate is basically constant during the discharge process (except for initial and final transients), while for elongated grains, this is not always true, as for large orifice sizes the flow rate is clearly increasing in time. For a smaller orifice, the flow rate remains nearly constant also for elongated grains, similarly to the case of beads. Note that we chose  $D/d^* \approx 11$  as the lower limit of orifices due to the clogging of  $L/d = 6$  particles below this orifice size.

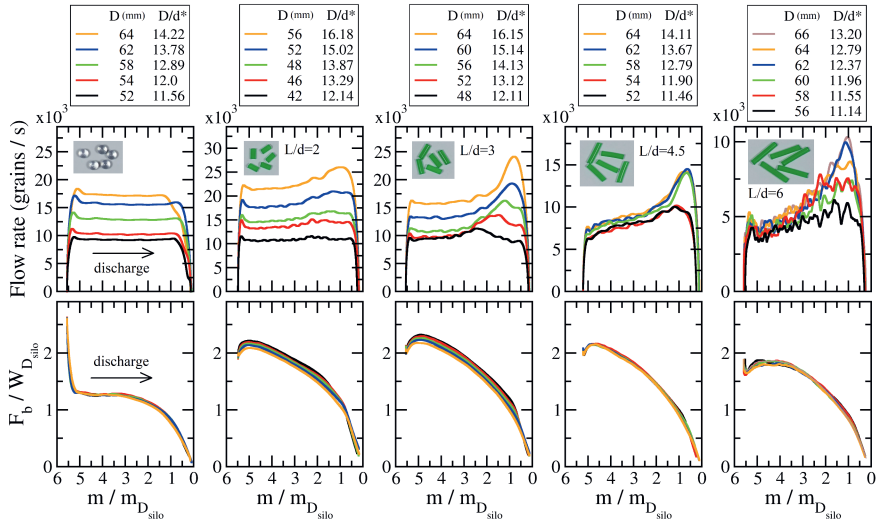


**Figure 2.2:** Experimental results: silo flow rate (top) and basal force  $F_b$  (bottom) as a function of the mass  $m$  in the silo. The different panels display data for samples of different grain shapes: glass beads and plastic rods with aspect ratios of  $L/d = 2, 3, 4.5$  and 6, as indicated by the pictures of the grains in the top row. The values of  $m$  and  $F_b$  were normalized by the mass  $m_{D_{\text{silo}}}$  and the weight  $W_{D_{\text{silo}}}$  of the material corresponding to a filling height equal to the diameter of the silo, respectively. Each curve corresponds to an average of 25 measurements for rods and 5 measurements for glass beads.

The basal force  $F_b$  was normalized by the weight  $W_{D_{\text{silo}}}$  of the material, corresponding to a filling height of the diameter of the silo. As we see in Fig. 2.2, the value of  $F_b$  is much smaller than the weight of the granular column for all cases. For glass beads, the evolution of  $F_b$  shows a plateau (right after the initial transient) and then a gradual decrease in the second half of the experiment. This behavior is in accordance with the Janssen effect, i.e., part of the weight of the granular column is held by the silo walls due to arches in the contact network. Interestingly, for elongated grains, the plateau is much less pronounced, and the value of  $F_b$  is larger. This is similar to our previous observations with lubricated (reduced friction) glass beads (see Fig. 5d of Ref. [24]). This might be an indication that the friction between the rods (which are mostly aligned parallel with boundaries) and the silo wall is smaller than that in the case of glass beads. Note that for each material, the curves measured for different orifice sizes overlap, which shows that the basal force does not depend on the flow rate (at least in the examined range of orifice sizes.).

The measurements presented in Fig. 2.2 were obtained in the orifice range of  $42 \text{ mm} \leq D \leq 64 \text{ mm}$  corresponding to  $11.14 \leq D/d^* \leq 16.18$ . Increasing the orifice size to very large values would lead to an accelerated flow regime, basically the same as without constriction at the bottom of the cylinder. Are the curves with increasing flow rate in Fig. 2.2 already the precursors of such a transition?

Fig. 2.3 confirms that this is not the case. Here, we plot the flow rate curves for glass beads and rods with  $L/d = 4.5$  up to the orifice size of  $D = 102 \text{ mm}$ , i.e.,  $D/d^* = 22.5$ . The sequence of curves for elongated particles shows that the increasing flow rate scenario is present in a limited range of orifice sizes, and at around  $D/d^* = 22$ , we recover the constant flow rate scenario. The flow rate as a function of time is shown in Fig. 2.3(c)-(d), presenting the typical timescales of the process. Another important observation is that the flow rate increase is not particularly sensitive to the initial filling height. In Fig. 2.3(b), three measurements are presented for the orifice of  $D/d^* = 18.5$ , with the initial fill heights of  $H/D_{\text{silo}} = 5.5, 4.2,$  and  $2.8$ . We see that the three curves nicely overlap, i.e., the flow rate increase is the same for all three measurements.

We can characterize the flow rate increase by two quantities: the peak flow rate and the initial flow rate. The initial flow rate is defined as the flow rate right after the transient when the material in the silo is between  $5m_{D_{\text{silo}}} > m > 4m_{D_{\text{silo}}}$ . Fig. 2.4(a)-(b) show the initial and final flow rates as a function of the reduced orifice size  $D/d^*$  for all five samples. We see that while the final flow rate increases similarly for all materials (at least up to about  $D/d^* = 15$ ), the increasing trend of the initial flow rate is getting significantly weaker with increasing aspect ratio  $L/d$ . This leads to an increasing value of the ratio of the final and initial flow rates with increasing aspect ratio of the particles, as we see in Fig. 2.4(c).

## 2.3. Results and discussion

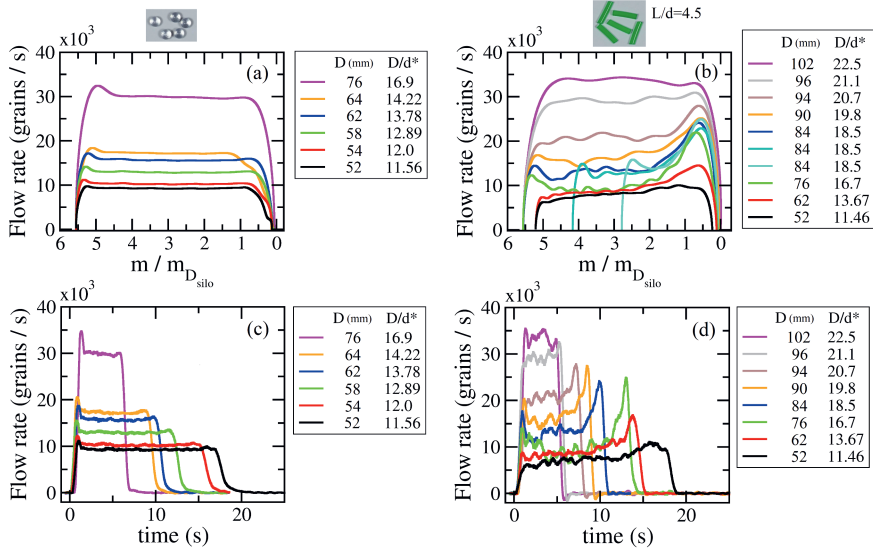


**Figure 2.3:** Experimental results of flow rate during discharge for glass beads (left column: (a) evolution with the normalized remaining mass in the silo, and (c) evolution with time), and plastic rods with an aspect ratio of 4.5 (right column: (b) and (d) shown in the same methods as (a) and (c) respectively). The normalized remaining mass is defined as the ratio of remaining mass in the silo to the mass of material filled up to a height of  $D_{\text{sil}o}$  in the silo. In Panel (a), (b) and (d), the curves are the average of 2 to 5, 2 to 25 and 2 measurements, respectively, whereas there is one measurement for each curve in Panel (c).

### 2.3.2 Numerical results

#### Macroscopic response

Discrete Element Method (DEM) simulations were performed for a direct comparison with the experimental system. In Fig. 2.5, we plot the flow rate and the basal force  $F_b$  as a function of the mass in the silo. For clarity, the data corresponding to the same cases discussed in Fig. 2.5 are shown.

In general, the numerical and experimental results are in quantitative agreement with a difference of up to 20% – 30%, which can be attributed to the slightly different particle shapes (spherocylinders vs. rods with slightly irregular ends) or surface friction of the grains. As we can see, DEM simulations reproduce the most relevant features of the discharge process, with constant flow rate for spherical particles and a complex

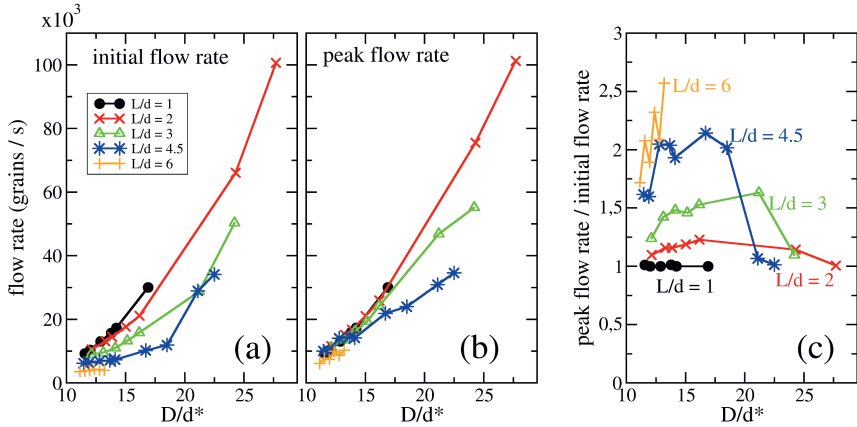


**Figure 2.4:** Experimental results: (a) initial flow rate, (b) peak flow rate and (c) ratio of the peak and initial flow rates as a function of the reduced orifice diameter  $D/d^*$ . The initial flow rate is measured when the material in the silo is between  $5m_{D_{\text{silo}}} > m > 4m_{D_{\text{silo}}}$ . The different curves correspond to particles with different aspect ratios  $L/d$ .

behavior for elongated grains. Thus, the flow rate for elongated grains shows an increasing trend for large orifices. However, the behavior changes as the orifice size reduces, resulting in a nearly constant value. For very small orifices, and after half of the process, the flow rate slightly decreases towards the end of the process, denoting the increasing risk of getting clogged.

The basal force  $F_b$  in the numerical simulations also shows a similar trend as the experimental data, with overlapping curves for different orifice sizes (no flow rate dependence) and after a nearly constant value in the first half of the discharge process, there is a gradual decrease in the second half.

In order to calculate the relevant macroscopic fields from the DEM data, we execute a coarse-graining analysis. As a first step, our analysis focuses on the behavior of the mean packing fraction  $\langle \phi \rangle$ , grain velocity in the vertical direction  $\langle v_z \rangle$ , and vertical component of the orientation tensor  $\langle O_{zz} \rangle$ , averaged in the orifice region. We define this region as a cylindrical volume centered around the silo axis with its base at the orifice level, with the same diameter as the orifice size and a height of  $L/2$ . The evolution of these quantities is presented in Fig. 2.6. We observe an overall non-monotonic trend of

### 2.3. Results and discussion

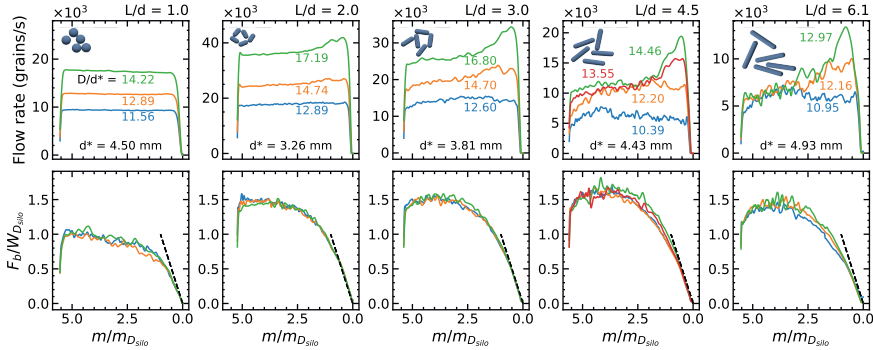


**Figure 2.5:** DEM results: silo flow rate (top) and basal force  $F_b$  (bottom) as a function of the mass  $m$  in the silo. The different panels display data for samples of different grain shapes: spheres and spherocylinders with aspect ratios of  $L/d = 2, 3, 4.5$  and  $6.1$  as indicated by the pictures of the grains in the top row. The values of  $m$  and  $F_b$  were normalized by the mass  $m_{D_{\text{silo}}}$  and the weight  $W_{D_{\text{silo}}}$  of the material corresponding to a filling height of the diameter of the silo, respectively. The dashed line represents the force which would be measured if the walls would not have friction (hydrostatic behavior). For spheres and particles with elongations  $L/d = 2$  and  $3$ , the curves correspond to an average of 4 simulation runs, while for particles with  $L/d = 4.5$  and  $6.1$ , they are derived from 8 runs.

$\langle \phi \rangle$  by increasing the particle aspect ratio  $L/d$  with the largest value of  $\langle \phi \rangle$  for particles with  $L/d = 2$ . This is coherent with earlier observations on the packing fraction of disordered jammed granular materials, where a similar non-monotonic dependence was found as a function of the particle elongation  $L/d$ , with the largest value of  $\langle \phi \rangle$  at around  $L/d = 1.5$  [43, 44]. For particles with  $L/d > 2$ , the value of  $\langle \phi \rangle$  monotonically decreases, since particles with larger elongation tend to form more dilute packing with a lower degree of orientational ordering [44].

In detail, examining spheres (Fig. 2.6, top row, first panel), we see that  $\langle \phi \rangle$  is practically constant during the discharge, and it is slightly growing with increasing orifice size  $D/d^*$ , in agreement with previous numerical findings [45]. Focusing the attention on moderately elongated particles, i.e., for  $L/d < 4.5$ ,  $\langle \phi \rangle$  varies only slightly during the discharge process, regardless of the orifice size  $D/d^*$ . Typically, we obtain a slightly increasing value of  $\langle \phi \rangle$  throughout the discharge process, with the largest  $\langle \phi \rangle$  values are always detected near the end. This trend also holds for very long rods  $L/d > 4.5$  and small orifices, but a distinct behavior is depicted for large orifices. In those cases, the flow is getting significantly diluted in the beginning, and a growing



## 2. Elongated grains discharged from a narrow 3D silo

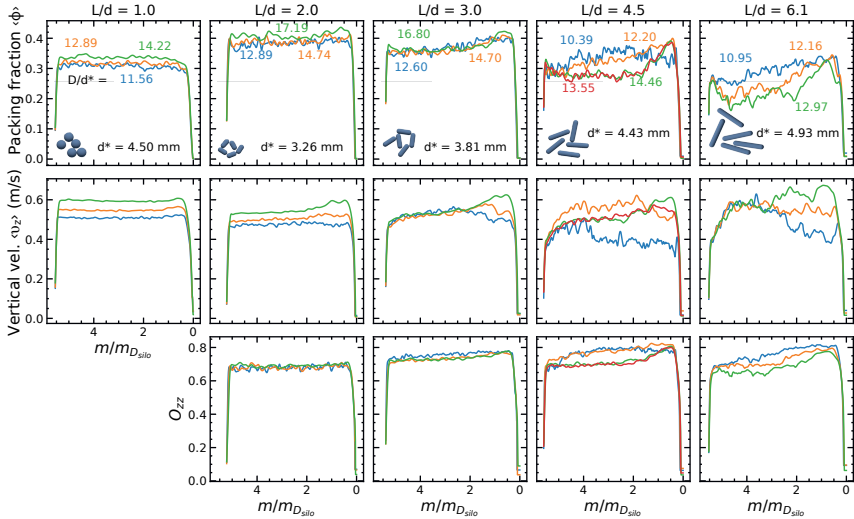


**Figure 2.6:** DEM results: average packing fraction (top row), vertical grain velocity (middle row) and vertical component of the orientation tensor (bottom row) as a function of the mass in the silo during the discharge process for spheres and spherocylinders with aspect ratios of  $L/d = 2, 3, 4.5, 6.1$ . We do not show this quantity for spherical particles since they do not have an orientation. The curves represent data averaged in a cylindrical region based at the orifice with a diameter of the orifice and a height of  $L/2$ .

value of  $\langle \phi \rangle$  is observed only in the second half of the process.

When inspecting the evolution of  $\langle v_z \rangle$  (Fig. 2.6, middle row) for spheres, we obtain  $\langle v_z \rangle$  practically constant during the discharge. As expected, the value of  $\langle v_z \rangle$  typically rises with increasing the relative orifice size  $D/d^*$ . For elongated particles, however, near the end of the process, we find increasing velocity for large orifices but decreasing velocity for small orifices. Consistently, this behavior is in line with the obtained trends for the particle flow rate when varying  $D/d^*$ , both experimentally and numerically. Here, we can argue that changes in the flow patterns cause these different trends.

The behaviors of  $\langle \phi \rangle$  and  $\langle v_z \rangle$  suggest that there are significant changes in the morphology of the flow during the discharge. In Fig. 2.6, bottom row, we present the mean value of the vertical component of the orientation tensor  $\langle O_{zz} \rangle$ , which shows that the particle orientation also changes during discharge. In general, its behavior correlates with the trend of  $\langle \phi \rangle$  in all cases. This indicates that the level of alignment

and order of the flowing structures determines the macroscopic volume fraction at the orifice. Accordingly, these microstructural changes also correlate with the macroscopic particle flow rate obtained numerically and experimentally.

### Spatial profiles of the main quantities in the silo

In order to better understand the complex nature of the data presented above, in the following, we extend our analysis by investigating the spatial profiles in the whole silo. Fig. 2.7 illustrates packing fraction  $\phi(r, z)$ , velocity  $v(r, z)$ , contact pressure  $p_c(r, z) = \frac{1}{3}Tr(\sigma^c(r, z))$ , and shear rate  $\dot{\gamma}(r, z)$  by presenting four snapshots of the discharge process, corresponding to 80%, 60%, 40% and 20% of the initial bed height. These moments are indicated by vertical red lines on the flow rate curves on the top of the figure. The plots are shown for four cases (see Fig. 2.7 from left to right): (column I) spheres, and (columns II-IV) rods with (column II) small orifice, (column III) large orifice and (IV) large orifice and wide silo with  $D_{\text{silo}} = 204$  mm. Note that the colormaps were created by azimuthal averaging, therefore some irregularities are present around the central axis, where less data are available for the averaging.

The results shown in Fig. 2.7 indicate that the nature of the discharge process is very different for beads and rods. For beads (column I), the macroscopic fields are relatively homogeneous, while for rods (II-IV) strong gradients are observed. For rods, we see a fast flowing central region surrounded by a slowly moving (or stagnant) zone, with a strongly sheared region in between. This is coherent with our earlier observations in a quasi-two-dimensional hopper [12].

Looking for the cause of the flow rate increase near the end of the discharge process in case III, we now compare cases II and III, corresponding to the same particle elongation  $L/d = 6.1$  but different orifice sizes  $D/d^* = 10.95$  and  $D/d^* = 12.97$ , respectively. Focusing the attention on the  $\phi$  colormaps in Fig. 2.7 at the orifice region, it is noticeable that in the last stage, the values are comparable in both cases. However, in case III,  $\phi$  is significantly lower in the first three snapshots than in case II, while in case II such flow-dilation is only observed in the first snapshot, after which the packing fraction at the orifice quickly increases. Examining the velocity fields in Fig. 2.7, they also indicate important differences in the nature of the flow field. For case II, a well developed stagnant zone is formed, and it also expands in time. It seems to increase the systems' effective friction, leading to a decrease in the flow velocity in the orifice region (see the blue velocity curve for  $L/d = 6.1$  in Fig. 2.6). This compensates for the slight increase in the packing fraction and altogether leads to an approximately constant flow rate for case II. In contrast, it does not occur in case III where the material around the surging inner region is also flowing, and it is hard to identify a stable stagnant zone. As a result, there is a significant increase of the flow velocity near the end of the discharge

## 2. Elongated grains discharged from a narrow 3D silo

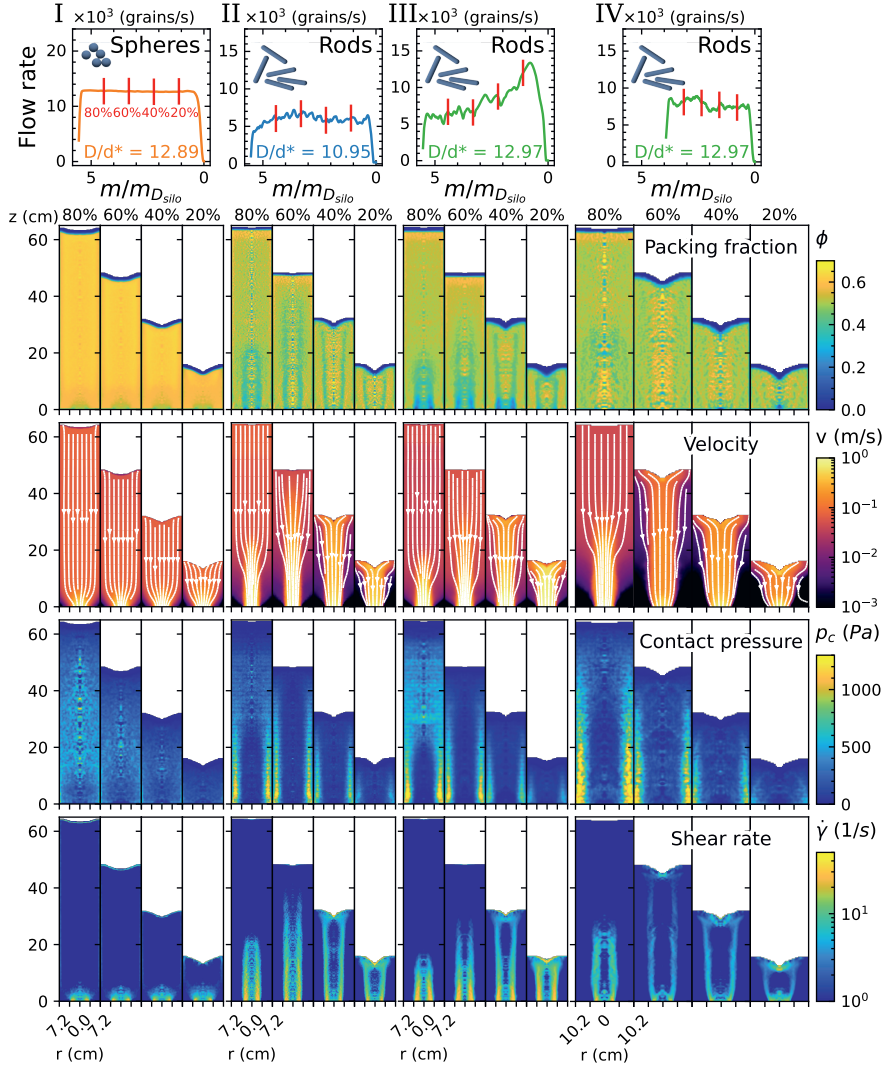


**Figure 2.7:** Evolution of the coarse-grained macroscopic fields for the spherical (I) and elongated particles (II-IV). Each subplot contains the colormaps of four snapshots during the flow, at 80%, 60%, 40% and 20% of the initial bed height in order. These moments are indicated with vertical red lines on the flow rate curves on the top of the figure. The rows display the spatial distribution of the following quantities in order: packing fraction  $\phi$ , velocity  $v$ , contact pressure  $p_c$  and shear rate  $\dot{\gamma}$ .

### 2.3. Results and discussion

process (see the green velocity curve for  $L/d = 6.1$  in Fig. 2.6). The above described two ingredients: (i) the increase in the packing fraction in the orifice region and the suppressed stagnant zone together lead to an increased flow rate for case III near the end of the discharge process.

As we have seen, the scenario of case III is only observed for a relatively large orifice (in relation to the inner silo diameter), when the stagnant zone is suppressed. Can we get back to the constant flow rate scenario by increasing the silo width and thereby recovering the stagnant zone? This configuration is shown in our last test (case IV in Fig. 2.7) in a silo with a 40% larger diameter. As we see, the velocity field of case IV resembles that of case II with a clearly developed stagnant zone. With the reappearance of the stagnant zone, the dilation in the region above the orifice also disappeared. Altogether, this results in a constant flow rate throughout the discharge process in case IV, similar to case II. We also note that when the orifice size is further increased we have observed a high constant flow rate as shown in Fig. 2.3 for  $D/d^* = 22.5$ . The mesoscopic fields for this case (not shown here) are very similar to the ones observed for spherical grains (case I in Fig. 2.7) without strong gradients.

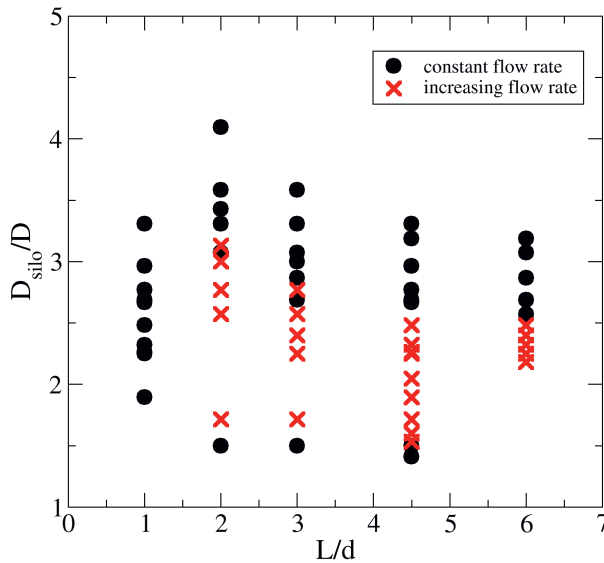


**Figure 2.8:** The two types of flow regimes: silo discharge with constant and increasing flow rates as a function of the particles aspect ratio  $L/d$  and the normalized silo diameter  $D_{\text{silo}}/D$ .

In Fig. 2.8 we visualize the obtained experimental discharge flow regimes in the explored range of the parameters. The black circles and red crosses indicate where the system exhibits constant or increasing flow rates, respectively. The increasing flow rate scenario is only observed in a finite range of the parameters. As expected, in the limit of a very large silo diameter compared to the orifice size, the classical constant flow rate response is achieved, regardless of particle shape and size. In the opposite limit, when the orifice size is comparable with the silo dimension, the constant flow rate is recovered.

### 2.4 Summary

We have shown that the discharge of elongated particles from a narrow silo can lead to strongly time-dependent outflow rates with a significant increase before the end of the discharge process. This is not observed for spherical particles of similar size in the same silo. The peculiar scenario for elongated grains is observed both in a typical size lab experiment and in corresponding numerical (DEM) simulation using 100,000 - 400,000 particles. The analysis of the numerical data revealed that the difference between the case of beads (constant flow rate) and elongated particles (time-dependent flow rate) originates from the difference in the flow field. Namely, for spherical grains, we observe smooth, homogeneous fields for the packing fraction, velocity, or contact pressure, representing a mass flow type discharge. For elongated grains, however, these quantities show large spatial variations inside the silo, with a strong gradient representing funnel flow behavior. In particular, a fast-flowing region is observed in the middle of the silo, which is surrounded by a slowly moving (or stagnant) zone. This is in accordance with our earlier observations in a quasi-two-dimensional silo [12], and it leads to slower discharge than for beads. For a large enough orifice size, however, the stagnant zone is suppressed, leading to an increase in the packing fraction and in the flow velocity before the end of the process. Altogether, the increasing flow rate scenario is observed in a finite range of the parameters.

---

## BIBLIOGRAPHY

- [1] Beverloo, W., Leniger, H., and van de Velde, J. “The flow of granular solids through orifices”. In: *Chemical Engineering Science* **15** (1961), 260–269.
- [2] Nedderman, R. M. et al. “The Flow of Granular Materials I: Discharge Rates from Hoppers”. In: *Chemical Engineering Science* **37** (1982), 1597.
- [3] Mankoc, C. et al. “The flow rate of granular materials through an orifice”. In: *Granular Matter* **9** (2007), 407–414.
- [4] Hilton, J. and Cleary, P. “Granular flow during hopper discharge”. In: *Physical Review E* **84** (2011), 011307.
- [5] Rubio-Largo, S. M. et al. “Disentangling the Free-Fall Arch Paradox in Silo Discharge”. In: *Physical Review Letters* **114** (2015), 238002.
- [6] Zuriguel, I. et al. “Jamming during the discharge of granular matter from a silo”. In: *Physical Review E* **71** (2005), 051303.
- [7] Thomas, C. C. and Durian, D. J. “Geometry dependence of the clogging transition in tilted hoppers”. In: *Physical Review E* **87** (2013), 052201.
- [8] Thomas, C. C. and Durian, D. J. “Fraction of clogging configurations sampled by granular hopper flow”. In: *Physical Review Letters* **114** (2015), 178001.
- [9] Ashour, A. et al. “Outflow and clogging of shape-anisotropic grains in hoppers with small apertures”. In: *Soft Matter* **13** (2017), 402.
- [10] Choi, J., Kudrolli, A., and Bazant, M. “Velocity profile of granular flows inside silos and hoppers”. In: *Journal of Physics: Condensed Matter* **17** (2005), S2533.

- 
- [11] Weinhart, T. et al. “Influence of coarse-graining parameters on the analysis of DEM simulations of silo flow”. In: *Powder Technology* **293** (2016), 138.
- [12] Szabó, B. et al. “Flow of anisometric particles in a quasi-2D hopper”. In: *Physical Review E* **97** (2018), 062904.
- [13] Ge, L. et al. “Effects of aspect ratio and component ratio on binary-mixed discharging pebble flow in hoppers”. In: *Powder Technology* **355** (2019), 320–332.
- [14] Golshan, S. et al. “Experimental and DEM studies of velocity profiles and residence time distribution of non-spherical particles in silos”. In: *Powder Technology* **373** (2020), 510–521.
- [15] Escudero, F. et al. “Silo discharge: influence of the particle shape on the velocity profiles”. In: *EPJ Web of Conferences* **249** (2021), 03029.
- [16] Janda, A. et al. “Flow-rate fluctuations in the outpouring of grains from a two-dimensional silo”. In: *Physical Review E* **79** (2009), 031302.
- [17] Unac, O. et al. “Experimental study of discharge rate fluctuations in a silo with different hopper geometries”. In: *Powder Technology* **225** (2012), 214.
- [18] Muite, B. et al. “Silo Music and Silo Quake: Granular Flow-Induced Vibration”. In: *Powder Technology* **145** (2004), 190.
- [19] Wilde, K. et al. “Experimental and Theoretical Investigations of Silo Music”. In: *Powder Technology* **198** (2010), 38.
- [20] Börzsönyi, T. and Kovács, Z. “High speed imaging of traveling waves in a granular material during silo discharge”. In: *Physical Review E* **83** (2011), 032301.
- [21] Wang, S., Fan, Y., and Ji, S. “Interaction between super-quadric particles and triangular elements and its application to hopper discharge”. In: *Powder Technology* **339** (2018), 534–549.
- [22] Masson, S. and Martinez, J. “Effect of particle mechanical properties on silo flow and stresses from distinct element simulations”. In: *Powder Technology* **109** (2000), 164.
- [23] Darias, J., Madrid, M., and Pugnali, L. “Differential equation for the flow rate of discharging silos based on energy balance”. In: *Physical Review E* **101** (2020), 052905.
- [24] Pongó, T. et al. “Flow in an hourglass: particle friction and stiffness matter”. In: *New Journal of Physics* **28** (2021), 023001.

## Bibliography

---

- [25] Ashour, A. et al. “Silo outflow of soft frictionless spheres”. In: *Physical Review Fluids* **2** (2017), 123302.
- [26] Harth, K. et al. “Intermittent flow and transient congestions of soft spheres passing narrow orifices”. In: *Soft Matter* **16** (2020), 8013.
- [27] Liu, S. D. et al. “Flow characteristics and discharge rate of ellipsoidal particles in a flat bottom hopper”. In: *Powder Technology* **253** (2014), 70.
- [28] Langston, P. A. et al. “Distinct element modelling of non-spherical frictionless particle flow”. In: *Chemical Engineering Science* **59** (2004), 425–435.
- [29] Jin, B., Tao, H., and Zhong, W. “Flow Behaviors of Non-spherical Granules in Rectangular Hopper”. In: *Chinese Journal of Chemical Engineering* **18** (2010), 931.
- [30] González-Montellano, C. et al. “Validation and experimental calibration of 3D discrete element models for the simulation of the discharge flow in silos”. In: *Chemical Engineering Science* **66** (2011), 5116–5126.
- [31] Calderón, C. et al. “Correlations between flow rate parameters and the shape of the grains in a silo discharge”. In: *Powder Technology* **320** (2017), 43.
- [32] Soltanbeigi, B. et al. “DEM study of mechanical characteristics of multi-spherical and superquadric particles at micro and macro scales”. In: *Powder Technology* **329** (2018), 288.
- [33] Markauskas, D. and Kacianauskas, R. “Investigation of rice grain flow by multi-sphere particle model with rolling resistance”. In: *Granular Matter* **13** (2011), 143.
- [34] Hilton, J. and Cleary, P. “Granular flow during hopper discharge”. In: *Physical Review E* **84** (2011), 011307.
- [35] Staron, L., Lagrée, P.-Y., and Popinet, S. “The granular silo as a continuum plastic flow: The hour-glass vs the clepsydra”. In: *Physics of Fluids* **24** (2012), 103301.
- [36] Rubio-Largo, S. M. et al. “Disentangling the Free-Fall Arch Paradox in Silo Discharge”. In: *Physical Review Letters* **114** (2015), 238002.
- [37] Dunatunga, S. and Kamrin, K. “Modelling silo clogging with non-local granular rheology”. In: *Journal of Fluid Mechanics* **940** (2022), A14.
- [38] Börzsönyi, T. et al. “Shear-induced alignment and dynamics of elongated granular particles”. In: *Physical Review E* **86** (2012), 051304.
- [39] Börzsönyi, T. et al. “Orientational Order and Alignment of Elongated Particles Induced by Shear”. In: *Physical Review Letters* **108** (2012), 228302.



- [40] Börzsönyi, T. et al. “Packing, alignment and flow of shape-anisotropic grains in a 3D silo experiment”. In: *New Journal of Physics* **18** (2016), 093017.
- [41] Tang, J. and Behringer, R. P. “Orientation, flow, and clogging in a two-dimensional hopper: Ellipses vs. disks”. In: *EPL (Europhysics Letters)* **114** (2016), 34002.
- [42] Guillard, F., Marks, B., and Einav, I. “Dynamic X-ray radiography reveals particle size and shape orientation fields during granular flow”. In: *Scientific Reports* **7** (2017), 8155.
- [43] Donev, A. et al. “Improving the Density of Jammed Disordered Packings Using Ellipsoids”. In: *Science* **303** (2004), 990.
- [44] Delaney, G. W. and Cleary, P. W. “The packing properties of superellipsoids”. In: *Europhysics Letters* **89** (2010), 34002.
- [45] Rubio-Largo, S. M., Maza, D., and Hidalgo, R. C. “Large-scale numerical simulations of polydisperse particle flow in a silo”. In: *Computational Particle Mechanics* **4** (2017), 419.

---

## From rice to lentil: the effect of different ellipsoidal shapes on the hourglass flow

*This chapter concentrates on the flow rate of a granulate out of a cylindrical container as a function of particle shape for flat and elongated ellipsoids experimentally and numerically. We find a non-monotonic dependence of the flow rate on the grain aspect ratio  $a/b$ . Starting from spheres the flow rate grows and has two maxima around the aspect ratios of  $a/b \approx 0.6$  (lentil-like ellipsoids) and  $a/b \approx 1.5$  (rice-like ellipsoids) reaching a flow rate increase of about 15% for lentils compared to spheres. For even more anisotropic shapes ( $a/b = 0.25$  and  $a/b = 4$ ) the flow rate drops. Our results reveal two contributing factors (with similar strength) to the non-monotonic nature of the flow rate: both the packing fraction and the particle velocity through the orifice are non-monotonic functions of the grain shape. Thus, particles with slightly non-spherical shapes not only form a better packing in the silo but also flow faster through the orifice than spheres. We also show that the resistance of the granulate against shearing increases with aspect ratio for both elongated and flat particles, thus change in the effective friction of the granulate due to changing particle shape does not coincide with the trend in the flow rate.*

This chapter is submitted as:

**Bo Fan, Tivadar Pongó, Raúl Cruz Hidalgo and Tamás Börzsönyi**  
“Effect of particle shape on the flow of an hourglass”

### 3.1 Introduction

As we have seen in the previous chapter, the elongated shape can alter the evolution of the discharge process of particles from a silo. In this chapter, we will focus on the average flow rate in the range of orifice sizes where the elongated shape does not change the nature of constant flow rate during the discharge process. We know that flow of a granular material out of a container is a common process in everyday life, agriculture and industrial operations. Typically, a granulate discharges through the orifice with a constant flow rate, independent of the filling height [1, 2]. This feature was used when the hourglass was constructed as a time measuring device long ago, and it is very useful as the required flow rate can be easily set by simply choosing the appropriate orifice size. The flow rate changes with increasing orifice size as a power law function (Beverloo law [2–7]) and also depends on the internal friction of the granular material, which is changing with the surface roughness as well as the shape of the grains. Naturally, increasing particle roughness negatively impacts the flow rate [8], but it is much less obvious how it should change with grain shape. On one end of the spectrum, very irregular grains can get entangled during the discharge and flow less easily, but what should we expect from shapes which deviate only slightly from a sphere: ellipsoids with rice-like or lentil-like shapes?

Elongated or flat particles are observed to develop orientational ordering in a shear flow, with their smallest cross-section facing almost in the flow direction [9–12]. The average orientation angle is decreasing with increasing grain anisometry, and e.g. is around  $10^\circ$  for a rice-like ellipsoid with elongation  $a/b = 3$ . Naively, this would then suggest easier flow and thus faster flow rate through a constriction for simple elongated or flat ellipsoids than for spherical particles. However, taking a closer look at the dynamics of such particles in a shear flow, we observe that they perform irregular rotation as dictated by the shear stress related to the interaction with their neighbors. On average, they rotate slower when they are nearly parallel to the flow direction and rotate faster when they are perpendicular to it [10]. So during their rotation, they spend most of the time nearly parallel to the flow, which leads to the above-described average orientation. But as they rotate, neighboring particles actually get into conflict and hinder each other's motion. This leads to a nontrivial rheology for such types of granular materials.

Previous studies focusing on the fundamental question of the effect of the grain shape on the rheology of a granular material or discharge rate from a silo are mostly numerical. This is because discrete element model (DEM) simulations offer a straightforward way to systematically change the particle shape without changing the other parameters (microscopic surface friction, etc.). As for the rheology, recent DEM studies show that for frictional particles the effective friction  $\mu_{\text{eff}}$  of the system is increasing with

## 3.2. Experimental setup

---

grain anisometry. This was found for spherocylinders in quasistatic shear flow for interparticle friction  $\mu_p > 0.4$  [13], or in more dynamic inclined plane flows for  $\mu_p \geq 0.5$  [14]. Similar observations were made in a simplified two-dimensional (2D) system [15]. Interestingly, for systems with lower interparticle friction ( $\mu_p < 0.4$ ) a non-monotonic tendency was found: starting from a spherical shape  $\mu_{\text{eff}}$  first increases and then decreases with  $a/b$ . Focusing on previous DEM results on the discharge of a 3D silo with frictional grains one finds contradictory observations. On one hand, Liu et al. found a reduced discharge rate for both elongated and flat ellipsoids compared to the case of spheres [16], on the other hand, Li et al. reported a larger flow rate for round disks than for spheres [17]. In a recent work by Hesse et al. decreased/increased flow rate was found for elongated/flat ellipsoids compared to spheres, respectively [18]. Finally, for frictionless grains Langston et al. reported the same flow rate for spherocylinders and spheres [19].

To the best of our knowledge, so far no systematic experimental tests have been performed to measure how the discharge rate changes with particle shape when all other parameters (surface roughness, density, hardness, etc...) are identical [20]. For rod-like shapes, a flow rate decrease was detected with increasing aspect ratio comparing 2 samples of glass rods with two samples of plastic rods [21].

In the present chapter, we investigate experimentally the effect of particle shape on the flow rate of a granulate out of a container. Notably, we use custom-made particles which differ only in shape, while their volume and all other parameters are identical [**borzsonyi\_particles**]. We also test the resistance of our samples against quasistatic shearing. Our experiments are complemented with numerical simulations using the discrete element model (DEM).

## 3.2 Experimental setup

In the experiments, we used 9 different samples of Polyoxymethylene (POM) ellipsoids (produced by injection moulding by Yuyao Strong Co., China). Each sample contained 50000 identical particles. Tab. 3.1 shows photographs of the particles and give their characteristic dimensions. The flow rate experiments were performed using an acrylic cylinder with an inner diameter of either  $D_c = 172$  mm or 144 mm and a length of 800 mm with an orifice at the bottom with adjustable diameter  $D$  (see Fig. 3.1(a)). The granulate was filled into the cylinder manually and after opening the orifice we recorded the flow rate by simply measuring the weight of the discharged mass with a load cell. In a complementary experiment we measured the resistance of the granulate against shearing in a cylindrical split-bottom shear cell (see Fig. 3.1(b)). Here the middle part of a granular sample was rotated with a rotating plate under it and thereby stationary

### 3. From rice to lentil: the effect of different ellipsoidal shapes on the hourglass flow

shear was applied in the shear zone (see red region in Fig. 3.1(b)) between the moving and standing regions. The applied torque was measured during stationary shearing.

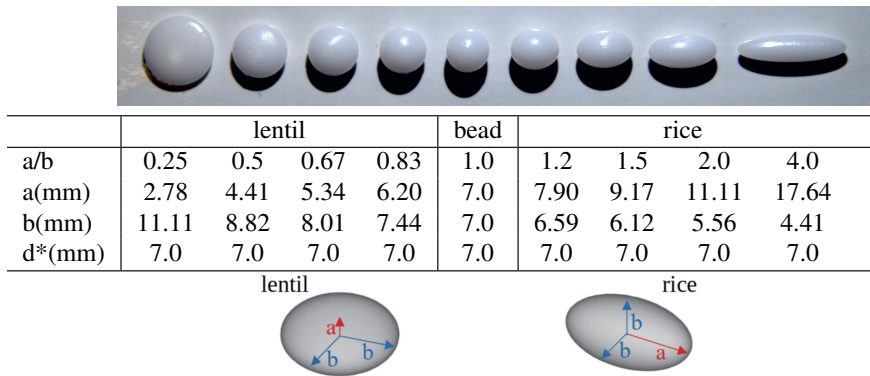


**Table 3.1:** Experimental materials. Top: ellipsoids with different aspect ratios, but with the same mass and volume.  $a$  and  $b$  are the two axis about which the elliptical cross section of the ellipsoid is symmetrical.

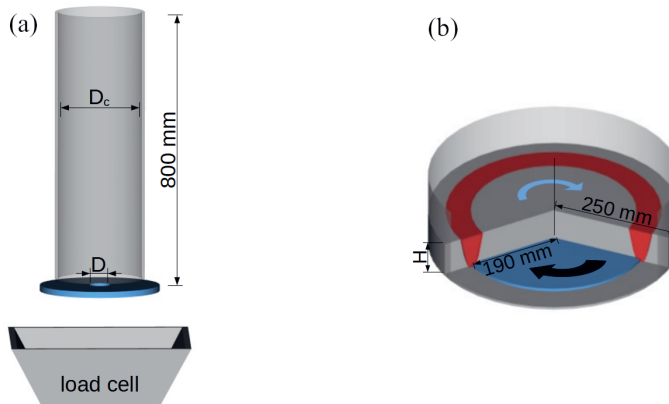


**Figure 3.1:** Schematic diagrams of experimental setups. (a) Silo. (b) Cylindrical split-bottom shear cell.

### 3.3 Results and discussion

The evolution of the normalized flow rate obtained in both experiments and simulations are presented as a function of the mass in the cylinder during the discharge process in Fig. 3.2. The mass in the cylinder is normalized by the mass corresponding to the filling height of  $D_c$ . The data-sets are normalized by the average flow rate of beads. The average flow rate is calculated using data in the middle of the discharge process, i.e. in the range of  $1.4 < m/m_{D_c} < 2.8$ . Similar plots were obtained in the smaller silo ( $D_c = 144$  mm). We mention that for a narrow cylinder, a surge is observed at the end of the discharge process[22] for a certain range of the orifice diameter as shown in chapter 2. For most of our current measurements, there was no surge, and for those where a surge occurs, we average the flow rate before the surge.

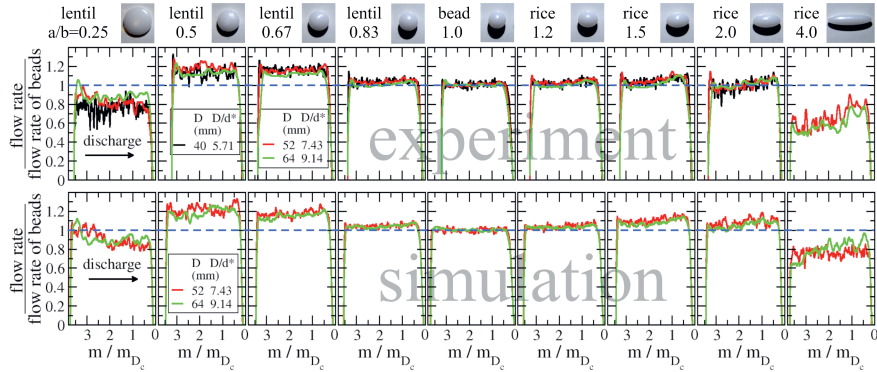


**Figure 3.2:** Normalized flow rate as a function of the mass in the cylinder for all 9 ellipsoidal samples during the discharge process. The average flow rate for beads is calculated in the range of  $1.4 < m/m_{D_c} < 2.8$ . Top row: experimental data obtained in the cylinder with  $D_c = 172$  mm with orifice sizes of  $D = 40, 52$  and  $64$  mm. Each curve corresponds to the average of 2 measurements. Bottom row: numerical results for the same setting. The curves correspond to a single run except for the cases of  $a/b = 0.25$  and  $a/b = 4.0$  for which 4 runs are averaged.

We summarize our findings by plotting the average flow rate as a function of the particle aspect ratio in Figs. 3.3(a),(d). Starting from the spherical shape and going towards lentil-like shapes we first find a clear increase of the flow rate having a maximum around the aspect ratio of  $a/b \approx 0.6$  and then a strong decrease for the grains with  $a/b = 0.25$ . When we go in the direction of elongated grains, around the aspect ratio of about  $a/b \approx 1.5$  we again find a peak, but this is smaller than for the case of lentils, and the effect is more pronounced for the DEM data than in

### 3. From rice to lentil: the effect of different ellipsoidal shapes on the hourglass flow

experiments (compare Figs. 3.3(a) and 3.3(d)). Above the aspect ratio of  $a/b = 2$  the flow rate clearly decreases. We mention that the above results are coherent with other experimental observations in a conical hopper, where the discharge rate is found to be larger for lentil-like grains ( $a/b = 0.6$ ) and slightly lower for rice-like grains ( $a/b = 3$ ) compared to spheres [23].

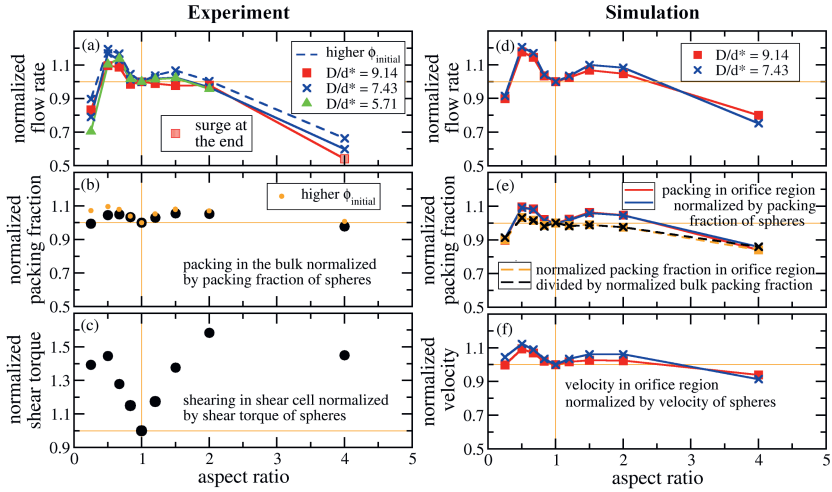


**Figure 3.3:** (a-c) Experimental results: (a) average flow rate (b) static packing fraction and (c) shear torque as a function of particle aspect ratio. All quantities normalized by the value obtained for beads. The average flow rate was obtained by averaging the data in the range of  $1.4 < m/m_{D_c} < 2.8$ . (d-f) Numerical results: (d) average flow rate, (e) packing fraction and (f) velocity as a function of aspect ratio.

In order to explore the non-monotonic nature of the flow rate curves (Figs. 3.3(a),(d)), we first investigate whether this can be rather related to variations in packing fraction or grain velocities through the orifice.

In the experiments, we can measure the bulk packing fraction of the initial state of each sample by measuring the weight of the sample in dry state and then submerged in water. This is done in a similar cylinder than the silo, but with closed bottom. As we see in Fig. 3.3(b) the initial packing in the cylinder slightly depends on the grain shape with a non-monotonic dependence for both lentil-like and rice-like shapes. The densest packings correspond to the aspect ratios of  $a/b = 0.5$  and  $a/b = 2$ , and are about 6% denser than the packing of spherical particles. A very similar dataset (not shown here) is obtained from our DEM simulations. All this is consistent with the

results of earlier numerical calculations predicting similar shape dependence for the random close packed density [24] and poured density [25] for both elongated and flat ellipsoids. Altogether, for the case of lentils the modulation of the initial bulk packing fraction with shape is small compared to the changes in flow rate, so it does not fully explain the flow rate behavior (Figs. 3.3(a),(d)).

In the numerical simulations, we can quantify the packing fraction as well as the velocity of the grains in the orifice region (see (Figs. 3.3(e),(f)). As we see, they both show non-monotonic shape dependence, and they give approximately an equal contribution to form the trend observed in the flow rate. Analyzing the data for the packing fraction first, we find that dividing the normalized packing fraction in the orifice region by the normalized bulk packing fraction the resulting curve becomes nearly shape independent in the range of  $0.5 \leq a/b \leq 2$ . This means, that the flow does not significantly improve the packing in the orifice region for slightly elongated or flat ellipsoids, so the two peaks on the packing fraction curves basically come from the peaks in the bulk packing fraction. Thus, the first major contribution to the non-monotonic trend in the flow rate curves basically comes from the bulk packing fraction. In order to analyze the origin of the second contribution – the non-monotonic trend of the velocity data – we plot the average grain velocity and acceleration above the orifice as a function of the distance from the orifice in Fig. 3.4. As we see, far from the orifice, the velocity of all types of grains is practically the same, and their acceleration is negligible. The interesting thing is, that the grains with non-spherical shape start accelerating from a higher position than the spheres, but as they get close to the orifice their acceleration becomes slightly smaller (compared to the case of spheres), probably due to larger dissipation. The final velocity is a result of the combination of these two factors: the position where the velocity starts growing and the growth rate of the velocity. The optimum corresponds to lentil-like shapes with an aspect ratio of  $a/b = 0.5$ , which cross the orifice with the largest speed.

Finally, coming back to the experimental data, we analyze how the resistance of the material against shearing is changing with grain shape, and whether this correlates with the flow rate behavior. We quantify this by measuring the shear torque needed for a stationary quasi-static rotation of the sample in the split-bottom shear cell. The normalized shear torque is presented as a function of the aspect ratio in Fig. 3.3(c). The data were obtained using samples with the volume of 7 liters corresponding to a filling height of  $H \approx 3.5$  cm. The data were normalized first by the weight of the sample and then by the normalized shear torque obtained for the case of beads. As we see both elongated and flat shapes are characterized by an increased shear resistance compared to the case of spheres. The increase in the shear torque reaches about 50% for both rice-like and lentil-like ellipsoids, with aspect ratios of  $a/b = 2$  and  $0.5$ , respectively. The increasing tendency is in accordance with our previous numerical



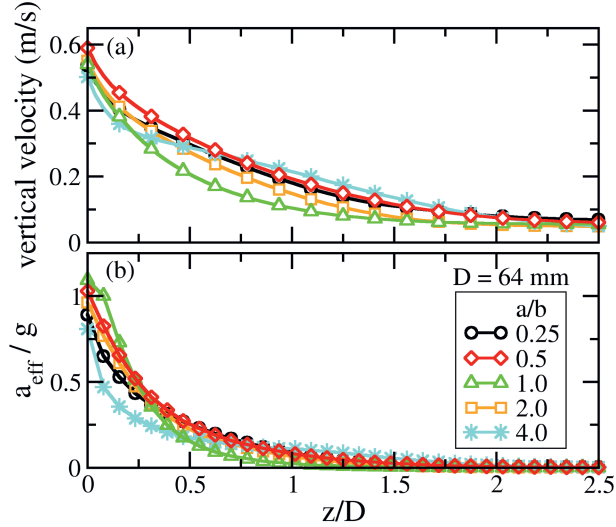


**Figure 3.4:** Numerical results: (a) average vertical velocity and (b) normalized acceleration of the grains above the orifice as a function of the normalized distance  $z/D$  from the orifice.

findings on elongated shapes in simple shear [13] and inclined plane flow [14]. This would suggest decreasing flow rate through a constriction for both elongated and flat grains compared to the case of spherical particles, which does not coincide with our observations described above. Thus, the non-monotonic behavior of the flow rate can not be explained by the shape dependence of the shear resistance.

### 3.4 Summary

In summary, we find a surprising non-monotonic behaviour of the silo flow rate as a function of grain shape for ellipsoidal particles. Slightly non-spherical particles discharge faster than spheres, the effect is stronger for lentil-like shapes than for rice-like shapes. Analyzing the packing fraction and grain velocity in the orifice region, we find that they contribute equally to the non-monotonic tendency of the flow rate. The contribution of the packing fraction mainly originates from the non-monotonic shape dependence of the bulk packing fraction, while the contribution of grain velocity is related to two factors: (i) what is the height above the orifice line at which grains start accelerating (this is larger for non-spherical grains than for spheres), and (ii) at what

### 3.4. Summary

---

rate they speed up, which certainly depends on the dissipation in the region right above the orifice. The optimum of these two effects is found for the slightly flat lentil-like shapes which produce the largest discharge rate in the silo. Finally, the resistance of the granulate against shearing considerably increases for both lentil-like and rice-like particles (compared to spheres), thus its trend does not directly coincide with the non-monotonic trend of the flow rate.



---

## BIBLIOGRAPHY

- [1] Fowler, R. and Glastonbury, J. “The flow of granular solids through orifices”. In: *Chemical Engineering Science* **10** (1959), 150.
- [2] Beverloo, W., Leniger, H., and van de Velde, J. “The flow of granular solids through orifices”. In: *Chemical Engineering Science* **15** (1961), 260–269.
- [3] Nedderman, R. M. et al. “The Flow of Granular Materials I: Discharge Rates from Hoppers”. In: *Chemical Engineering Science* **37** (1982), 1597.
- [4] Mankoc, C. et al. “The flow rate of granular materials through an orifice”. In: *Granular Matter* **9** (2007), 407–414.
- [5] Hilton, J. and Cleary, P. “Granular flow during hopper discharge”. In: *Physical Review E* **84** (2011), 011307.
- [6] Rubio-Largo, S. M. et al. “Disentangling the Free-Fall Arch Paradox in Silo Discharge”. In: *Physical Review Letters* **114** (2015), 238002.
- [7] Calderón, C. et al. “Correlations between flow rate parameters and the shape of the grains in a silo discharge”. In: *Powder Technology* **320** (2017), 43.
- [8] Pongó, T. et al. “Flow in an hourglass: particle friction and stiffness matter”. In: *New Journal of Physics* **28** (2021), 023001.
- [9] Börzsönyi, T. et al. “Orientational Order and Alignment of Elongated Particles Induced by Shear”. In: *Physical Review Letters* **108** (2012), 228302.
- [10] Börzsönyi, T. et al. “Shear-induced alignment and dynamics of elongated granular particles”. In: *Physical Review E* **86** (2012), 051304.

- 
- [11] Börzsönyi, T. and Stannarius, R. “Granular materials composed of shape-anisotropic grains”. In: *Soft Matter* **9** (2013), 7401–7418.
- [12] Botton, M. et al. “Quasistatic rheology and microstructural description of sheared granular materials composed of platy particles”. In: *Physical Review E* **87** (2013), 032206.
- [13] Nagy, D. et al. “Flow and rheology of frictional elongated grains”. In: *New Journal of Physics* **22** (2020), 073008.
- [14] Hidalgo, R. C. et al. “Rheological response of nonspherical granular flows down an incline”. In: *Physical Review Fluids* **3** (2018), 074301.
- [15] Trulsson, M. “Rheology and shear jamming of frictional ellipses”. In: *Journal of Fluid Mechanics* **849** (2018), 718–740.
- [16] Liu, S. D. et al. “Flow characteristics and discharge rate of ellipsoidal particles in a flat bottom hopper”. In: *Powder Technology* **253** (2014), 70.
- [17] Li, J. et al. “Flow of sphero-disc particles in rectangular hoppers—a DEM and experimental comparison in 3D”. In: *Chemical Engineering Science* **59** (2004), 5917–5929.
- [18] Hesse, R., Krull, F., and Antonyuk, S. “Prediction of random packing density and flowability for non-spherical particles by deep convolutional neural networks and Discrete Element Method simulations”. In: *Powder Technology* **393** (2021), 559–581.
- [19] Langston, P. A. et al. “Distinct element modelling of non-spherical frictionless particle flow”. In: *Chemical Engineering Science* **59** (2004), 425–435.
- [20] Borzsönyi, T. et al. *CaliParticles: A Benchmark Standard for Experiments in Granular Materials*. 2022.
- [21] Ashour, A. et al. “Outflow and clogging of shape-anisotropic grains in hoppers with small apertures”. In: *Soft Matter* **13** (2017), 402–414.
- [22] Pongó, T. et al. “The role of the particle aspect ratio in the discharge of a narrow silo”. In: *New Journal of Physics* **24** (2022), 103036.
- [23] Hanif, M. A. et al. “In preparation”. In: *To be determined* (2023).
- [24] Donev, A. et al. “Improving the Density of Jammed Disordered Packings Using Ellipsoids”. In: *Science* **303** (2004), 990.
- [25] Gan, J., Zhou, Z., and Yu, A. “Structure analysis on the packing of ellipsoids under one-dimensional vibration and periodic boundary conditions”. In: *Powder Technology* **335** (2018), 327–333.

## Asymmetric grains in a 3D silo and shear flow

*In this chapter, shear induced orientational ordering of asymmetric elongated particles is investigated experimentally. Corn grains and pegs with one end sharpened are studied using X-ray Computed Tomography (CT) during quasistatic shearing and silo discharge. We show that asymmetries can be detected in the orientational distributions of the particles, which are related to the modulated rotation of the particles during shear flow. Namely, when the particles rotate in a plane that is not horizontal, they spend more time with the sharper (lighter) end pointing up, which can be explained using energy arguments. We quantify the resulting asymmetry of the orientational distribution in a split bottom Couette cell and in a silo discharge process.*

This chapter is submitted as:

**Viktor Nagy, Bo Fan, Ellák Somfai, Ralf Stannarius and Tamás Börzsönyi**

“Flow of asymmetric elongated particles”

## 4.1 Introduction

When a granular material consisting of elongated particles is subjected to shear, the particles get aligned. The average alignment of the particles' long axis is nearly parallel to the flow, it is characterized by a small angle  $\theta_{av}$ , which decreases with increasing particle elongation as it was shown in numerical simulations [1–6] and laboratory experiments [5–9]. Several works have shown that for elongated or flat particles increasing shape anisotropy of the grains leads to stronger orientational ordering, higher effective friction of the sample or stronger shear banding [5, 10–16]. As we have seen in chapters 2 and 3, the shape anisotropy can also result in a surge of flow rate near the end of the discharge process or a higher flow rate for slightly non-spherical grains compared to spheres. For particles with low interparticle friction ( $\mu_p \leq 0.4$  in 3D and  $\mu_p \leq 0.15$  in 2D) an interesting non-monotonic dependence of the effective friction was found as a function of grain elongation [13, 15]. The effect of grain shape on the flow field in a silo, the discharge rate and the clogging probability was also investigated [17–28]. For elongated grains, the flow field was found to be more concentrated to the silo center and had larger temporal fluctuations compared to the case of spherical grains [17, 21, 22]. Even if some of the above investigations involved asymmetric elongated grains e.g. corn seeds, sesame seeds [18, 19, 21, 29] or dumbbells [20], the role of grain shape asymmetry is not well explored in shear flow or silo flow.

In the present chapter, we use two types of elongated asymmetric grains: sharpened pegs and corn seeds in a shear flow and in silo flow. We use a non-invasive method (X-ray computed tomography) to detect the location and orientation of each particle inside our 3-dimensional experimental system. We analyze the orientation distributions and focus on effects related to the asymmetric shape of the grains.

## 4.2 Experimental system

In this chapter, two experimental geometries have been employed to study the flow of a granular assembly of elongated asymmetric particles. In the first experiment, the granular material was exposed to shear in the so called cylindrical split-bottom shear cell (see Fig. 4.1(a), also introduced in chapter 1 in Fig. 1.5(a)). In this device, the central part of the granular sample is rotated, while the outer part of the sample is not moving. The sheared region is between the moving and standing parts, with the highest shear rate in the middle of this region. We define the core of the shear zone as the region where the time averaged rotation rate is in between 5% and 95% of the rotation rate of the inner part. This shear zone core is indicated with red contours and white particles in Figs. 4.1(a), 4.2(a) and a dashed red line in Figs. 4.3(a-f). The

## 4.2. Experimental system

---

width of the shear zone is expected to scale linearly with particle size and to be larger for spherical particles than for irregular ones [30]. As we will see later, the geometry of the shear zone in our experiments was very similar for the two types of grains we used. The radius of the cell was 28.5 cm, the radius of the rotating plate was 19.5 cm, while the height of the granular layer was 6 cm. Before recording the data, the sample was presheared with 15 full rotations, in order to eliminate any transient effects and to ensure stationary shear throughout the experiment. During the experiment, quasistatic shearing was applied which was stopped at regular intervals of  $360^\circ$  of rotation of the inner part, and then a pair of X-ray computed tomograms (CT) was taken of the sample. The plate was rotated by a small amount ( $2^\circ$ ) between the two tomograms, with the aim of enabling the detection of particle displacements for the determination of the flow field. We recorded 50 pairs of tomograms for sharpened wooden pegs and 19 pairs of tomograms for corn seeds. In the second experiment, the granular material was discharged from a nearly cylindrical silo with a circular orifice at the bottom (Fig. 4.1(b)). The diameter of the orifice was relatively small so that the flow often clogged. Each clogged configuration was recorded with X-ray CT. We recorded 109 tomograms for sharpened pegs and 30 tomograms for corn seeds. The container had a height of 21.4 cm and a diameter of 19 cm. The tomograms for both experiments were obtained with the Siemens Artis zeego X-ray Tomograph of the STIMULATE-lab of the Otto von Guericke University in Magdeburg. The recorded volume was  $25.2 \text{ cm} \times 25.2 \text{ cm} \times 19 \text{ cm}$ , with a spatial resolution of 2.03 pixel/mm, resulting in tomograms of  $512 \times 512 \times 386$  pixels. The recording of a single tomogram took about 2 minutes.

The particles used here share a common feature: in addition to being elongated, both are asymmetric in the sense that the two ends are different: the corn seeds have a wedge shape, while for the pegs one of the ends is sharpened (see the photographs in Fig. 4.1(c)). The pegs had a diameter of  $d = 5 \text{ mm}$  and a length of  $L = 25 \text{ mm}$ , while the typical dimensions of the corn seeds were about  $d_1 = 5 \text{ mm}$ ,  $d_2 = 8 \text{ mm}$ , and  $L = 12 \text{ mm}$ . The particle positions and orientations were obtained by tailored 3D image processing. After an initial adaptive binarization of the 3D absorbance field obtained by the X-ray CT measurements, particles were separated by binary erosion and reconstructed by subsequent regrowth. The pictures in Fig. 4.1(a,b) show reconstructed pegs from actual measurements. In the shear cell (Fig. 4.1(a)) the particles are colored according to their location in order to visualize the core of the shear zone. In the silo (Fig. 4.1(b)), the colors represent the local nematic orientational order parameter, which was obtained by averaging over particles in rings of similar height and radius from the central axis.



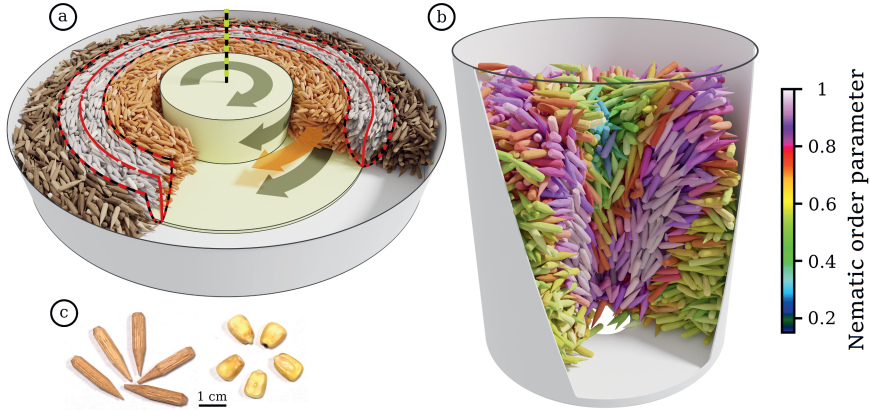


**Figure 4.1:** Sketches of the experimental configurations: (a) cylindrical split-bottom shear cell (b) silo. Both pictures include grains as detected in tomograms. In panel (a) the shear zone is indicated with red lines, while particles in the shear zone are colored white. In panel (b) particle colors represent the local nematic order parameter, according to the colorbar next to the cylinder. (c) Photographs of the samples: sharpened wooden pegs and corn seeds.

## 4.3 Results and Discussion

### 4.3.1 Shear flow

In the first experiment, we characterize the flow field and the orientation of the particles in stationary shear flow in the split bottom shear cell. Fig. 4.2 indicates the main features of the velocity field in this system: the flow velocity is strictly tangential, while the velocity gradient is nearly horizontal. The side view in Fig. 4.2(b) shows that the lines parallel to the local velocity gradient are somewhat curved. This results in a practically horizontal velocity gradient in the outer half of the shear zone core (filled with orange) and a slightly tilted velocity gradient in the inner half of the shear zone core (filled with light blue). As discussed in earlier works [5–8], elongated particles in a shear flow get oriented with their long axis predominantly in the shear plane (spanned by the flow velocity and velocity gradient). They perform a rotation within the shear plane with a fluctuating angular velocity which depends on the actual interactions with neighbours. The ensemble averaged angular velocity, however, shows a clear orientation dependence: particles with their long axis nearly parallel to the flow rotate

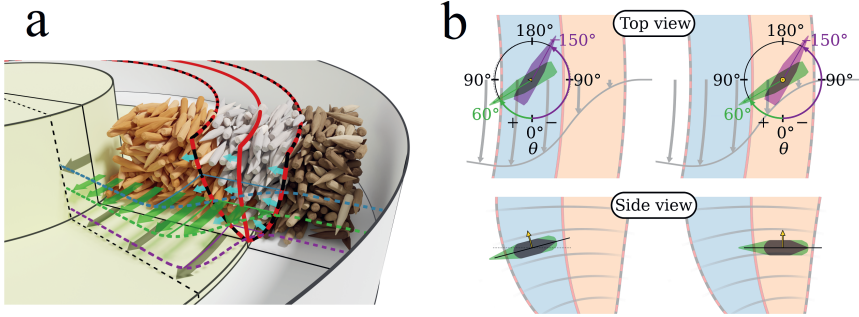


**Figure 4.2:** Geometry of the shear flow in a cylindrical split bottom cell. In panel (a) the contours and the middle of the shear zone are indicated with red lines, the particles in the shear zone are colored white. The velocity profiles at three different heights are indicated with three different colors, the green arrows indicate the velocity profile in the middle of the granular layer. In panel (b) a top view and a side view of the shear zone is sketched. In the top view the flow velocity is indicated by arrows. In the side view, the direction of the local velocity gradient is indicated by lines: it is nearly horizontal in the outer half of the shear zone (orange) and slightly tilted in the inner part of the shear zone (light blue). Two particles lying in the shear plane with orientation angles  $\theta = -150^\circ$  and  $\theta = 60^\circ$  are shown as examples.

slower than those perpendicular to the flow. This results in orientational ordering with an average alignment of the longest axis of the grains nearly parallel to the main flow.

As a first step, we consider the particles as simple elongated grains (i.e. in the first approximation we prescind from the difference between the non-sharpened and sharpened ends) and characterize the shear-induced alignment by a nematic order parameter  $S$ . This is calculated by diagonalizing the symmetric traceless order tensor [6, 31, 32]:

$$T_{ij} = \frac{3}{2N} \sum_{n=1}^N \left[ \ell_i^{(n)} \ell_j^{(n)} - \frac{1}{3} \delta_{ij} \right] , \quad (4.1)$$

where  $\vec{\ell}^{(n)}$  is a unit vector along the long axis of particle  $n$ , and the sum is over all  $N$  detected particles in a certain volume element within the container. The largest eigenvalue of is the primary nematic order parameter  $S$  [5, 6]. Random grain orientations would lead to  $S = 0$ , while  $S = 1$  corresponds to a perfect alignment with all grains parallel to each other. Figs. 4.3(a) and (d) show the maps of the nematic order parameter  $S$ , while Figs. 4.3(b) and (e) show the maps of the average alignment angle for sharpened pegs and corn seeds, respectively, in dependence of the height and

#### 4. Asymmetric grains in a 3D silo and shear flow

the distance from the central axis. The data are averaged over rings around the center, where the local coordinate system always has one coordinate in vertical direction and a second one directed radially. These figures clearly show that both systems get aligned

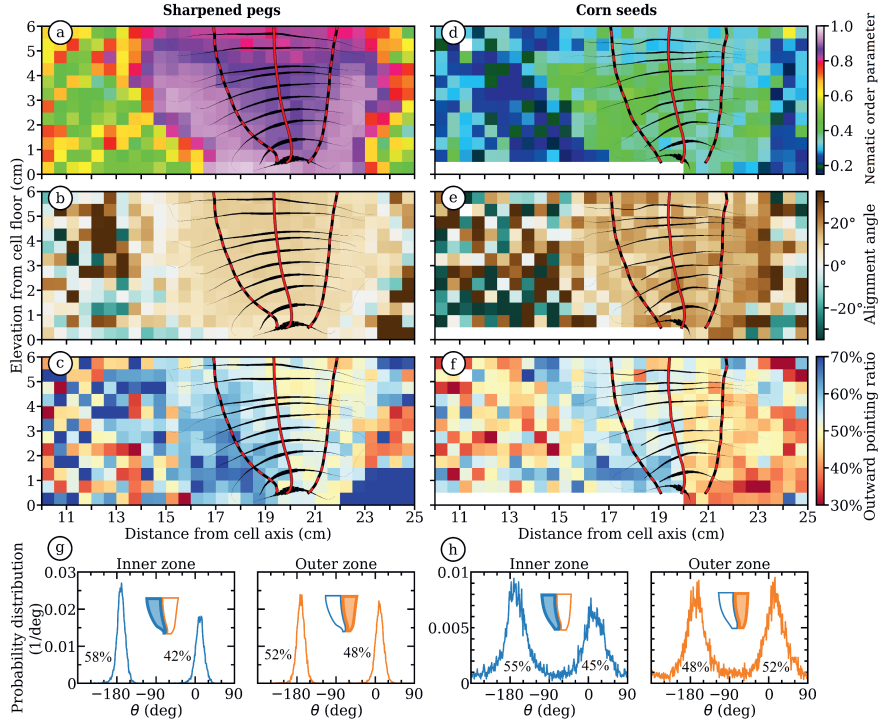


**Figure 4.3:** Maps of the orientational order parameter (row 1), average alignment angle (row 2) ratio of outward pointing particles (row 3) and the distributions of particle orientations (row 4) for sharpened pegs (left) and corn seeds (right) in the cylindrical split-bottom shear cell.

in the sheared region, with the strongest alignment in the core of the shear zone. The order parameter reaches a larger value for sharpened pegs ( $S \approx 0.9$ ) than for the less elongated corn seeds ( $S \approx 0.5$ ). The alignment angle is slightly smaller for sharpened pegs ( $\theta_{av} \approx 10^\circ$ ) than for corn seeds ( $\theta_{av} \approx 14^\circ$ ). All this is in accordance with earlier observations on normal (not sharpened) pegs and rice particles [5, 6].

As a second step, we determine the orientation distribution of the particles by fully

considering their asymmetric shapes (i.e. taking into account the difference between their two ends). Figs. 4.3(g,h) show the distribution of the orientation angle  $\theta$ , defined as the angle between the long axis of the particle and the flow direction as shown in Fig. 4.2(b) (top view). The orientation distribution is separately shown in the outer and inner half of the core of the shear zone for both grain types: sharpened pegs and corn. The distributions have narrower peaks for pegs, i.e. shear induced ordering is stronger for more elongated grains, and the peaks are slightly shifted with respect to the flow direction ( $0^\circ$  and  $180^\circ$ ), in accordance with earlier observations on other elongated particles [5, 6]. Interestingly, in the outer half of the shear zone core the peaks are symmetric, while in the inner half of the shear zone core they are asymmetric. One method to quantify the asymmetry is to calculate the fraction of grains corresponding to each peak. This turns to be 58% : 42% and 55% : 45% in the inner half of the zone for sharpened pegs and corn, respectively (see Figs. 4.3(g,h)). In the outer half of the zone we find 52% : 48%, which is consistent with a symmetric distribution within our statistical uncertainty. An other method to quantify the asymmetry is to introduce the polar order parameter  $P = |\langle \cos(\theta - \theta_{av}) \rangle|$ . This yields  $P = 0.16$  and  $0.09$  in the inner half and  $P = 0.038$  and  $0.023$  in the outer half of the shear zone core for sharpened pegs and corn, respectively. In order to understand this asymmetry, we should consider that the shear gradient is nearly horizontal in the outer half, while it is slightly tilted in the inner half, as discussed above. Thus the deviation of the particle's orientation from the flow direction has a vertical component in the inner half, while it is nearly horizontal in the outer half. The asymmetry of the distributions in the inner half means, that there is a higher probability to find grains with their sharper end pointing outwards than inwards. This can be rationalized by the argument, that the two configurations are energetically different, since outward pointing grains have their thicker end at a lower position, while inward pointing grains have their thicker end at a higher position (see the two grains presented as examples in Fig. 4.2(b) on the left side of the side view). For a horizontal shear gradient there is no such difference (see the two grains on the right side of the side view), so the distributions in the outer half of the zone (see again Figs. 4.3(g,h)) are nearly symmetric. The maps of the outward pointing ratio thus nicely visualize this asymmetry throughout the whole cell (see Figs. 4.3(c,f)). The asymmetry is more pronounced towards the inner side of the shear zone (blue colors) and is larger for the case of sharpened pegs than for corn seeds.

#### 4.3.2 Clogging in a silo

In the second experiment, we investigate the grain orientations during the discharge of a nearly cylindrical silo with a circular orifice at the bottom. The size of the orifice was relatively small:  $D = 3.3$  cm for sharpened pegs, and  $D = 2.6, 2.8$  and  $3.0$  cm

for corn seeds. This ensured frequent clogs during the discharge process. A typical avalanche size between two subsequent clogs corresponds to a handful of grains. A tomogram was recorded of each clogged configuration. The vertical cross sections of two example tomograms are shown in Fig. 4.4. As we see that the clogs are not uniform, the figure shows two cases with a typical high and shallow dome. During the avalanches the grains sink towards the orifice in a cone shaped region (indicated with red lines in Fig. 4.4), while other grains in a stagnant zone near the silo wall do not move. The region with the strongest shear is nicely visualized by the shear induced orientational ordering of the grains, see the region with pink color in Fig. 4.1(b), and it is also visible by the grain orientations in Fig. 4.4. Grains in the stagnant zone (outside of the shear zone) are mostly horizontal, as they keep the orientation that they obtained during the filling procedure, similarly to earlier observations [33]. Our goal is

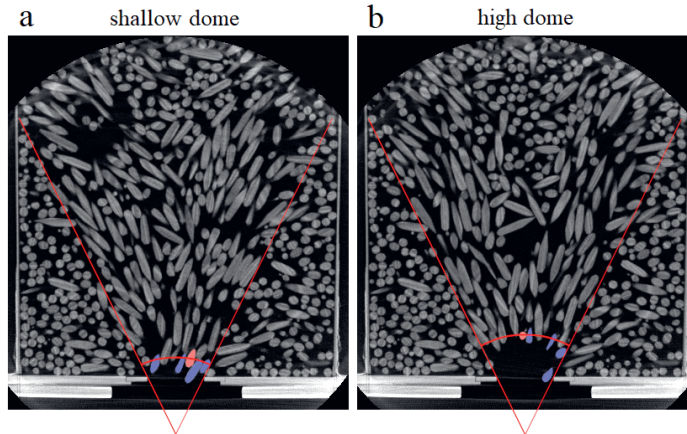


**Figure 4.4:** Vertical cross sections of two clogged configurations of sharpened pegs, and illustration of the definition of the dome. Straight red lines indicate the cone of moving particles. Within this cone, the first 4 particles closest to the cone apex are marked blue; the 5<sup>th</sup> closest, which is sitting on the dome surface (red arc), is labeled light red. In the actual analysis, the 5<sup>th</sup> closest particle within the complete 3D cone is selected, not just in a 2D cross section as in this illustration.

to determine the particle orientations in the sheared region, and compare the statistics in the layer forming the dome and above. For this we need to define the approximate position of the dome for each tomogram. This is done by drawing a spherical cap centered around the cone apex, and going through the center of mass of the 5<sup>th</sup> closest

### 4.3. Results and Discussion

---

particle to the apex. In Fig. 4.4 particles No. 1-4 are colored blue, while particle No 5. is colored red. Using the 5<sup>th</sup> closest particle instead of the closest one reduces the fluctuations caused by the position of a single particle.

In order to identify the sheared region of our granular sample in the silo, we plot the map of the orientational order parameter in a vertical cross section of the silo (see Figs. 4.5(a,b)) by averaging the data in the azimuthal direction. As we see, orientational ordering is observed in a tilted region with a much larger order parameter for sharpened pegs than for corn seeds. This is similar to the observations in the split bottom shear cell described above. In the following, we analyze particle orientations in the regions in between the dashed lines in Figs. 4.5(a,b), up to about 10 cm above the orifice. First we plot the distributions of the orientation angle  $\theta$  measured with respect to the streamlines (see Figs. 4.5(d,e)). Here the streamlines are approximated by straight lines converging towards the apex of the cone corresponding to the flowing region as shown in Fig. 4.5(c). As we see in Figs. 4.5(d,e), the grains are oriented nearly parallel to the flow with a slight majority of tip up particles (54%) for corn and a practically equal fraction of tip up/down particles for sharpened pegs. The related polar order parameters are 0.06 and 0.003, respectively. For the case of corn, the asymmetry in the silo is similar to the asymmetry observed in the inner zone of the shear cell (55% : 45%, see Fig. 4.3(h)). But for the case of sharpened pegs, the global symmetric distribution observed in the silo is very different from the asymmetric one (58% : 42%, Fig. 4.3(g)) observed in the shear cell. This difference can be related to the fact, that the time period of rotation of a more elongated particle in a shear flow is larger. In the shear cell we ensured a stationary state with extensive shearing of the sample, but in the silo the sample is subjected to a limited shear deformation, which is not enough to reach a stationary state for the relatively long pegs.

We continue the analysis by looking for differences between the orifice region (where the clog occurs) and above. Namely, it might be expected that clogs are formed with a higher probability with “wedge down” particles. For this analysis we chose a different visualization of the data characterizing the orientation of the long axis of the particles: in Figs. 4.5(f,g), we show the value of the component parallel to the streamlines as a function of the particles distance from the dome, which forms the clog above the silo outlet. The component parallel to the streamlines is positive when the sharper end of the particle points away from the orifice and it is negative when it points towards the orifice. In Figs. 4.5(f) and (g) we see two clouds of points, one on the positive and one on the negative side of the graph. These clouds indicate the orientational ordering of the grains, and show stronger ordering for sharpened pegs than for corn seeds. The balance between the two clouds is visualized by the red data curve. Red data points above zero mean more particles pointing up (i.e. away from the orifice) than down.

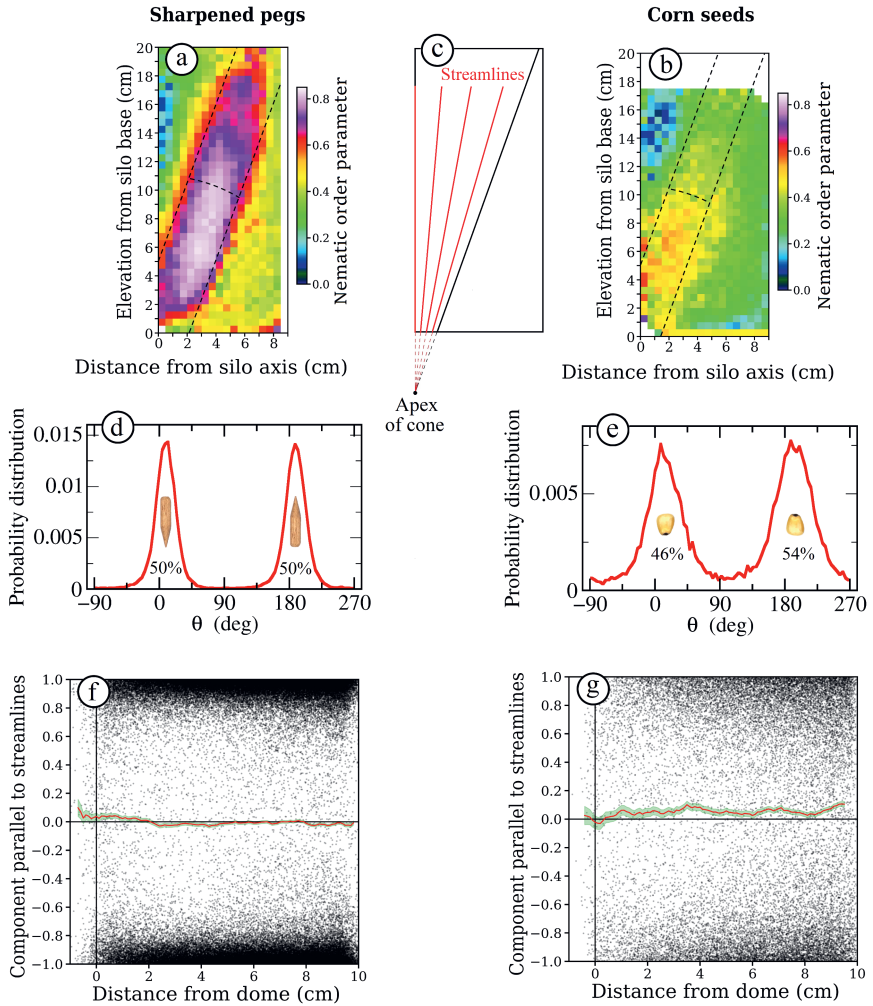


**Figure 4.5:** Grain orientation data for sharpened pegs and corn seeds in the silo. Panels (a) and (b) show the order parameter maps, panel (c) shows the approximate streamlines. Half of the silo cross section is shown, with the center at the left edge of the image and the outer wall at the right edge. Panels (d) and (e) show the orientation distribution of the particles' long axis with respect to the streamlines, while panels (f) and (g) quantify the orientations by showing the value of the component parallel to the streamlines as a function of the distance from the dome which forms the clog above the silo outlet. The red line corresponds to the average of the data, while the green band indicates its uncertainty. The horizontal black line at 0 indicates that the particle is perpendicular to the streamline.

#### 4.4. Conclusion

---

As we see, for corn seeds the balance is slightly positive above the dome, but is around zero near the dome. This means that above the dome the wedge shaped corn seeds slightly favour the “sharp end up” configuration against the “sharp end down” configuration (in accordance with the energy argument described above), while in the dome, where the clog is formed, this difference seems to disappear. This is coherent with the argument that a dome forms more easily with wedge shaped particles pointing down. Note that the distributions shown represent the clogged state. When the system is in free flow, the distributions of the polar axes in the orifice region may differ.

The scenario is different for the case of sharpened pegs. There, the balance is practically zero in the upper region, meaning equal number of “sharp end up” and “sharp end down” particles. In the lower part (including the dome region) however, the balance becomes slightly positive, meaning slightly more “sharp end up” particles. Such distribution of particle orientations is consistent with our previous observations in the same silo on similar pegs without sharpened ends [34]. Namely, the pegs with elongation  $L/d = 5$  gradually developed orientational ordering during sinking in the silo, and the orientation distribution did not fully reach the distribution observed in stationary shear flow even in their lowest position near the silo exit. The red curve in Fig. 4.5(f) thus indicates two things: (i) due to the limited amount of shear in the course of silo flow, the sharpened pegs only start exploring the energetically more favoured “sharp end up” configuration in the lower part of the silo, (ii) since their fat side has a cylindrical shape (i.e it is not a wedge) the tendency to form a clogging arch rather with a “sharp end down” is not observed. Altogether, although the difference between the case of sharpened pegs and corn seeds is small, it indicates that the particle configurations and the mechanism for clog formation is different for these two types of particles.

#### 4.4 Conclusion

Our experimental observations on the flow of asymmetric elongated particles in a sheared system and during silo discharge show, that for both corn grains and pegs sharpened at one end one can detect the effect of the particle asymmetry on the shear induced orientational ordering process. Namely, elongated grains in general rotate in a shear flow with modulated angular velocity: faster rotation when perpendicular to the flow and slowing down when their orientation is near the flow direction. This leads to orientational ordering, as grains spend more time with their long axis oriented near the flow direction. This general behavior of elongated grains is slightly modified for the asymmetric particles investigated here: if their plane of rotation is not perpendicular to gravity, they are expected to spend more time in the “sharper end up” than in the



“sharper end down” configuration, so the orientational distribution is expected to become asymmetric. We experimentally detect this asymmetry in the particle orientations in a cylindrical split bottom shear cell for both corn seeds and sharpened pegs. For the case of silo discharge, the asymmetry is detected in most of the sheared region for corn seeds, except in the vicinity of the orifice. This indicates, that for wedge shaped particles clog formation is slightly enhanced when more “sharper end down” particles are present in the region where the clogging arch is formed. For sharpened pegs the asymmetry only appears in the orifice region with a small amplitude, indicating that (i) for longer grains, larger shear deformation is needed to reach the stationary state and (ii) for sharpened pegs (which are not true wedges, but have a cylindrical part at the thick side) clog formation does not seem to be influenced by the particles asymmetry. Future numerical simulations might help to get more insight into the processes of grain rotation leading to the asymmetric orientational distributions observed in our experiments as well as in the clogging process of asymmetric grains.

---

## BIBLIOGRAPHY

- [1] Anki-Reddy, K., Kumaran, V., and Talbot, J. “Orientational ordering in sheared inelastic dumbbells”. In: *Physical Review E* **80** (2009), 031304.
- [2] Campbell, C. “Elastic granular flows of ellipsoidal particles”. In: *Physics of Fluids* **23** (2011), 013306.
- [3] Guo, Y. et al. “A numerical study of granular shear flows of rod-like particles using the discrete element method”. In: *Journal of Fluid Mechanics* **713** (2012), 1–26.
- [4] Nadler, B., Guillard, F., and Einav, I. “Kinematic Model of Transient Shape-Induced Anisotropy in Dense Granular Flow”. In: *Physical Review Letters* **120** (2018), 198003.
- [5] Börzsönyi, T. et al. “Orientational Order and Alignment of Elongated Particles Induced by Shear”. In: *Physical Review Letters* **108** (2012), 228302.
- [6] Börzsönyi, T. et al. “Shear-induced alignment and dynamics of elongated granular particles”. In: *Physical Review E* **86** (2012), 051304.
- [7] Börzsönyi, T. and Stannarius, R. “Granular materials composed of shape-anisotropic grains”. In: *Soft Matter* **9** (2013), 7401–7418.
- [8] Wegner, S. et al. “Alignment and dynamics of elongated cylinders under shear”. In: *Soft Matter* **8** (2012), 10950.
- [9] Guillard, F., Marks, B., and Einav, I. “Dynamic X-ray radiography reveals particle size and shape orientation fields during granular flow”. In: *Scientific Reports* **7** (2017), 8155.

- 
- [10] Marschall, T. and Teitel, S. “Athermal shearing of frictionless cross-shaped particles of varying aspect ratio”. In: *Granular Matter* **22** (2020), 4.
- [11] Botton, M. et al. “Quasistatic rheology and microstructural description of sheared granular materials composed of platy particles”. In: *Physical Review E* **87** (2013), 032206.
- [12] Botton, M. et al. “Particle alignment and clustering in sheared granular materials composed of platy particles”. In: *European Physical Journal E* **37** (2014), 116.
- [13] Nagy, D. et al. “Flow and rheology of frictional elongated grains”. In: *New Journal of Physics* **22** (2020), 073008.
- [14] Hidalgo, R. C. et al. “Rheological response of nonspherical granular flows down an incline”. In: *Physical Review Fluids* **3** (2018), 074301.
- [15] Trulsson, M. “Rheology and shear jamming of frictional ellipses”. In: *Journal of Fluid Mechanics* **849** (2018), 718–740.
- [16] Nouguier-Lehon, C. “Effect of the grain elongation on the behaviour of granular materials in biaxial compression”. In: *Comptes Rendus Mécanique* **338** (2010), 587.
- [17] Szabó, B. et al. “Flow of anisometric particles in a quasi-2D hopper”. In: *Physical Review E* **97** (2018), 062904.
- [18] Escudero, F. et al. “Silo discharge: influence of the particle shape on the velocity profiles”. In: *EPJ Web of Conferences* **249** (2021), 03029.
- [19] Calderón, C. et al. “Correlations between flow rate parameters and the shape of the grains in a silo discharge”. In: *Powder Technology* **320** (2017), 43.
- [20] Reddy, A. et al. “Clogging phenomena in a system of asymmetric dumbbells”. In: *Journal of Statistical Mechanics: Theory and Experiment* (2021), 063201.
- [21] Tao, H. et al. “Discrete element method modeling of non-spherical granular flow in rectangular hopper”. In: *Chemical Engineering and Processing: Process Intensification* **49** (2010), 151.
- [22] Markauskas, D. and Kacianauskas, R. “Investigation of rice grain flow by multi-sphere particle model with rolling resistance”. In: *Granular Matter* **13** (2011), 143.
- [23] Cleary, P. W. “The effect of particle shape on hopper discharge”. In: *Second International Conference on CFD in the Minerals and Process Industries*. CSIRO. 1999, pp. 71–76.

## Bibliography

---

- [24] Cleary, P. and Sawley, M. “DEM modelling of industrial granular flows: 3D case studies and the effect of particle shape on hopper discharge”. In: *Applied Mathematical Modelling* **26** (2002), 89–111.
- [25] Liu, S. D. et al. “Flow characteristics and discharge rate of ellipsoidal particles in a flat bottom hopper”. In: *Powder Technology* **253** (2014), 70.
- [26] Li, J. et al. “Flow of sphero-disc particles in rectangular hoppers—a DEM and experimental comparison in 3D”. In: *Chemical Engineering Science* **59** (2004), 5917–5929.
- [27] Langston, P. A. et al. “Distinct element modelling of non-spherical frictionless particle flow”. In: *Chemical Engineering Science* **59** (2004), 425–435.
- [28] Ashour, A. et al. “Outflow and clogging of shape-anisotropic grains in hoppers with small apertures”. In: *Soft Matter* **13** (2017), 402–414.
- [29] González-Montellano, C. et al. “Validation and experimental calibration of 3D discrete element models for the simulation of the discharge flow in silos”. In: *Chemical Engineering Science* **66** (2011), 5116–5126.
- [30] Fenistein, D., van de Meent, J., and van Hecke, M. “Universal and Wide Shear Zones in Granular Bulk Flow”. In: *Physical Review Letters* **92** (2004), 094301.
- [31] De Gennes, P.-G. and Prost, J. *The physics of liquid crystals*. 83. Oxford university press, 1993.
- [32] Bates, M. A. and Luckhurst, G. R. “Biaxial nematic phases and V-shaped molecules: A Monte Carlo simulation study”. In: *Physical Review E* **72** (2005), 051702.
- [33] Hidalgo, R. C. et al. “Granular packings of elongated faceted particles deposited under gravity”. In: *Journal of Statistical Mechanics: Theory and Experiment* **2010** (2010), P06025.
- [34] Börzsönyi, T. et al. “Packing, alignment and flow of shape-anisotropic grains in a 3D silo experiment”. In: *New Journal of Physics* **18** (2016), 093017.



## Elliptical grains in a two-dimensional silo discharged with a conveyor belt

*In this chapter, the flow of elliptical particles out of a 2-dimensional silo when extracted with a conveyor belt is analyzed experimentally. The conveyor belt placed directly below the silo outlet reduces the flow rate, increases the size of the stagnant zone, and it has a very strong influence on the relative velocity fluctuations as they strongly increase everywhere in the silo with decreasing belt speed. In other words, instead of slower but smooth flow, flow reduction by belt leads to intermittent flow. Interestingly, we show that this intermittency correlates with a strong reduction of the orientational order of the particles at the orifice region. Moreover, we observe that the average orientation of the grains passing through the outlet is modified when they are extracted with the belt, a feature that becomes more evident for large orifices.*

**Bo Fan, Iker Zuriguel, Joshua Dijkstra, Jasper van der Gucht and Tamás Börzsönyi**

“Elongated particles discharged with a conveyor belt in a two-dimensional silo”

## 5.1 Introduction

Flow of a granulate out of a container or a silo is widely used in various industrial applications. A very useful feature of such flows is that the flow rate does not depend on the filling height of the silo, as it was already pointed out in pioneering works long ago [1, 2]. For large enough orifices there is a clear relation between the size of the orifice and the flow rate [1, 3, 4]. Thus, one can tune the flow rate by simply changing the orifice size. Unfortunately, this only works for relatively large flow rates, because below a certain orifice size the system clogs [5–7]. In industrial applications, however, one often needs small flow rates. There are several ways to overcome this problem, e.g. reducing the probability of clogging by vibration [8–11], by placing an obstacle above the orifice to prevent arch formation [12–14], or simply using a conveyor system (screw conveyor, or conveyor belt) placed directly below the silo outlet so that it limits the flow rate [15]. Then, one can use a large orifice (clogging is avoided) and the flow rate is set by the speed of the conveyor system.

In this chapter, we investigate how the presence of a conveyor belt influences the flow field, packing fraction, and grain orientation during the discharge of a 2-dimensional (2D) silo filled with ellipses. In previous works [16–18], for the case of spheres, it was proved that the belt importantly altered these different fields. In particular, a transition was shown from belt controlled flow to outlet size controlled flow (by gravity) as the belt velocity increased and the orifice reduced. The advantage of 2D model silos is that one can obtain detailed microscopic information about the flow and clogging of the granulate by using high speed digital imaging [19]. Such access to the internal flow structure is more difficult to obtain in 3-dimensional systems, where one has to use more sophisticated detection techniques (e.g. X-ray tomography) [20–22].

The majority of previous experimental or numerical works focusing on microscopic details of silo discharge used spherical (3D) or disk shaped (2D) particles. Some studies provided data for shape-anisotropic grains [20, 21, 23–26]. For elongated particles, orientational ordering develops in the sheared regions [20], where the average alignment of the particles long axis is nearly parallel to the flow direction, similarly to the observations in other shear flows [27, 28]. For such grains, the flow field in the silo showed stronger funneling and larger velocity fluctuations [20, 21, 23–26] and the probability of clog formation was also higher [29, 30] than for spherical grains. Therefore, as a natural extension of these works, in this study we focus on determining the influence of the conveyor belt extraction system on the flow of elliptical grains, with special focus on grain orientation, ordering and the flow fields.

### 5.2 Experimental setup

The experimental setup (Fig. 5.1 (a)) and procedures are the same implemented in previous works using spherical particles [16–18]. The system comprises a two-dimensional (2D) silo, a removable conveyor belt below the silo outlet and a high-speed camera focusing on the lower part of the silo above the orifice (the rectangle area drawn with dashed lines). The silo is formed by two parallel glass plates with a height of 1600 mm, a width of 700 mm and a thickness of 6 mm, between which there are two vertical 4 mm thick and 40 mm wide aluminum bars at both sides with a distance of 520 mm. The particles filled in the silo are elliptical cylinders (see Fig. 5.1(b)) of 10 mm in length, 5 mm in width, and 3 mm in thickness. Therefore, a single layer can fit in the 4 mm gap between the two glass plates. In addition, the width  $D$  of the silo outlet at the bottom can be adjusted with two 11 mm wide horizontal sliders. Lastly, a conveyor belt with a width of 105 mm is mounted below the silo outlet with a gap of approximately 13 mm between the glass plate edge and the conveyor's top surface to control the outflow rate. For comparison, we have also implemented experiments in which the conveyor belt is not mounted, hence obtaining the so called free-flow case. In Fig. 5.1 (c)-(e), photos from the experiments with a 40 mm orifice are presented for free flow and flow-rate-controlled flow with a conveyor belt speed at 5.1 mm/s and 55.7 mm/s. We note that when using identical spheres hexagonal ordering of the grains was observed (see Fig. 1(b) in Ref. [18]), which is not present here for the case of elliptic particles. In this work, four belt speeds were used: 1.5 mm/s, 5.1 mm/s, 10.5 mm/s, 55.7 mm/s. Note that 1.5 mm/s corresponds to the so-called quasi-static regime in Refs. [16–18].

The silo was filled from the top with elliptical particles up to a height of about 40 cm. To image the flow, we used a high-speed camera at a frequency of either 1000 Hz (for free flow) or 125 Hz (for flow-rate-controlled flow) to capture the movement of grains in a rectangular area (marked with a dashed-line in Fig. 5.1 (a)) while the grains are discharged through an outlet of  $D = 40$  mm, 50 mm, 60 mm or 80 mm. The flow field, grain orientations and packing fraction were determined by digital image analysis, and the flow rate was measured by counting the number of grains passing through the orifice line.

### 5.3 Results and discussion

The flow rate is shown as a function of time for the case of free flow in Fig. 5.2(e) and for flow-rate-controlled cases with different belt speeds in Figs. 5.2(a-d). Clearly, the flow rate is considerably reduced by the presence of the belt while the fluctuations seem



## 5. Elliptical grains in a two-dimensional silo discharged with a conveyor belt

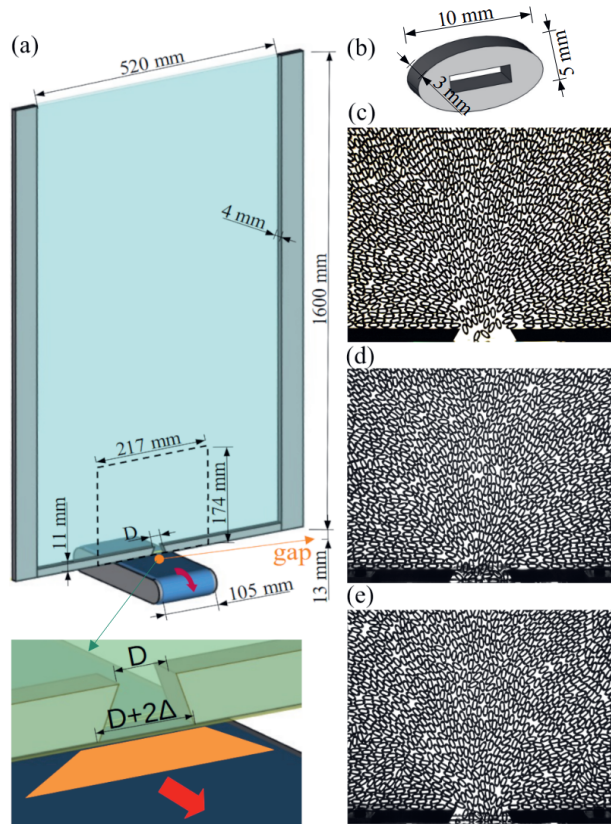


**Figure 5.1:** Experimental setup. (a) A sketch of the experimental setup. The rectangle area formed by the dashed lines is the camera's scope. For belt controlled silo discharge the flow expands below the orifice due to the trapezoid shape of the outlet characterized by the parameter  $\Delta = 5.7$  mm and the non-zero gap (13 mm) between the bottom of the silo walls and the belt. On the right column, (b) sketch of the elliptical particle, photos of (c) the free flow discharge (without the belt below the outlet), and flow-rate-controlled flow with belt speeds of (d) 5.1 mm/s and (e) 55.7 mm/s. The orifice size in the photos is the same, which is 40 mm.

### 5.3. Results and discussion

to decrease only moderately. In order to better quantify this, we represent the average flow rate as a function of belt speed (Fig. 5.3(a)) and the orifice size (Fig. 5.3(b)). The results obtained reveal the same main features reported for the case of spheres (see Fig. 2 of Ref. [18]); i.e. i) the flow rate grows with the belt speed in a non-linear manner (Fig. 5.3(a)) with deviations from linearity being more important as the belt speed ( $v_b$ ) increases; ii) the flow rate is strongly dependent on the belt velocity, and even for the fastest case, is far from approaching the values of the free flow (see inset of Fig. 5.3(b)). Concerning the fluctuations, their characterization by means of the standard deviation (Fig. 5.3(c)) evidences an increase with the outlet size and the belt speed. However, when normalized by the average value of the flow rate (Fig. 5.3(d)), the tendency is inverted, and the rescaled value reduces with both, the outlet size and the belt speed. As expected, when the grains are discharged in a quasi-static manner ( $v_b = 1.5$  mm/s), the fluctuations become much larger than the average.

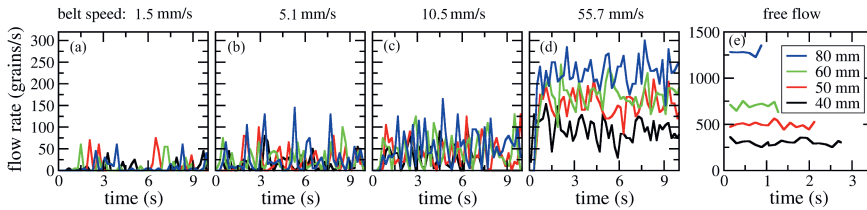


**Figure 5.2:** Flow rate evolution for different orifice sizes (40 mm, 50 mm, 60 mm and 80 mm) as indicated in the legend of panel (e). (a)-(d) Flow with a conveyor belt speed of 1.5 mm/s, 5.1 mm/s, 10.5 mm/s, and 55.7 mm/s respectively, (e) free flow.

After characterizing the general features of the flow rate, we now turn to investigate the spatial structure of the flow field. In Fig. 5.4 we present the flowing region (by overlapped images), the packing fraction, order parameter and the relative velocity fluctuations for free flow (top row) and for the quasi-static discharge ( $v_b = 1.5$  mm/s) in the rectangular area shown in Fig. 5.1. Orientational ordering is measured by the usual nematic order parameter  $S$ , which is defined as the average of  $2 \cos^2(\theta - \bar{\theta}) - 1$  in a certain area, where  $\theta$  is the orientation of individual particles and  $\bar{\theta}$  is the average orientation of the particles in the selected area.

As we see in the left column of Fig. 5.4, the stagnant zone on the two sides of the flowing region is considerably larger for the case of flow controlled by the conveyor belt than for free flow. Note that for correct comparison we constructed these 2 images by overlapping the snapshots obtained within a given time period in such a way that the number of grains leaving the silo was very similar (about 2300). For the case of flow with belt, those snapshots where nothing moved in the silo were not included.

## 5. Elliptical grains in a two-dimensional silo discharged with a conveyor belt

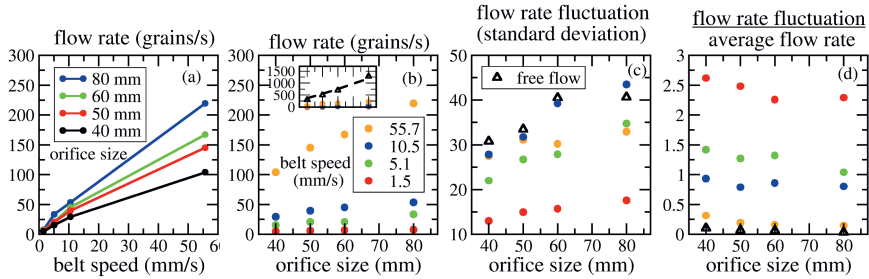


**Figure 5.3:** (a) Time averaged flow rate as a function of belt speed (different colors correspond to different outlet sizes). (b) Time averaged flow rate as a function of orifice size. In the inset the flow rate of the free-flow case (open triangular symbols) is compared with the flow-rate-controlled cases (colored solid circular symbols). (c) Flow rate fluctuation characterized by the standard deviation of the flow rate data shown in Fig. 5.2. (d) Relative flow rate fluctuation defined as the ratio of the standard deviation to the average flow rate.

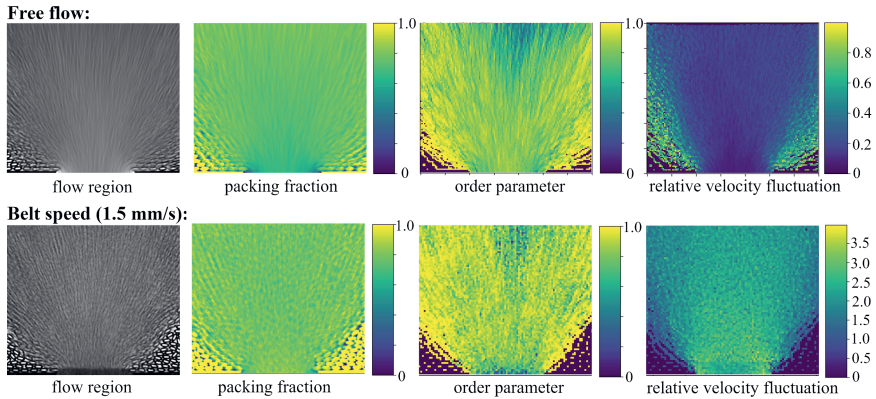


**Figure 5.4:** Flow field maps from left to right: flow region (super-positioned image to show the flowing particles), packing fraction, order parameter, and relative velocity fluctuation. The relative velocity fluctuation is defined as the ratio of the velocity standard deviation to the average velocity. The orifice size is always 80 mm in these maps.

The plots for the packing fraction and orientational order parameter (second and third columns of Fig. 5.4) both show that the presence of the conveyor belt influences these quantities mostly in the orifice region. For free flow there is a region above the orifice in which the grains accelerate towards the orifice and consequently the packing fraction is smaller compared to other regions in the silo (more blue in the map). On the contrary, when we reduce the flow rate with the conveyor belt, the packing fraction in this region becomes large (yellow), reaching a value similar to what we observe elsewhere in the silo. Looking at the maps of the orientational order parameter, we see that in the outlet region (where the belt makes the packing denser) the order is decreased. As we will see later on, the shear induced orientational order (the grains above the orifice are typically aligned with their long axis towards the orifice) is destroyed by the belt, since the orientation of the grains changes in the orifice.

Finally, we investigate the relative velocity fluctuations. This quantity is defined as the standard deviation of the flow velocity divided by the average flow velocity and is presented in the last column of Fig. 5.4. Clearly, the relative velocity fluctuations get significantly increased when the grains are discharged with the belt, a phenomenon that occurs in the majority of the flowing region and not only at the orifice. This means that reducing the flow speed by the belt results in slower but more fluctuating flow all throughout the silo.

Despite this, since the influence of the conveyor belt on the other variables (such as packing fraction and order parameter) is mostly localized in the orifice region, we proceed to its characterization in the following. We study the profiles at the orifice of velocity, packing fraction, particle orientation and order parameter, first for the free-flow case, and then for the discharge with a conveyor belt.

#### 5.3.1 Free flow

In Fig. 5.5, we evidence that the vertical velocity (Fig. 5.5(a) and (f)) and the packing fraction profiles (Fig. 5.5(c) and (h)) of the elliptical particles show similar trends to those reported for spherical particles in Ref. [31]. In short, the vertical velocity (Fig. 5.5(a)) gets higher as the orifice size is increased, and the profiles of vertical velocity  $v_z$  show self-similarity (Fig. 5.5(f)), since the data nicely collapse when the horizontal coordinate is divided by the half size of the orifice ( $R$ ) and the vertical velocity is normalized by its maximum value at the center of the silo ( $v_c$ ). These collapsed datasets agree with the function of  $v_z/v_c = \sqrt{1 - (x/R)^2}$  which originates from the assumption of the existence of a parabolic free fall arch above the orifice [31].

The packing fraction (Fig. 5.5(c)) shows a similar trend to the vertical velocity: the packing is denser in the middle of the orifice than near the edge. Thus, there is a correlation between the velocity gradient (shear rate) and the packing, which is not

## 5. Elliptical grains in a two-dimensional silo discharged with a conveyor belt

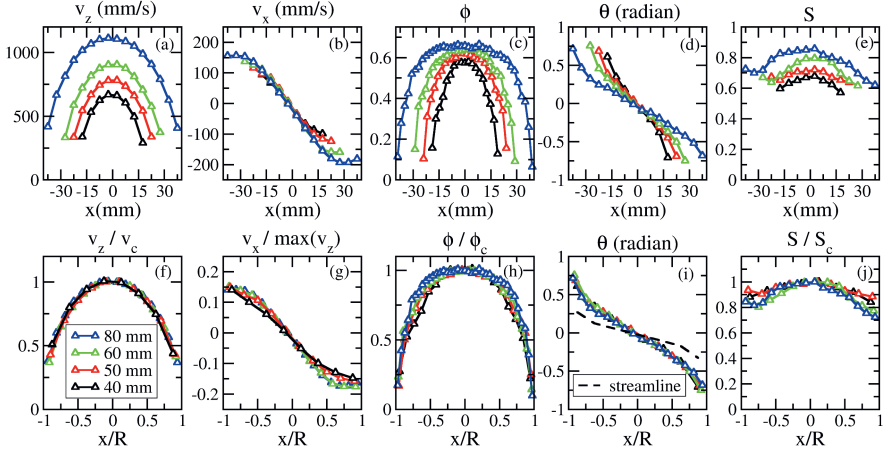


**Figure 5.5:** Profiles of different quantities at the orifice for the free flow case. (a)-(e) original data and (f)-(j) normalized data for vertical velocity  $v_z$ , horizontal velocity  $v_x$ , packing fraction  $\phi$ , average orientation  $\theta$  and order parameter  $S$ , respectively.  $x$  denoted on the  $x$  axis represents the position at the outlet line.  $R$  is a half of the corresponding orifice size  $D$ .  $v_c$ ,  $\phi_c$  and  $S_c$  are the values of vertical velocity, packing fraction and order parameter at the orifice center respectively. The orientation of the particle is defined as the angle between the major axis of the particle and the vertical direction. The dashed line in (i) shows the direction of the streamline at the orifice as a reference. Order parameter in (e) and (j) is a quantity measuring the extent of alignment of the particles, defined in the range between 0 and 1, corresponding to random orientation and perfect alignment, respectively. Different colors correspond to different orifice size as indicated in the legend of panel (f).

surprising as larger shear rate means more intensive collisions and thus the expansion of the material. In Fig. 5.6(a) we evidence this feature by representing the packing fraction as a function of shear rate. Interestingly, the curves obtained for different orifice sizes show the same trend and are near to each other, but they do not perfectly collapse. The packing fraction for the same shear rate is reduced when the outlet size decreases. Again, non-dimensionalizing the packing fraction curves shown in Fig. 5.5(c) as we did with the velocity profiles, the data approximately collapse to a single curve (see Fig. 5.5(h)), although not as precisely as the vertical velocity case. Again, we see slightly smaller packing fractions when the orifice size reduces.

Regarding the horizontal velocity, in Fig. 5.5(b) we observe that the particles move towards the orifice center. Noteworthy, the curves measured for different orifice sizes

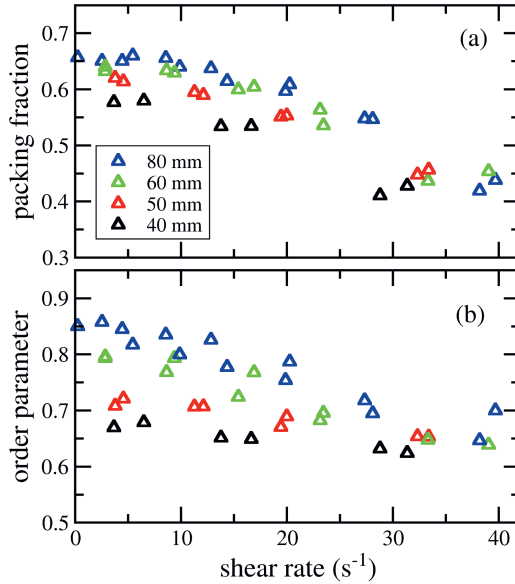


**Figure 5.6:** Free flow: (a) packing fraction, and (b) order parameter as a function of shear rate.

fall very close to each other, with the horizontal velocity increasing with the distance from the orifice center. Normalizing the horizontal velocity by the maximum of the vertical velocity also leads to a reasonably good collapse, and helps to visualize that the maximum horizontal velocity (at the edge of the orifice) is about 10 % of the maximum vertical velocity.

For a complete description of the flow of elliptical particles, in addition to their position, velocity and packing fraction, we also need to characterize their orientation, which is measured by the angle between the major axis of the ellipse and the vertical direction. Fig. 5.5(d) and (i) show the distribution of particle orientation at the outlet line in the original and normalized forms respectively. Once more, when the  $x$  axis is normalized by  $R$ , the curves of the average orientation at the outlet line overlap. We can compare the grain orientation and the flow direction (streamlines). The streamline curve is obtained from the direction of the average velocity and is shown with a dashed line in Fig. 5.5(i). The collapsed curves for the average grain orientation show a similar tendency as the streamline direction curve, but slightly deviates from it. This is in accordance with the observations on the direction of the elongated particles under shear

in which the long axis of the particle in average was found to be aligned near to the flow direction [27, 28, 32]. In the silo, this means that the orientation of the grains with respect to vertical is slightly more tilted than the flow lines themselves [20].

The order parameter (Fig. 5.5 (e)) is larger in the middle of the orifice than it is near the orifice edge. We can also easily derive from Fig. 5.5(a) that the shear rate in the middle is lower than that near the orifice edge. Similarly to the packing fraction, the order parameter correlates with the shear rate: larger shear rate leads to decreased order parameter, as we see in Fig. 5.6(b). This tendency is also consistent with previous observations in shear flows [27, 28]. Thus, more intensive collisions lead to expansion of the material and decreased orientational ordering. Again, Fig. 5.5(j) shows that similarly to what occurs with the vertical velocity, a rescaling of the horizontal coordinate by  $R$  and the order parameter by its maximum value measured in the center of the silo ( $S_c$ ), leads to a reasonably good collapse of the data.

In summary, the results of this section corroborate that, as it occurs for spheres, in the free discharge of elliptical particles the outlet size imposes a characteristic length scale in the system. This scaling extends to quantities never explored before with the precision reached here, such as the particle orientation and the order parameter.

### 5.3.2 Comparison of free-flow with the flow-rate-controlled case

#### Vertical velocity and packing fraction

After the analysis of the free discharges we now compare these results with the conveyor belt discharges. First, we analyze the vertical velocity at the outlet line. The profiles for different orifice sizes (from left to right: 40 mm, 50 mm, 60 mm and 80 mm) are plotted in Fig. 5.7 where we show results for the free-flow case (top row), and the flow-rate-controlled cases with different belt speeds, both in physical units (middle row) and in normalized form (bottom row).

As expected, for all orifices the vertical velocity rises as the belt speed grows (see middle row). More counterintuitively, we observe that for the highest belt speed (orange curves), the mean vertical velocity at the outlet reduces as the orifice size enlarges. This behavior also occurs for the other belt speeds as it becomes evident in Fig. 5.9 where we represented, for each belt speed, the mean vertical velocity normalized by the value it takes for the largest orifice (80 mm). Remarkably, the reduction of the vertical velocity with the outlet size contrasts the increasing trend observed for the free-flow case, but is in good agreement with the results reported for spheres [18]. The reason given in that work is based on mass conservation and the fact that flow expands after crossing the orifice line, i.e. the belt removes a wider band of grains than the orifice size, and the relative strength of this effect is larger for a smaller orifice. The reason for

### 5.3. Results and discussion

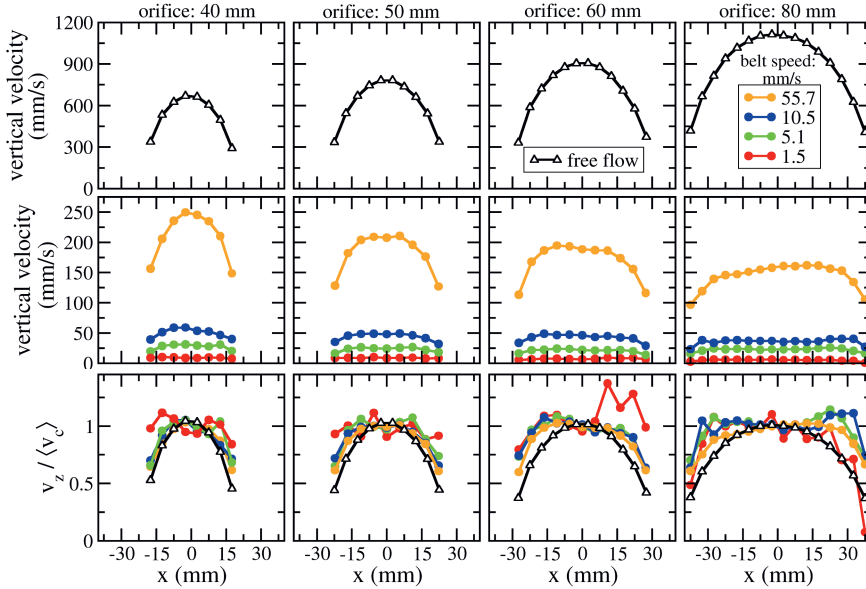


**Figure 5.7:** Vertical velocity at the orifice for different orifice sizes (from left to right: 40 mm, 50 mm, 60 mm and 80 mm). Top row: black lines with open triangular symbols represent the case of free flow. Middle row: colored lines with solid circular symbols represent the cases of flow-rate-controlled flow with different conveyor belt speeds (1.5 mm/s, 5.1 mm/s, 10.5 mm/s, 55.7 mm/s) as indicated in the legend of the top right panel. Bottom row: vertical velocity normalized by the central mean velocity  $\langle v_c \rangle$ .

the expansion below the orifice is twofold: (i) the trapezoid shape of the region below the orifice line and (ii) the gap between the bottom of the silo wall and the belt (see the enlarged orifice region at the bottom of Fig. 5.1(a)).

By normalizing the vertical velocity with the maximum value (developed in the middle region of the orifice) we get the curves presented in the bottom row of Fig. 5.7. As it could be envisaged from the profiles reported in the medium row, the collapse is not good at all because the curves flatten as the orifice enlarges. We also note that the normalized vertical velocity profiles become increasingly noisy with decreasing belt speed. This behavior is attributed to the augment of the relative velocity fluctuations when reducing belt speed described before.

The packing fraction curves at the orifice line for free flow and the belt extraction



## 5. Elliptical grains in a two-dimensional silo discharged with a conveyor belt

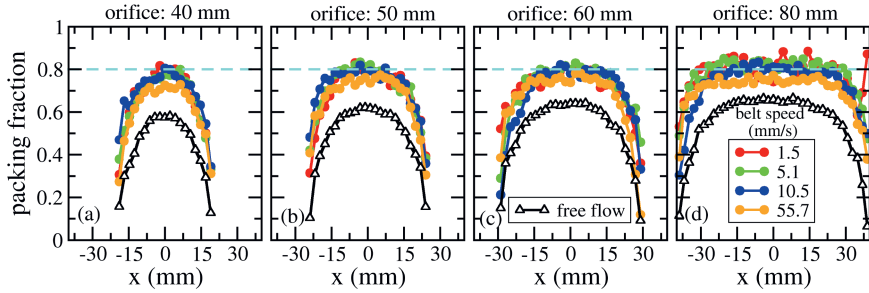


**Figure 5.8:** Packing fraction at the orifice for different orifice sizes (from left to right: 40 mm, 50 mm, 60 mm and 80 mm). The dashed line is a guide at the packing fraction of 0.8. Black lines with open triangular symbols represent the case of free flow. Colored lines with solid circular symbols represent the cases of flow-rate-controlled flow with different conveyor belt speeds (1.5 mm/s, 5.1 mm/s, 10.5 mm/s, 55.7 mm/s) as indicated in the legend of panel (d).

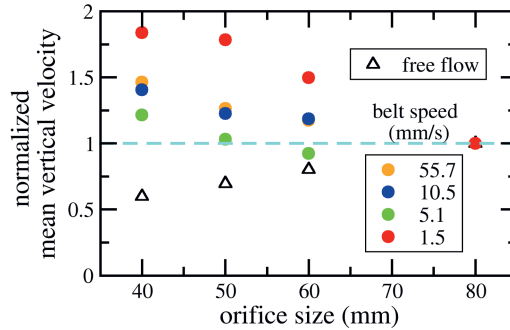


**Figure 5.9:** Normalized mean vertical velocity as a function of orifice size. The average vertical velocity values are normalized with the corresponding value for the orifice of 80 mm. Open triangles represent the case of free flow. Colored solid circles represent the flow-rate-controlled cases as indicated in the legend. The dashed line is a guide at the normalized value of 1.

system are compared in Fig. 5.8. The first thing to note is that decreasing belt speed leads to higher packing fraction as it was already reported for spheres [18]. In the same way, we find increasing packing fractions with enlarging the orifice sizes (see the relative position of the colored curves to the dashed cyan guide line). This is in accordance with the above described observation of decreasing flow velocity with increasing orifice size (Fig. 5.7, middle row). Although the noisy nature of the velocity curves (see bottom row of Fig. 5.7) does not allow a meaningful calculation of the shear rate, the increasing trend of the packing fractions with decreasing belt velocity suggests that packing fraction increases with decreasing shear rate, just like for the free flow case (Fig. 5.6(a)). At this stage it should be recalled that, in the belt discharges, the flow becomes increasingly intermittent with decreasing belt speed. Therefore, as the packing fraction curves contain data from both flowing and arrested configurations, the smaller the belt velocity, the higher the number of times in which the flow is arrested that are used to compute the time averaged packing fraction profiles. Accordingly, the average packing fraction values obtained increase as the belt velocity reduces.

#### **Orientation and order parameter**

Next, in Fig. 5.10 we present the profiles at the outlet of i) the average orientation, ii) the horizontal velocity and iii) the order parameter. As for the other quantities, we represent results for different orifice sizes and for both, free-flow and several flow-rate-controlled scenarios. Concerning the average orientation of the grains (top row), when the orifice is relatively small (40 mm) we observe similar behavior in the belt discharged system than in the free flow case: the average orientation decreases more or less linearly as  $x$  increases, taking positive values when  $x < 0$  and negative values when  $x > 0$ . This implies that in average grains point towards the center of the orifice. However, as the orifice enlarges, this trend is altered and the differences among the belt discharges and the free case become increasingly larger. The most important difference is observed for  $D = 80$  mm, where for the belt controlled case, the average orientation of the grains passing through the orifice is rather vertical, or even slightly pointing towards the two edges. This could be attributed to the expansion of the flow below the orifice explained above. The average grain alignment is sketched in the presence of the belt for small, middle and large orifices in Figs. 5.11(a), (b) and (c), respectively. In line with this, the profiles of the horizontal velocity (Fig. 5.10, middle row) reveal that while for the free flow case the grains at the orifice line move towards the center, for the belt discharges they do the opposite, i.e. move towards the edges. Again, this result corroborates the diverging nature of the flow below the orifice line.

Additionally, the curves of the average particle orientation (Fig. 5.10, top row) reveal that the flow-rate-controlled cases are not as smooth as the ones in the free-flow

## 5. Elliptical grains in a two-dimensional silo discharged with a conveyor belt

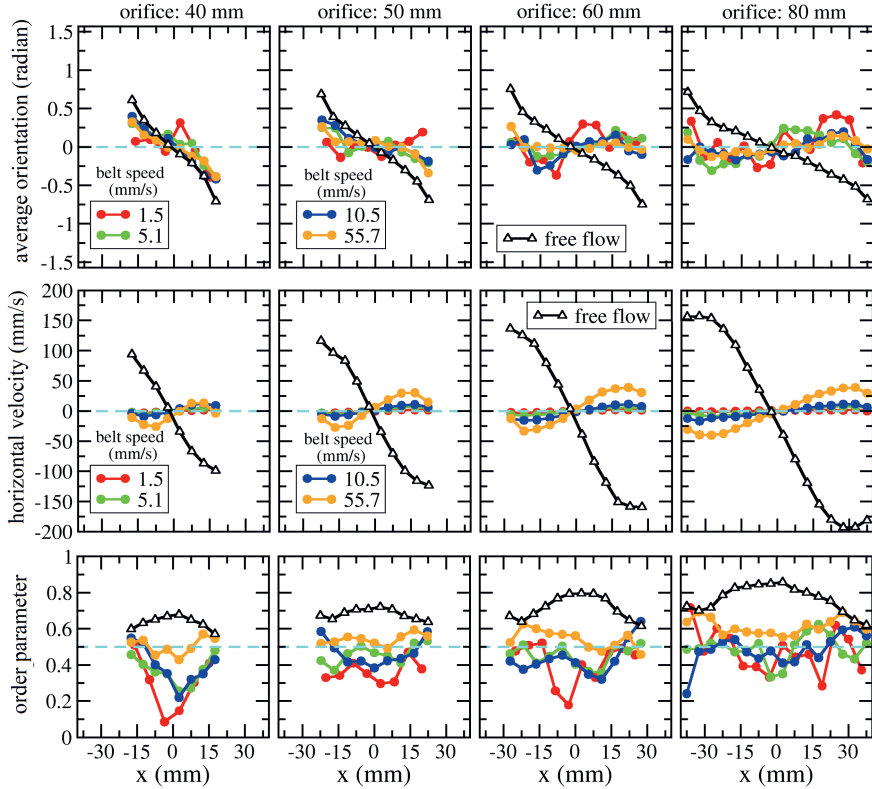


**Figure 5.10:** Top row: average particle orientation at the orifice. The orientation is defined as the angle in radian between the vertical line and the particle's major axis. Middle row: horizontal velocity at the orifice. Black lines with open triangular symbols represent the case of free flow. Colored lines with solid circular symbols represent the cases of flow-rate-controlled flow with different conveyor belt speeds (1.5 mm/s, 5.1 mm/s, 10.5 mm/s, 55.7 mm/s) as indicated in the legend. Bottom row: Orientational order parameter at the orifice. The dashed line is a guide at 0.5 that can be taken as a reference to visualize the profiles evolution as the orifice size increases.

## 5.4. Summary

---

case, and their smoothness gets improved once the belt speed reaches the highest value (orange curves). The higher noise on the orientation profile for lower belt speeds is related to the intermittent nature of the flow. When the flow stops, grain orientations are perturbed.

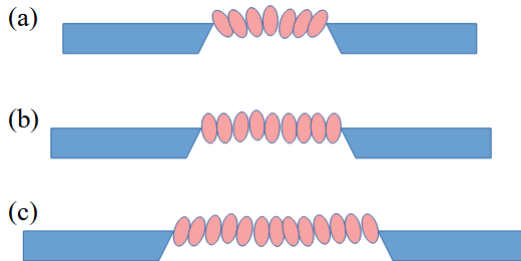


**Figure 5.11:** Diagram of configurations of the particles' orientation at the orifice for the flow-rate-controlled case with increasing the orifice size from (a) to (c).

Regarding the order parameter (bottom row in Fig. 5.10), we globally find lower values for the case of belt controlled flows than for the free flow, indicating that the presence of the belt destroys the orientational order. Intriguingly, the curves of the free-flow case have a convex shape for all the orifice sizes, with the largest order parameter in the middle of the orifice, while the ones for the flow-rate-controlled cases – especially for low belt speed – have a dip in the middle. We attribute this feature to the following behavior. In the middle of the orifice the average orientation of the particles is vertical for both free flow and belt controlled flow. However, for the case with belt, when the system is arrested due to the intrinsic intermitencies of the flow, the grains tend to turn (left or right with equal probability). As a consequence, the order parameter reduces while the average orientation remains vertical. In this sense, the concavity of the order parameter curves can be seen as an indicator of the degree of flow intermitencies developed within the system.

## 5.4 Summary

Our results show that the presence of a conveyor belt strongly modifies the flow dynamics of elliptical grains inside the silo. We find that limiting the flow with the belt leads to a larger stagnant zone in the two sides of the silo. Decreasing the belt speed naturally leads to decreasing flow velocity in the silo, but the amplitude of velocity fluctuations decreases much more slowly than that of the average velocity. This means that the relative velocity fluctuations defined as the ratio of velocity fluctuations and

## 5. Elliptical grains in a two-dimensional silo discharged with a conveyor belt

---

average flow velocity are considerably increased in most parts of the silo when we are limiting the discharge with the belt. In other words, decreasing belt speed leads to fluctuating, intermittent flow instead of smooth but slower flow. This effect (already known for spheres) leads to *a priori* unexpected behavior of the order parameter, which can be seen as an indicator of the degree of intermittencies developed in the system.

Another interesting feature introduced by the presence of the belt and the geometry of our system is the lateral spreading of the grains below the orifice. This behavior was also reported for spherical particles and can be clearly detected looking at the profiles of horizontal velocities at the outlet: for free discharges, grains move towards the center of the orifice, while for discharges with the belt, grains move towards the edges. Interestingly, for the case of particles with anisotropic shape, the lateral spreading of the grains has a side effect that affects their average orientation: contrary to the alignment pointing towards the center of the orifice observed in the free discharge, in the presence of the belt the average orientation of the particles passing through the orifice is vertical or even slightly inclined towards the orifice edges.

---

## BIBLIOGRAPHY

- [1] Hagen, G. “Ueber die Bewegung des Wassers in engen cylindrischen Röhren”. In: *Annalen der Physik* **122** (1839), 423–442.
- [2] Tighe, B. P. and Sperl, M. “Pressure and motion of dry sand: translation of Hagen’s paper from 1852.” In: *Granular Matter* **9** (2007), 141–144.
- [3] Beverloo, W., Leniger, H., and van de Velde, J. “The flow of granular solids through orifices”. In: *Chemical Engineering Science* **15** (1961), 260–269.
- [4] Mankoc, C. et al. “The flow rate of granular materials through an orifice”. In: *Granular Matter* **9** (2007), 407–414.
- [5] Zuriguel, I. et al. “Jamming during the discharge of granular matter from a silo”. In: *Physical Review E* **71** (2005), 051303.
- [6] Thomas, C. C. and Durian, D. J. “Geometry dependence of the clogging transition in tilted hoppers”. In: *Physical Review E* **87** (2013), 052201.
- [7] Thomas, C. C. and Durian, D. J. “Fraction of Clogging Configurations Sampled by Granular Hopper Flow”. In: *Physical Review Letters* **114** (2015), 178001.
- [8] Pacheco-Martinez, H., Gerner, H. J. van, and Ruíz-Suarez, J. C. “Storage and discharge of a granular fluid”. In: *Physical Review E* **77** (2008), 021303.
- [9] Mankoc, C. et al. “Role of vibrations in the jamming and unjamming of grains discharging from a silo”. In: *Physical Review E* **80** (2009), 011309.
- [10] Lozano, C. et al. “Breaking Arches with Vibrations: The Role of Defects”. In: *Physical Review Letters* **109** (2012), 068001.

- 
- [11] Zuriguel, I. et al. “Clogging transition of many-particle systems flowing through bottlenecks”. In: *Scientific Reports* **4** (2014), 7324.
- [12] Zuriguel, I. et al. “Silo Clogging Reduction by the Presence of an Obstacle”. In: *Physical Review Letters* **107** (2011), 278001.
- [13] Endo, K., Anki Reddy, K., and Katsuragi, H. “Obstacle-shape effect in a two-dimensional granular silo flow field”. In: *Physical Review Fluids* **2** (2017), 094302.
- [14] Vamsi Krishna Reddy, A. et al. “Granular silo flow of inelastic dumbbells: clogging and its reduction”. In: *Physical Review E* **98** (2018), 022904.
- [15] Fernandez, J. W., Cleary, P. W., and McBride, W. “Effect of screw design on hopper drawdown of spherical particles in a horizontal screw feeder”. In: *Chemical Engineering Science* **66** (2011), 5585–5601.
- [16] Gella, D., Zuriguel, I., and Maza, D. “Decoupling Geometrical and Kinematic Contributions to the Silo Clogging Process”. In: *Physical Review Letters* **121** (2018), 138001.
- [17] Gella, D., Zuriguel, I., and Ortín, J. “Multifractal Intermittency in Granular Flow through Bottlenecks”. In: *Physical Review Letters* **123** (2019), 218004.
- [18] Gella, D., Maza, D., and Zuriguel, I. “Granular flow in a silo discharged with a conveyor belt”. In: *Powder Technology* **360** (2020), 104–111.
- [19] Rubio-Largo, S. M. et al. “Disentangling the Free-Fall Arch Paradox in Silo Discharge”. In: *Physical Review Letters* **114** (2015), 238002.
- [20] Börzsönyi, T. et al. “Packing, alignment and flow of shape-anisotropic grains in a 3D silo experiment”. In: *New Journal of Physics* **18** (2016), 093017.
- [21] Guillard, F., Marks, B., and Einav, I. “Dynamic X-ray radiography reveals particle size and shape orientation fields during granular flow”. In: *Scientific Reports* **7** (2017), 8155.
- [22] Stannarius, R. et al. “High-speed x-ray tomography of silo discharge”. In: *New Journal of Physics* **21** (2019), 113054.
- [23] Cleary, P. and Sawley, M. “DEM modelling of industrial granular flows: 3D case studies and the effect of particle shape on hopper discharge”. In: *Applied Mathematical Modelling* **26** (2002), 89–111.
- [24] Tao, H. et al. “Discrete element method modeling of non-spherical granular flow in rectangular hopper”. In: *Chemical Engineering and Processing: Process Intensification* **49** (2010), 151–158.

## Bibliography

---

- [25] Liu, S. D. et al. “Flow characteristics and discharge rate of ellipsoidal particles in a flat bottom hopper”. In: *Powder Technology* **253** (2014), 70.
- [26] Szabó, B. et al. “Flow of anisometric particles in a quasi-2D hopper”. In: *Physical Review E* **97** (2018), 062904.
- [27] Börzsönyi, T. et al. “Orientational Order and Alignment of Elongated Particles Induced by Shear”. In: *Physical Review Letters* **108** (2012), 228302.
- [28] Börzsönyi, T. et al. “Shear-induced alignment and dynamics of elongated granular particles”. In: *Physical Review E* **86** (2012), 051304.
- [29] Ashour, A. et al. “Outflow and clogging of shape-anisotropic grains in hoppers with small apertures”. In: *Soft Matter* **13** (2017), 402–414.
- [30] Reddy, A. et al. “Clogging phenomena in a system of asymmetric dumbbells”. In: *Journal of Statistical Mechanics: Theory and Experiment* (2021), 063201.
- [31] Janda, A., Zuriguel, I., and Maza, D. “Flow Rate of Particles through Apertures Obtained from Self-Similar Density and Velocity Profiles”. In: *Physical Review Letters* **108** (2012), 248001.
- [32] Börzsönyi, T. and Stannarius, R. “Granular materials composed of shape-anisotropic grains”. In: *Soft Matter* **9** (2013), 7401–7418.





---

## Mixtures of hydrogel and airsoft beads in a 2D silo

*In this chapter, we study the outflow dynamics and clogging phenomena of mixtures of soft, elastic low-friction spherical grains and hard frictional spheres of similar size in a quasi-two-dimensional (2D) silo with narrow orifice at the bottom. Previous work has demonstrated the crucial influence of particle elasticity and friction on silo discharge. We show that the addition of small amounts, even as low as 5%, of hard grains to an ensemble of soft, low-friction grains already has significant consequences. We analyze the influence of hard frictional grains and compare outflow velocities and duration of non-permanent clogs for different compositions of the mixtures. Experimental results are compared with numerical simulations.*

This chapter is published as:

**Wang, J.\* , Fan, B.\* , Pongó, T.\* , Harth, K., Trittel, T., Stannarius, R., Illig, M., Börzsönyi, T., Cruz Hidalgo, R.**

“Silo discharge of mixtures of soft and rigid grains”

*Soft Matter* **17**, 4282–4295 (2021)

\*shared first authorship

## 6.1 Introduction

Storage of granular materials in silos and hoppers has an evident advantage over other containers for the processing of these materials in agriculture, chemical industry, construction industry and many other branches: Material is stowed into the silo through a top orifice, yet it can be withdrawn from the silo through an orifice at the bottom simply using gravity forces. No additional mechanical device is needed to maintain the outflow. However, one of the problems with these storage bins is congestion of the orifice, so-called clogging, which can occur even if the orifice diameter is much larger than the largest spatial extension of the individual grains. Particles can form stable arches (in 2D) or domes (in 3D) above the outlet and block further outflow. Intervention from outside is required to re-trigger discharge. From a physical point of view, this process is insufficiently understood even today, despite of hoppers being in use for millennia in human history. The flow of grains, even in the simplest form of hard monodisperse spheres, has retained many mysteries. Even the simplest problem of the outflow of monodisperse ensembles of spheres is still an active field of research. Through large enough orifices, such grains flow at constant rates given by geometrical and physical parameters. Flow rates have been derived from theoretical models [1–4] and the predictions were tested in numerous experiments (e.g. [4–9]). When the outlet diameter is small (less than about 5 particle diameters) [10–12], hard spheres tend to form clogs after some time at the orifice. These block further outflow until they are destroyed by shaking the container, by applying air flushes or by other mechanical disturbances. Spontaneous arch formation [13, 14], the preceding kinetics [15], as well as the inherent force distributions [16, 17] have been analyzed in the literature. Identical hard spheres are an idealized special system that has been considered in most of the experimental and theoretical studies. Since there are no principal differences between clogging of 2D and 3D silos, the former are often preferred in experiments because they offer the study of the inner dynamics and structure formation in the container with non-invasive observation methods.

Recently, it was found that soft particles with low friction differ considerably from common hard, frictional grains in their static and dynamic behavior in silos [18, 19]. The critical ratio  $\rho$  of orifice size and particle size below which clogging sets in is much smaller than for rigid grains. In addition, non-permanent, intermittent clogs are observed which spontaneously dissolve after some time. Such features are otherwise observed only in vibrated silos [20, 21], in colloidal systems [22–24] or in active matter [14]. In the earlier experiments with soft, slippery hydrogel grains, it remained unexplained whether the softness of the particles (elastic modulus of the order of a few dozen  $kPa$ ) or the low friction coefficient (in the order of 0.03), or a combination of both causes the quantitative differences to hard, frictional grains. Previous work on pure

monodisperse hydrogel sphere (HGS) ensembles [25] has identified the viscoelastic properties of these spheres as one important feature that causes qualitatively new features of the discharge through narrow orifices.

In practice, homogeneous granular ensembles are often the exception, even in industrial processes. One usually deals with materials that are non-uniform in size, shape, surface structure, or other properties. This motivated us to study mixtures of particles that differ in their elastic and frictional properties but are otherwise very similar. It turns out that an addition of even small portions of rigid particles to HGS ensembles has dramatic influence on silo discharge behavior.

This chapter describes an experimental and numerical study of the effects of doping soft HGS ensembles with hard, frictional particles of the same size and weight. Up to 10% of the latter will be added to the pure hydrogels, and three aspects will be focused on: (1) What is the influence of doping on the silo discharge characteristics?

(2) How is the concentration  $x_{h,f}$  of hard grains in the mixture represented in the composition of the blocking arches? This will allow us to extract the probabilities that hard or soft grains complete a blocking arch and cause clogging.

(3) Does the composition of the mixtures affect the outflow rates?

A quasi-two-dimensional setup with one layer of beads between two vertical glass plates is used. The mass of the discharged material is recorded by means of a balance beneath the orifice. Particle arrangements and flow inside the container are monitored by video imaging. In addition, numerical simulations are performed and compared to the experiment.

## 6.2 Experimental methods and materials

The setup consists of a flat container of 80 cm height, 40 cm and slightly more than 6 mm depth. In Fig. 6.1(a), vertical aluminum rails that support the front and rear glass plates hide 3 cm of the container interior on the left and right sides. Only 34 cm are visible. At the bottom, a rectangular opening of variable width can be adjusted with two horizontal sliders.

The container is filled with a mixture of soft, low-friction hydrogel spheres and hard frictional (HF) plastic airsoft ammunition. The concentration of HF plastic grains is low, typically 5% or 10%. We define the aspect ratio  $\rho$  as the quotient of the orifice  $D$  and the particle diameter  $d$ . In the present study, this ratio is in the range  $1.7 < \rho < 2.2$ . We note that at such small orifice sizes a pure sample of hard frictional grains would almost immediately clog. At large enough orifice sizes ( $\rho > 3$ ), the behaviour of our mixtures is practically identical to the pure hydrogel samples.

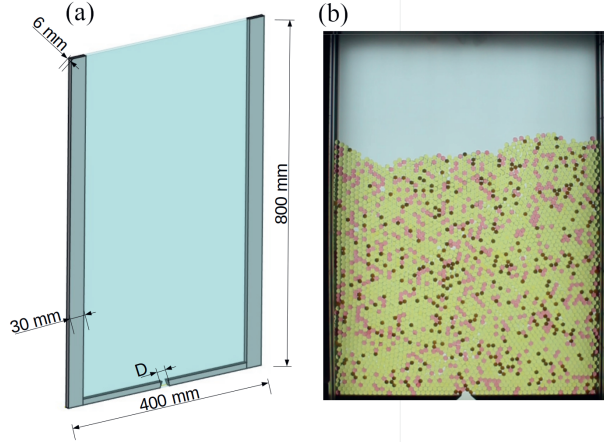


**Figure 6.1:** (a) Illustration of the experimental setup: two-dimensional silo. (b) Experimental photo: the two-dimensional silo filled with the mixture of 10% hard frictional spheres (HFS) and 90% hydrogel spheres (HGS). The orifice is 11 mm wide about two particle diameters.

Both species have densities of approximately  $1020 \text{ kg/m}^3$ . The 6 mm diameter airsoft beads were obtained from commercial providers. They are made from plastic, are perfectly monodisperse. The friction coefficient of the airsoft beads is 0.3. They are incompressible and can be considered rigid. The hydrogel spheres were obtained in dried state from a commercial provider (*Happy Store, Nanjing*). They were swollen in salted water with a NaCl concentration that determined the final radius of approximately 6.5 mm, with a polydispersity of about 3%. The mass of each hydrogel sphere is about 0.15 g. They have a friction coefficient one order of magnitude lower than the HF spheres, but the elastic modulus is of the order of only 50 kPa to 100 kPa. These particles are incompressible as well, but they deform slightly in the silo under the weight of the overlying grains. A rough estimate is that the Hertzian contacts between hydrogel spheres at the bottom of the container indent the grains by approximately 1.3 mm under the weight of the full silo.

The 2-dimensional ( $40 \times 80 \text{ cm}$ ) cell can accommodate about 10,000 grains corresponding to a weight of  $\approx 1.5 \text{ kg}$ . The cell is extended at the top with an additional 3-dimensional container, which can hold extra granular material.

## 6.3 Results and Discussion

### 6.3.1 Pressure characteristics

It was shown earlier that the low-frictional hydrogel shows an almost hydrostatic characteristics  $P(h)$  of the pressure  $P$  at the bottom of a quasi-2D container filled up to a height  $h$  [19]. In contrast, the hard, frictional grains exhibit Janssen effect - the typical saturation of the pressure [26]) at a fill height of several centimeters [19]. Fig 6.2 shows that the pressure characteristics of the pure hydrogel sample is changed significantly by addition of a small amount  $x_{hf}$  (10%) of HF spheres. The pressure in the mixtures clearly deviates from hydrostatic behavior. The data were obtained by measuring the force on a short (4 cm) horizontal bar that replaced part of the bottom container border. The weight of the material in upper layers is at least partially transferred to the container walls. The pressure characteristics differ slightly in individual runs, but the general trend is seen in all three graphs. This continuous pressure increase with fill height has direct consequences for the discharge characteristics of the mixtures, as will be demonstrated below.

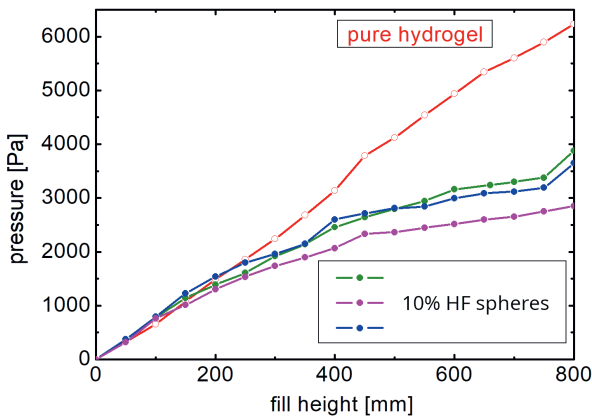


**Figure 6.2:** Pressure on the bottom area near the orifice as a function of the fill height of the grains in the silo. The line with open circles represents the pure HGS case; lines with closed circle represents three individual measurements for the case of the mixture of 10% HFS and 90% HGS.

One consequence of the increasing pressure towards the bottom of the silo in combination with the low elastic modulus of the hydrogels is that the packing fraction  $\phi$  increases towards the bottom. The closest packing of spheres with diameter  $d$  in a quasi-2D hexagonal lattice within a layer of thickness  $d$  is  $\phi_{\max} = \pi/\sqrt{27} \approx 0.604$ . This is indeed the mean packing fraction of pure hydrogel spheres, since they form a nearly defect-free hexagonal lattice in the depth of the granular bed. At the bottom, they even reach packing fractions up to about 0.65 where they are squeezed out of their original sphere shape. In the very top layers, owing to imperfections, the packing fraction drops to about 0.5. This may have some consequences for the outflow rates discussed in the next section.

### 6.3.2 Flow rate and clogging

Fig. 6.3(a) demonstrates how the character of the outflow is altered by changing the size of the orifice for a given mixture. One can see that the material flows practically uninterrupted through the largest orifice, with 13 mm in width, until the fill level has lowered to about 20...25 cm. In the silo with 12 mm orifice width, clogs interrupt avalanches of the order of 100 g (nearly 1000 particles), while in the silo with 11 mm opening, avalanches are on average one order of magnitude smaller.

The presence of a small fraction of hard frictional particles influences the outflow dynamics by having an impact on the statistics of clogs (permanent or non-permanent) as well as on the flow rate between clogs. The outflow curves are shown in Fig. 6.3(b) for 3 samples with hard frictional sphere contents  $x_{hf}$  of 0, 0.05 and 0.1. The orifice width was  $D \approx 11.5$  mm. The flow rate (between clogs) depends on the composition of the sample (fraction of HF spheres) and other parameters, such as the filling height and orifice size. We will further investigate the dependence of the flow rate as well as the duration of non-permanent clogs on the number of HF spheres in the proximity of the orifice.

For a visualization of the evolution of the flow rate (during avalanches) during the whole discharge process, Fig. 6.3(b) was trimmed by removing all clogs longer than 1 s. The result is shown in Fig. 6.3(c). The local slope of these curves gives the instantaneous discharge rate at any moment. In addition, the numerical simulation results presented in Fig. 6.3(d)-(e) were dealt with by the same methods as in Fig. 6.3(b)-(c), from which we can conclude the similar trends.

This rate is shown in Fig. 6.4(a) as a function of the bed height  $h$ . In accordance with our earlier observations in a 3D silo [27], the flow rate for pure hydrogel decreases with decreasing filling height. For the sample with 5 % HF grains, the height dependence is much weaker, while for the sample with 10 % HF grains this trend has essentially vanished. Thus, adding a small amount of frictional hard beads to a hydrogel bead

### 6.3. Results and Discussion

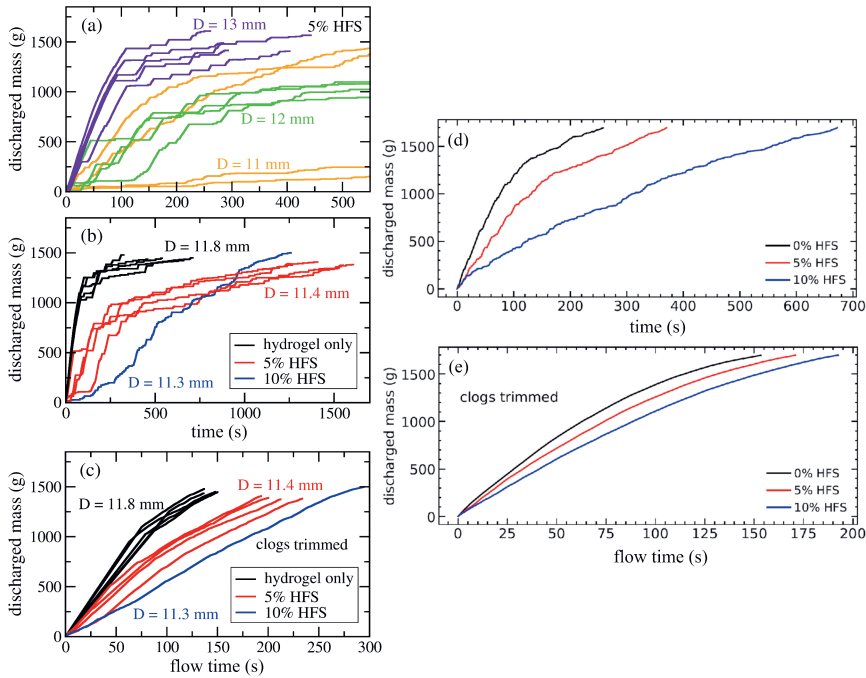


**Figure 6.3:** (a) Time dependence of the discharged mass for a sample containing 5% hard frictional spheres (HFS) for 3 values of the orifice width  $D$ . Smaller  $D$  mean more clogs, as visible in the reduced discharged mass for given time. (b) Time evolution of the discharged mass for 3 different samples: pure hydrogel, and mixtures containing 5% or 10% HF spheres. The orifice size  $D$  is indicated on the figure. The horizontal sections correspond to the clogs. (c) Same data as panel (b) but with clogs longer than 1 s trimmed. The flow rate is measured as the local slope of these trimmed curves. (d) Numerical simulation of the time evolution of discharged mass for the three cases of pure HGS, 5% HFS and 10% HFS in the samples respectively at the orifice size  $D = 11$  mm and with the friction coefficient  $\mu_{hyd-hf} = 0.2$ . (e) Same data as in Panel (d) but with clogs trimmed.



ensemble has a strong effect on the discharge kinetics of a 2-dimensional silo. Increasing the concentration of frictional hard grains, we quickly recover the typical behavior of granular materials characterized by a height independent (constant) flow rate.

It is obvious that Beverloo's original equation that relates the geometry of the particles and outlet to the discharge rate is not applicable for the hydrogels and at least the 5% HF spheres mixture since their discharge rates depend upon pressure at the outlet. Here, the low friction coefficient of the hydrogel may play a role [28], but the primary cause is the pressure dependence caused by the grain elasticity. Astonishingly, addition of 10% of rigid grains fully removes this pressure dependence.

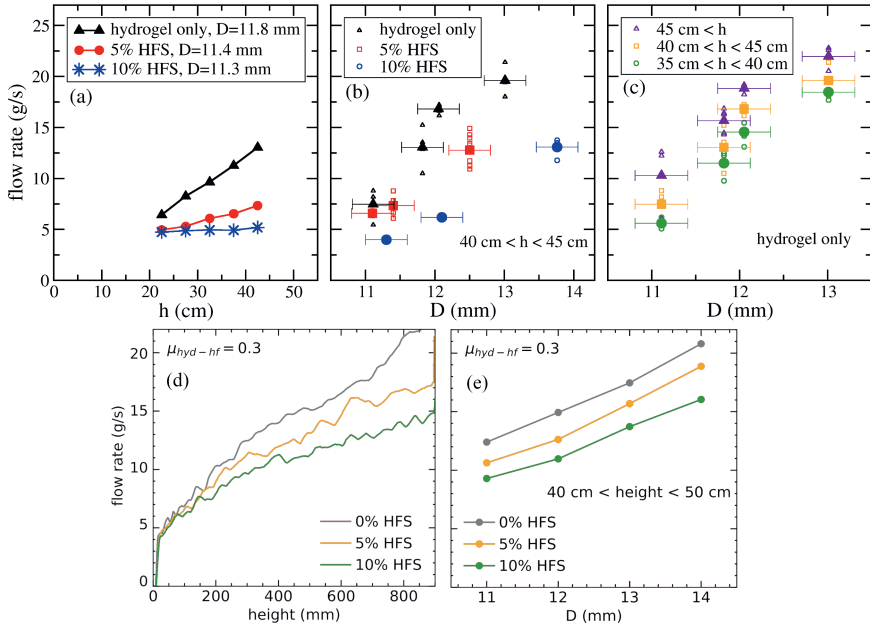


**Figure 6.4:** (a-c) Experimental results: (a) Flow rate as a function of the bed height  $h$  for pure hydrogel and for mixtures with 5% and 10% HF spheres. (b) Flow rate as a function of orifice size  $D$  for all three samples for a bed height from 40 cm to 45 cm and for (c) pure hydrogel samples at various bed heights  $h$ . Small open symbols represent individual experiments, large filled symbols show averages of the respective data sets (on average 4 experiments). (d)-(e) Numerical simulation results: (d) flow rate as a function of granular bed height and for the three samples mentioned above; (e) flow rate as a function of orifice size  $D$  in the height range of  $40 \text{ cm} < h < 45 \text{ cm}$  for the three sample mentioned above.

### 6.3. Results and Discussion

For an analysis how the flow rate depends on the orifice size  $D$ , and for comparison of all three mixtures, we present data of the height range between 40 cm and 45 cm in Fig. 6.4(b). As expected, the flow rate  $W$  decreases with  $D$ . An increased concentration of hard grains clearly reduces the flow rate, particularly at small orifice sizes. A dependence as predicted by Beverloo's model in 2D,  $W = C\phi\rho_0h\sqrt{g}(D - kd)^{1.5}$ , with the grain diameter  $d$ , the density  $\rho_0$  of the grains, packing fraction  $\phi$ , cell thickness  $h \approx d$  and adjustable constants  $k$  and  $C$  can be fitted for all three samples, but this is not surprising because of the small  $D/d$  range and the free parameters  $k$  and  $C$ . The product  $\rho_0\phi h$  amounts to approximately  $3.7 \text{ kg/m}^2$ . From Fig. 6.4(b), one finds  $k \approx 1.6$ , which is larger than the commonly reported value of about 1.4. The constant  $C$  to fit the graphs in Fig. 6.4(b) ranges from 3.5 for the 90% sample to about 6 for the pure hydrogels. This proportionality factor  $C$  accounts, for instance, for details of the orifice geometry. Considering Fig. 6.4(a), one has to conclude that this factor depends upon the instant fill height, viz. the pressure at the container bottom, in the pure hydrogel and the 5% HF spheres samples. This is also evident from the flow rate of the pure hydrogel sample as a function of  $D$  for three different height ranges, shown in Fig. 6.4(c). The results of numerical simulations demonstrated in Fig. 6.4(d) indicate that the addition of a few percent of HFS does not restore the typical granular feature of hard grains in terms of flow rate as a function of bed height but just weakens the height dependence. Fig. 6.4(e) tells us the similar trends as Fig. 6.4(b).

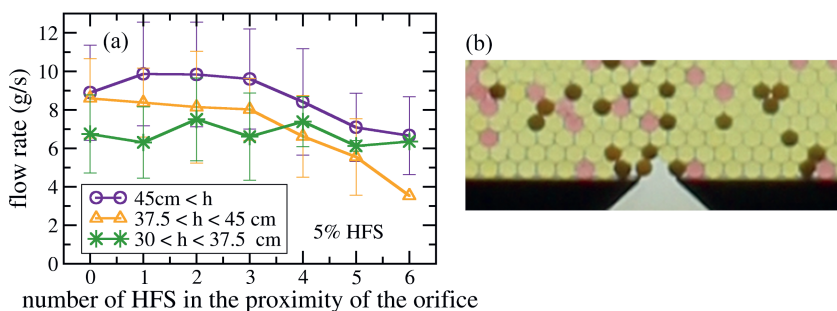


**Figure 6.5:** (a) Flow rate as a function of the number of HF grains in the proximity (5 particle diameters) of the orifice. Data taken for  $30 \text{ cm} < h < 80 \text{ cm}$ . Data points represent 18 measurements on average, error bars stand for the standard deviation. (b) A photo of the vicinity of the orifice while there is a clog.

Next, we analyze the dependence of the flow rate on the number of HF grains in the vicinity of the orifice. We consider a region with the shape of a half circle with a radius

of  $5d$  above the orifice. For large bed heights ( $h > 37.5$  cm) the flow rate is clearly decreasing when we have more than 3 hard grains in this region, i. e. the presence of hard, frictional grains near the bottleneck has a noticeable effect on the outflow (see Fig. 6.5). For  $h < 37.5$  cm, no such decrease was detected. When the pressure at the bottom is already very low, the addition of hard grains has little effect on the outflow dynamics. The explanation is straightforward: the elasticity of the hydrogel plays a role primarily when there is high pressure at the orifice. When the silo is filled by a 40 cm high granular bed, the pressure is approximately 3 kPa, and this pressure can deform the soft particles at the orifice by roughly 10% of their diameter. When the fill height and consequently the pressure lowers, the deformations are much less intense and the hydrogels gradually approach the mechanical properties of still low-frictional but hard grains.

### 6.3.3 Non-permanent clogging

Similar to earlier observations with pure hydrogel sphere ensembles [25], the system shows non-permanent clogging. This is seen, for example, in the mass curve shown

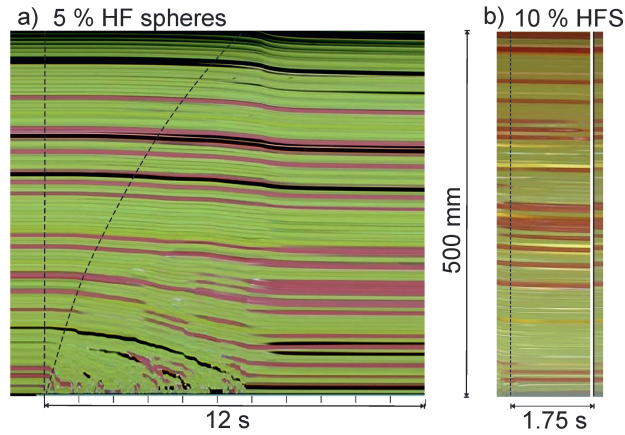


**Figure 6.6:** Kymographs of a vertical cross section of the silo in the central axis above the orifice ( $D = 12$  mm). a) Mixture with 5 % HF spheres. The grains start to flow only locally at the orifice after it is opened (vertical dashed line). The reaction of the material in the upper part is delayed considerably (bent dashed line). b) After the orifice at the bottom clogs (vertical dashed line), the material (with 10 % HF spheres) in the upper part still reorganizes for several seconds. The state immediately after the outflow stopped is re-plotted behind the white gap, to visualize the changes during the clogged state.

in Fig. 6.3. The plateaus are signatures of stopped outflow. In the experiment shown, with 11 mm orifice size and the silo emptied to about one fourth, roughly every second congestion of the orifice ends spontaneously, without external interference by air flushes or other. The reason for that is identified in the viscoelastic properties of the hydrogel. While the orifice is blocked, there is still motion in the upper parts of the silo that may cause an imbalance of forces in the blocking arches, with a considerable delay of up to several seconds. Fig. 6.6(b) demonstrates this delay. The granular material still reorganizes in the upper regions of the container after the outflow has already stopped. During a period of 1.75 seconds, no grain leaves the orifice but the material in the upper parts rearranges slowly. The blocking structure dissolves after 1.75 second. We have plotted the configuration immediately after the clog started on the right hand hand side of the figure, behind the solid line. Comparison with the state at the end of the clog evidences the shift of the grains during the congestion.

The viscoelastic character of the hydrogel is the reason for the slow dynamics of these processes. It is even more evident immediately after the outlet of the freshly filled container is opened for the first time, as shown in Fig. 6.6(a). The flow at the orifice sets in immediately, while the motion of the grains far above the orifice is delayed by up to several seconds. Note that in silos filled with hard grains, there is practically no such delay. This phenomenon has been reported for pure hydrogel samples before [25]. The delay times can vary slightly between individual runs of the experiment. Compared to the pure hydrogel samples, the addition of few percents of hard grains even seems to slightly enlarge the average delay times.

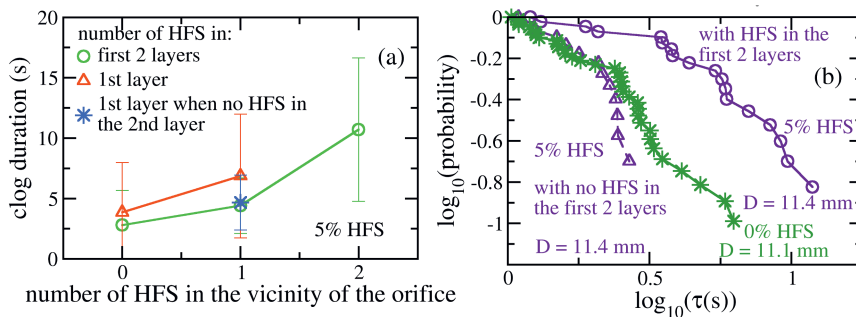


**Figure 6.7:** (a) Clog duration as a function of the number of high friction spheres (HFS) in the vicinity of the orifice. The data sets correspond to cases when only the first layer, or the first two layers are considered. Data points represent 13 clogs on average, error bars stand for the standard deviation. (b) Probability of non-permanent clogs longer than  $\tau$  as a function of  $\tau$  on a log-log scale.

We analyze now, how the duration of non-permanent clogs depends on the number of hard frictional spheres (HFS) in the vicinity of the orifice. As we see in Fig. 6.7(a), the clog duration increases with an increasing number of HFS. Hard frictional beads in the first and second layer both have an effect on the clog duration, with a slightly larger influence of the first layer. Another way to quantify how hard frictional beads in the vicinity of the orifice influence the duration of non-permanent clogs is to plot the probability that the clog is longer than a specific time interval  $\tau$  (this indicates that if the specific time interval is 0 second, then the probability of that clog lasting longer than this time interval is 1. Thus, the curves in Fig. 6.7(b) basically demonstrate the distribution of the clog duration.). This is shown in Fig. 6.7(b) as a function of  $\tau$  in a log-log plot. The curve characterizing a pure hydrogel sample is very close to the curve of a mixture with 5% HFS, when no HFS are present in the first two shells above the orifice. However the curve is considerably shifted for those clogs, when HFS are present in this region. Thus, the stability of blocking arches clearly increases when hard frictional grains are present in them.

## 6.4 Discussion

Our results clearly show that the addition of a small percentage of hard grains to an ensemble of soft, low-friction spheres has dramatic consequences for the flow through a narrow orifice and the clogging statistics in a quasi-2D silo. First, one finds that the outflow rate of pure soft grain ensembles through narrow orifices depends upon the pressure at the silo bottom, which is in contrast to Beverloo's model for hard grains. Second, one observes that the addition of a few percent of hard spheres restores the pressure-independent outflow characteristics predicted by Beverloo (Fig. 6.4(a)). Moreover, the discharge rates of all mixtures approach each other at low container fill heights (Fig. 6.4(a)). The reason is obviously that the elasticity of the soft grains is less important when the pressure near the orifice is low, then their deformability can be neglected. On the other hand, at high fill levels of the silo, the increased pressure at the bottom can deform the soft grains and squeeze them through the orifice efficiently. Therefore, the outflow rate for the pure hydrogel sample at a fill height of 40 cm (pressure  $\approx 3$  kPa) is approximately 2.5 times as high as that for the 10% mixture. This cannot be explained by the smaller friction coefficient [28] of the hydrogel compared to the hard frictional spheres, since the concentration of the latter is small. The effect of the number of hard frictional grains in the vicinity of the orifice on the flow rate is in accordance with the above described observations. At higher fill levels ( $h > 37.5$  cm), the flow rate is found to decrease when the number of HFS is larger than three in the proximity ( $5d$ ) of the orifice (Fig. 6.5). At low fill levels, when the pressure near the

orifice is low, increasing the number of HFS around the orifice does not affect the flow rate significantly.

We note that a comparison of outflow rates with those of a pure hard sphere ensemble is not possible because the latter will permanently clog at orifice widths smaller than  $2d$ , with mean avalanche sizes well below 10 particles.

We find a substantial influence of hard frictional particle doping on the clogging statistics, both in experiment and simulations. Besides, the time evolution shown in Fig. 6.3 shows that the effective discharge is considerably delayed by frequent intermittent stagnation of the flow in the doped mixtures.

The material forms non-permanent clogs which are resolved after some delay, because of slow reorganizations of the packing structure in the granular bed within the complete container above the orifice. This reorganization occurs on a timescale of a few seconds, as illustrated by Fig. 6.6(a). Interestingly, the probability distribution of clog durations is very similar for a pure hydrogel sample and a 5% mixture if no HFS are present in the first two layers above the orifice (Fig. 6.7(b)). The clog duration clearly increases when HFS are present near the orifice. This observation underlines the important role of hard frictional beads in the vicinity of the orifice. Both experiment and simulations are in good qualitative agreement, and allow a comprehensive analysis of the system from complementary points of view.

## 6.5 Summary

This study demonstrates that the behavior of mixtures of grains with different frictional and elastic properties cannot be described by a simple interpolation of dynamic parameters, but that already the presence of a low percentage of one of the species can alter the dynamics substantially. In many practical situations, for instance in agriculture, but also in natural phenomena like mud or debris flow, the coexistence of grains of very different sizes and mechanical properties is the rule, not the exception. It adds a new level of complexity that has been studied only scarcely in the past. Here, we have peeked into this complex field by restricting our study to monodisperse materials, in a quasi-2D geometry. The hard frictional grains slide more dissipatively against the wall, forming defects or obstacles in a 2D geometry more easily at a low concentration, which will not be expected in a 3D setting. We also restricted the discussion to small doping percentages. This is a considerable simplification of relevant practical cases, but it shines a light on the various phenomena expected in such systems.

Finally, further investigations should be carried out, addressing the significance of adding rigid grains in the evolution of the force chains and contact network.



---

## BIBLIOGRAPHY

- [1] Franklin, F. C. and Johanson, L. N. “Flow of granular material through a circular orifice”. In: *Chemical Engineering Science* **4** (1955), 119–129.
- [2] Beverloo, W. A., Leniger, H. A., and Van de Velde, J. J. “The flow of granular solids through orifices”. In: *Chemical Engineering Science* **15** (1961), 260.
- [3] Neddermann, R. M. et al. “The flow of granular materials discharge rates from hoppers”. In: *Chemical Engineering Science* **37** (1982), 1597–1609.
- [4] Mankoc, C. et al. “The flow rate of granular materials through an orifice”. In: *Granular Matter* **9** (2007), 407–414.
- [5] Aguirre, M. A. et al. “Pressure independence of granular flow through an aperture”. In: *Physical Review Letters* **104** (2010), 238002.
- [6] Sheldon, H. G. and Durian, D. J. “Granular discharge and clogging for tilted hoppers”. In: *Granular Matter* **12** (2010), 579.
- [7] Janda, A., Zuriguel, I., and Maza, D. “Flow rate of particles through apertures obtained from self-similar density and velocity profiles”. In: *Physical Review Letters* **108** (2012), 248001.
- [8] Koivisto, J. and Durian, D. J. “The sands of time run faster near the end”. In: *Nature Communications* **8** (2017), 015551.
- [9] Wilson, T. J. et al. “Granular Discharge Rate for Submerged Hoppers”. In: *Papers in Physics*. **6** (2014), 060009.
- [10] To, K. “Jamming transition in two-dimensional hoppers and silos”. In: *Physical Review E* **71** (2005), 060301.



- 
- [11] Zuriguel, I. et al. “Jamming during the discharge of granular matter from a silo”. In: *Physical Review E* **71** (2005), 051303.
- [12] Thomas, C. C. and Durian, D. J. “Fraction of clogging configurations sampled by granular hopper flow”. In: *Physical Review Letters* **114** (2015), 178001.
- [13] Tang, J. and Behringer, R. “How granular materials jam in a hopper”. In: *Chaos* **21** (2011), 041107.
- [14] Zuriguel, I. et al. “Clogging transition of many-particle systems flowing through bottlenecks”. In: *Scientific Reports* **4** (2014), 7324.
- [15] Rubio-Largo, S. M. et al. “Disentangling the Free-Fall Arch Paradox in Silo Discharge”. In: *Physical Review Letters* **114** (2015), 238002.
- [16] Hidalgo, R. C. et al. “Force analysis of clogging arches in a silo”. In: *Granular Matter* **15** (2013), 841–848.
- [17] Vivanco, F., Rica, S., and Melo, F. “Dynamical arching in a two dimensional granular flow”. In: *Granular Matter* **14** (2012), 563–576.
- [18] Hong, X., Kohne, M., and Weeks, E. R. “Clogging of soft particles in 2D hoppers”. In: *Physical Review E* **96** (2017), 062605.
- [19] Ashour, A. et al. “Silo outflow of soft frictionless spheres”. In: *Physical Review Fluids* **2** (2017), 123302.
- [20] Mankoc, C. et al. “Role of vibrations in the jamming and unjamming of grains discharging from a silo”. In: *Physical Review E* **80** (2009), 011309.
- [21] Guerrero, B. V. et al. “Slow relaxation dynamics of clogs in a vibrated granular silo”. In: *Physical Review E* **97** (2018), 042904.
- [22] Marin, A. et al. “Clogging in constricted suspension flows”. In: *Physical Review E* **97** (2018), 021102(R).
- [23] Hidalgo, R. C. et al. “Flow of colloidal suspensions through small orifices”. In: *Physical Review E* **97** (2018), 012611.
- [24] Souzy, M., Zuriguel, I., and Marin, A. “Clogging transitions in constricted particle suspension flows”. In: *Physical Review E* **101** (2020), 060901(R).
- [25] Harth, K. et al. “Intermittent flow and transient congestions of soft spheres passing narrow orifices”. In: *Soft Matter* **16** (2020), 8013.
- [26] Janssen, H. A. “Versuche über Getreidedrücke in Silozellen”. In: *Zeitschrift des Vereines Deutscher Ingenieure* **39** (1895), 1045.
- [27] Stannarius, R. et al. “High-speed x-ray tomography of silo discharge”. In: *New Journal of Physics* **21** (2019), 113054.

## Bibliography

---

- [28] Darias, J. R., Madrid, M., and Pugnali, L. “Differential equation for the flow rate of discharging silos based on energy balance”. In: *Physical Review E* **101** (2020), 052905.



---

## Mixtures of hydrogel and airsoft beads in a 3D silo and a shear cell

*In this chapter, the flow of granular mixtures composed of hard frictional beads and soft low-friction beads was investigated in a cylindrical silo as well as in a split-bottom shear cell. In a silo discharge process in the two limits we find a fill height dependent flow rate for 100% low friction soft grains and height independent flow rate for 100% hard frictional grains. When mixing the two types of grains, the transition between the soft, frictionless and hard, frictional particle limit occurs around 20% hard grains, and is rather abrupt. We verify that this abrupt change in flow rate is not due to (rate-dependent) effective frictional dissipation effects. Both quasi-static split-bottom shear tests and rate dependent “granular drag” tests reveal only modest increases of frictional dissipation with increased hard particle mixture content, both of which only emerge around 40%. We conclude that there must be an additional mechanism to explain the transition from height dependent flow rate to constant flow rate in granular mixtures of increasing hard particle content.*

**Bo Fan, Joshua Dijkstra, Jasper van der Gucht and Tamás Börzsönyi**  
“Granular flow of mixtures of soft and hard spheres”

## 7.1 Introduction

We usually think about a granular material as an assembly of hard frictional grains. The flow properties of such materials are complex and are still widely investigated nowadays. Such materials have a very useful feature: they flow out of a container with a constant rate, independent of the filling height, as it was pointed out in the pioneering works of Huber-Burnand, Hagen and Beverloo [1–4]. Interestingly, for deformable particles with low surface friction, recent work has shown that this classic perspective does not hold anymore. The flow rate becomes height dependent, similarly to the case of liquids [5], and for smaller orifices, where clogs occur, the probability of clogging also becomes height dependent [6, 7]. Moreover, we observed an increasing trend in flow rate during discharging elongated particles from a narrow silo in chapter 2. Furthermore, for immersed granular materials viscous effects resulting from the background fluid can also change the scaling relation between container flux and opening size [8].

Hydrogel beads are excellent examples of soft particles with low surface friction. Their use becomes increasingly important in various applications in food industry (delivery of drugs, nutrients or probiotics) or in agriculture and water purification (removal of dyes, metal ions, organic pollutants or bacteria) and various biomedical applications [9–12]. The effect of particle softness on the rheology of a granulate has been investigated previously in shear flows numerically [13–15], and hydrogel beads proved to be very useful to gain experimental insight into the microscopic dynamics by sophisticated non invasive 3-dimensional (3D) imaging techniques [16–18].

As mentioned above, the discharge of low friction soft particles out of a container is very different from the behavior of hard grains. Experiments in a 2-dimensional system allowed for the observation of the flow at the level of individual particles [6, 7, 19, 20]. At small orifice sizes temporary congestions occur which resolve after some time, unlike the permanent clogs observed for hard grains. Both, the statistics of the temporary congestions for small orifice (in the intermittent flow regime), as well as the discharge rate for larger orifice (in the continuous flow regime) are filling height dependent. Investigations in a 3D silo also unveiled strong differences in the flow field between the cases of hard grains and low friction soft hydrogel beads [21, 22] and a height dependent discharge rate [5]. This is related to the fact that for low friction soft grains the stability of force chains and arch formation is less pronounced. As a result of this, for low friction soft grains (i) the local vertical stress  $\sigma_{zz}$  above the orifice changes more during the discharge process and (ii) the value of  $\sigma_{zz}$  has a stronger impact on the outflow rate than for hard grains [5].

For a mixture of hard grains and hydrogel beads a transition is expected to happen as a function of concentration between the two different behaviors described above. Interestingly, in a 2D silo, chapter 6 showed that adding a small amount (5 or 10%)

of hard frictional grains to hydrogel beads strongly changes the flow [23]. By adding only 10% of hard grains the constant flow rate was already recovered. The probability of the formation of clogging arches also strongly changed with the concentration of hard grains in 2D silo experiments [23–25]. In view of the striking behavior of the 2D systems it is interesting to test how the flow characteristics of mixtures changes with concentration in 3-dimensional configurations.

In the present chapter, we therefore investigate the flow of mixtures of hydrogel beads and plastic beads in a 3-D silo, exploring the full range (0 – 100%) of concentrations. We complement the silo discharge measurements with two further experimental tests: (i) quasistatic shearing in a split-bottom shear cell and (ii) measuring the drag force on an object moved horizontally in the granulate.

## 7.2 Experimental procedures

For the silo discharge experiments we use an acrylic cylinder with an inner diameter of  $D_c = 144$  mm and a height of 800 mm with a circular orifice with diameter  $D$  in the middle of the silo base (see Fig. 7.1(a)). The silo base is separated from the cylinder by a gap of about 1 mm, and it is held by two load cells, which allows us to measure the force exerted on the silo bottom. The container below the silo was also held by a load cell. The sample was filled into the silo manually with a filling rate of about 500 g/s and then the orifice was opened, and the evolution of both the discharged mass and the basal force was monitored throughout the whole discharge process by reading the signals from the load cells with a sampling rate of 100 Hz.

In the second experiment the sample was exposed to shear deformation in a cylindrical split bottom device (see Fig. 7.1(b)). In this setup the middle of the sample is slowly rotated with a time period of 13 s, while the outer part is stationary, so the region between them (denoted with red color in Fig. 7.1(b)) is constantly sheared with a typical shear rate of  $3 \text{ s}^{-1}$ . In order to measure the resistance of the sample against shearing we measure the torque needed for maintaining stationary rotation of the middle part.

In the third type of experiment we move an object horizontally in the mixture and measure the force needed to maintain stationary motion. Two objects were used: an airsoft bead (same as for making the mixtures; glued at the end of a stainless steel needle with diameter of 0.7mm) or a vertical stainless steel cylinder with the diameter of 6 mm. For each experiment a 50 mm thick layer of the sample was placed in a cylindrical container with the diameter of 150 mm. Then the object was immersed at a depth of 22 mm and it was moved using a rheometer (Anton-Paar MCR-501) along a circular trajectory with a radius of 45 mm. The speed of the object was varied in the

range of  $0.47 \text{ cm/s} \leq v \leq 7.54 \text{ cm/s}$ . We can estimate the corresponding shear rate range by dividing the velocity difference of the moving object and the static neighboring grains by the grain size, which results in  $0.8 \text{ s}^{-1} \leq \dot{\gamma} \leq 13 \text{ s}^{-1}$ .

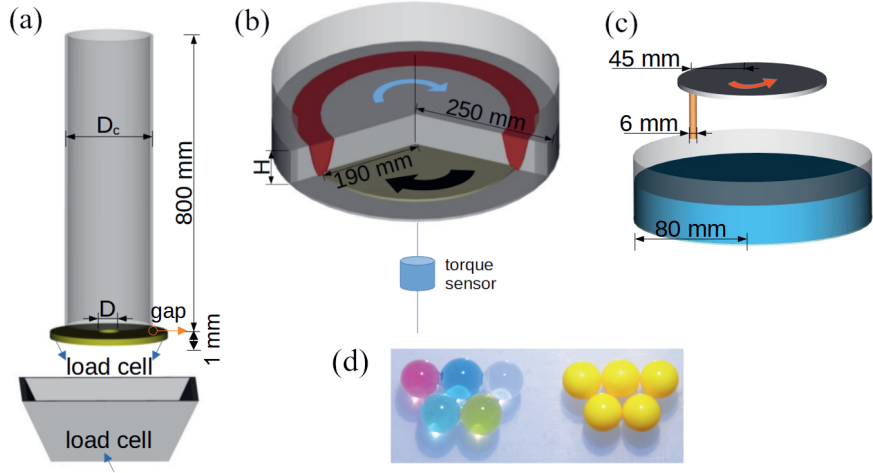


**Figure 7.1:** Experimental setups: (a) silo, (b) cylindrical split-bottom shear cell, (c) rheometer, (d) materials: hydrogels (left) and airsoft beads (right).

In the experiments presented here we used airsoft beads (ASB) with a diameter of  $d = 5.95 \pm 0.04 \text{ mm}$  and hydrogel beads with  $d = 6.4 \pm 0.3 \text{ mm}$  (for photographs of the beads see Fig. 7.1(c)). We have investigated 11 samples, spanning the whole concentration range 0 – 100%. The mass density of the two types of grains is identical within an accuracy of less than 1%, as both were slowly sinking/rising in salty water with salt concentrations of 3% or 4%, respectively.

For characterizing the shear resistance as a function of the concentration we prepared samples with the same volume ( $V = 10.9 \text{ liters}$ ), i.e. all samples had the same fill height  $h = 5.6 \text{ cm}$  in the shear cell. Since the HGS beads are deformable, their packing fraction depends on the pressure. For a layer with a thickness of  $h = 5.6 \text{ cm}$  the HGS packing fraction was about 0.7 while that of ASB was measured to be 0.62. Thus increasing ASB concentration leads to slightly decreasing mass of the sample. The measured torque was normalized by the mass of the sample. For the silo measurements the same samples were used. Fig. 7.2 shows the mass of the samples as well as the fill height in the silo as a function of the ASB concentration.

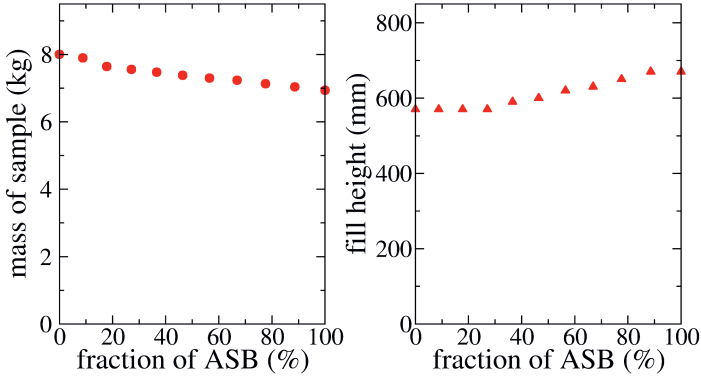


**Figure 7.2:** (a) Mass of the samples (b) fill height in the silo as a function of the ASB concentration.

## 7.3 Results and Discussion

### 7.3.1 Silo flow

In the first set of experiments we measure the evolution of the silo flow rate during the discharge process for all mixtures. The flow rate is presented as a function of the mass in the silo for mixtures with different ASB concentration in Fig. 7.3 (top row). Both the flow rate and the mass are normalized by the total mass  $m_{\text{total}}$  of the sample. The evolution of the basal force  $F_b$  is shown in the bottom row. For each sample 3 discharge curves were taken at orifice sizes of  $D=30, 40$  and  $52$  mm. As we see, by increasing the concentration of the ASB we find a gradual change from the hydrogel like discharge behavior with decreasing flow rate and almost hydrostatic pressure conditions at the bottom of the silo towards a traditional granular-like discharge with constant flow rate and saturating basal force according to the Janssen screening.

To quantify how the nature of the silo flow rate changes with the mixture concentration, we take the slope of the flow rate curve in the middle part of the discharge process which is free of the initial and final transients, and normalize it with the slope obtained for the pure hydrogel sample. The normalized slope is presented as a function of the percentage of ASB in Fig. 7.4(a). While we see a gradual change in the whole concentration range, the discharge characteristics change stronger in the beginning of the curve (up to about 20% ASB), i.e. adding a small amount of hard grains has a strong effect on the behaviour of the sample. However, the change at low



## 7. Mixtures of hydrogel and airsoft beads in a 3D silo and a shear cell

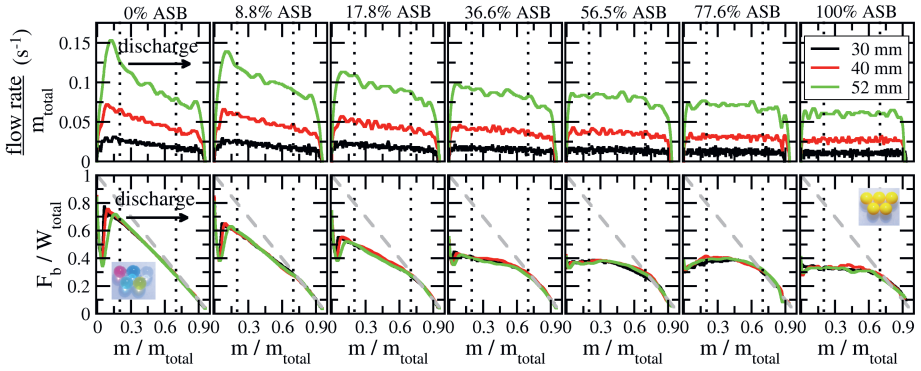


**Figure 7.3:** Flow rate (top row) and basal force  $F_b$  (bottom row) as a function of the discharged mass, normalized by the total mass ( $m_{\text{total}}$ ) or total weight ( $W_{\text{total}}$ ) of the sample. In the first panel on the left in the bottom row (for the 0% ASB sample) the hydrostatic pressure condition is indicated with a grey dashed line as a reference. For each sample three discharge curves are shown corresponding to the orifice sizes of  $D = 30, 40$  and  $52$  mm. Each curve is a result of the average of two measurements.

concentration is not so dramatic as it was in previous experiments in a 2-dimensional silo [23] in chapter 6, where a constant discharge rate scenario was already reached at 10% ASB. Note, that the curves obtained for different orifice sizes nicely overlap, when normalized by the flow rate obtained for pure hydrogel for the given orifice.

### 7.3.2 Shear test in the split-bottom shear cell

How can we understand the ASB fraction dependence of the discharge rate? One mechanism can be that the mixtures experience a larger frictional drag, as the ASB-wall and ASB-hydrogel contacts have a higher friction coefficient than any hydrogel-contact. During the course of silo discharge the sample is subject to shear deformation within the silo which triggers such frictional dissipation. It is thus interesting to compare the effect of mixture concentration on the silo discharge and on the resistance of the sample against shearing. The shear resistance was measured in the cylindrical split bottom shear cell [26, 27], by measuring the torque needed for maintaining stationary rotation of the middle part of the sample, and thereby inducing quasistatic shearing of the material in the shearzone (see red region in Fig. 7.1(b)). The normalized shear resistance is presented as a function of ASB concentration in Fig. 7.4(b). The graph shows two curves, obtained during the first full rotation (13 s), and during the

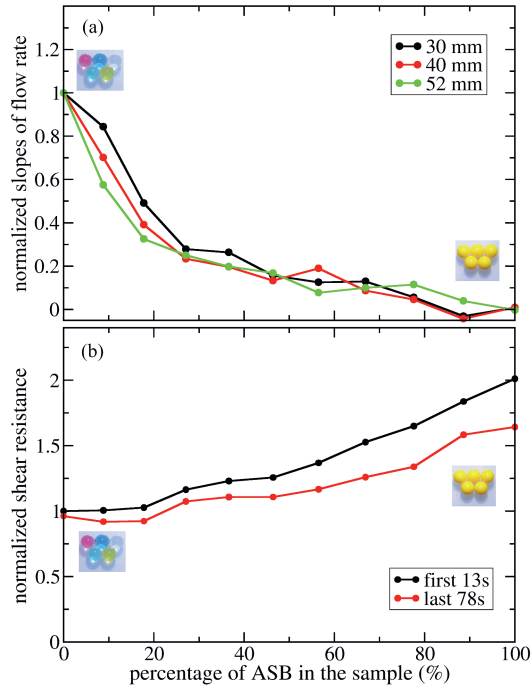


**Figure 7.4:** (a) The slope of flow rate curve obtained by linear fitting between  $0.2 < m/m_{total} < 0.7$  (see the two black dotted lines in Figure 7.3) as a function of ASB concentration. The slope is normalized by the slope value obtained for 0% ASB. (b) Shear resistance per mass as a function of the of ASB concentration. The shear resistance data are normalized by the value of the first 13s of the curve at 0% ASB.

subsequent 6 rotations (78 s), respectively. As we see, the shear torque is larger in the beginning of the experiment (black data points), which is most probably connected to the fact, that during the course of shearing the grains in the shear zone organize themselves into chains along the streamlines [28]. As a demonstration we show pictures of the quarter of the cylindrical shear cell for the two limiting cases: a pure ASB and a pure HGS sample (Fig. 7.5). The initial configuration is random for both samples (left hand side). For ASB with uniform size shearing the sample results in ordering of the grains in the shear zone, while no such ordering is seen for HGS most probably due to the polydispersity of grain sizes (right hand side).

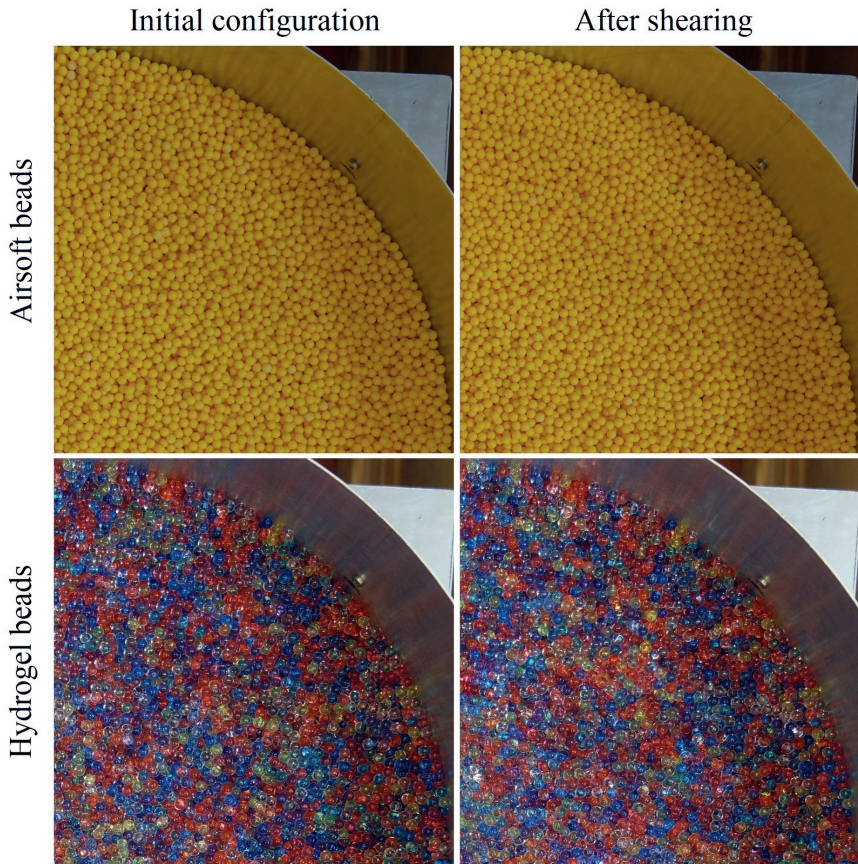


**Figure 7.5:** Top view of a quarter of the cylindrical shear cell for a pure ASB and HGS sample (top and bottom images) for the initial configuration (left side) and after shearing the sample with 6 full rotations of the bottom plate.

The shear measurement was always started with a random packing, which is harder to shear, and during the course of the experiment the shear resistance slightly decreases due to the above described ordering process. With increasing the concentration of the monodisperse airsoft beads the shear induced ordering of the samples becomes stronger. Therefore the two curves showing the shear resistance in the disordered state (first 13

s of the measurement) and in the ordered state (following 78 s of the measurement) separate with increasing ASB concentration. Apart from the separation, both curves show the same tendency: a gradual increase of the shear resistance with increasing ASB concentration. Thus, the general trends of the flow rate (Fig. 7.4(a)) and shear resistance (Fig. 7.4(b)) are consistent: with increasing hard grain concentration we get stronger resistance against shearing and smaller flow rate in the silo.

Another important observation regarding the samples' shear resistance is that even if the microscopic surface friction of common hard grains is about one order of magnitude larger than the value of HGS ( $\mu = 0.3$  vs.  $\mu = 0.02$  [5]), we see in Fig. 7.4 (b) that the shear resistance (effective friction) of the sample increases only by about a factor of 2 when going from 0% ASB to 100% ASB. This is perfectly consistent with the result of earlier numerical simulations [29] and work on frictional hydrogel experiments [30], and shows the importance of the geometrical origin of the effective friction of a sheared granulate.

Altogether, comparing the two measurements more carefully we find a mismatch: the change in the shear resistance is minor at low ASB concentration and becomes stronger in ASB rich samples, while the tendency is opposite for the silo discharge rate curves, where a small amount of added ASB had a strong influence on the discharge behavior, and in ASB rich samples the flow rate changes less with concentration. This discrepancy clearly shows that in addition to the role of the effective friction of the sample, other factors have a significant contribution to the evolution of the flow rate as a function of mixture concentration.

#### 7.3.3 Drag force on an object moved in the mixture

As we observe that rate independent friction cannot be solely responsible for the weakening height dependence of flow rate, we turn to verifying whether rate dependent effects play a role. To test this, in the third set of experiments an object is moved horizontally in the sample (see Fig. 7.1(c)) and the drag force is measured with the help of a rheometer at various driving rates. For this drag force experiment, we used two test objects: an airsoft bead (ASB) and a stainless steel cylinder with a diameter of 6 mm, both immersed at a depth of 22 mm. The velocity of the object was varied in the range of  $0.47 \text{ cm/s} \leq v \leq 7.54 \text{ cm/s}$ , corresponding to a shear rate range of  $0.8 \text{ s}^{-1} \leq \dot{\gamma} \leq 13 \text{ s}^{-1}$ . The results of these measurements confirm the observations we made in the split bottom shear cell. First, as we see in Figs. 7.6(a-b) the drag force changes with the mixture concentration in a very similar way as the shear torque changed under quasistatic shear in the split bottom shear cell. Generally, the force increases with ASB concentration, and the rate of change is much larger in ASB rich samples than at low ASB concentrations. The drag force is about 2.5-3 times larger in

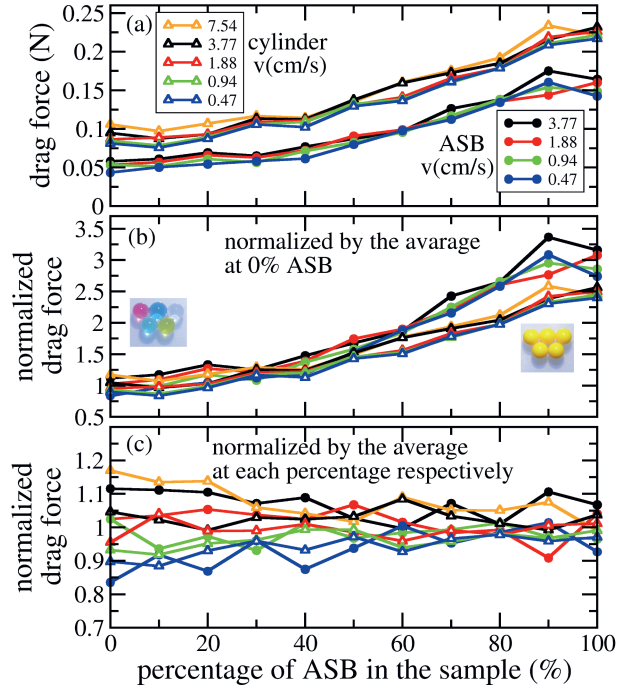


**Figure 7.6:** (a) Drag force on an object (ASB bead or vertical cylinder) moved horizontally in the HGS-ASB mixture, immersed at a depth of 22 mm. The curves correspond to different velocities  $v$  of the object, the values of  $v$  are indicated in the figure. (b-c) Same data as in panel (a) normalized by the average force at 0% ASB (panel b), and normalized by the average force calculated for each concentration (panel c).

## 7.4. Summary

---

ASB rich samples than at small concentrations. Naturally, we get a larger drag force for a cylinder than for a single ASB. Second, the shear rate dependence of the drag force appears to be minor, as the data values are very similar even if the shear rate is increased by a factor of 16. In order to better visualize the weak shear rate dependence, we present the data in a normalized form in Fig. 7.6(c). For high ASB concentration, the data obtained for low and high shear rates are very similar within the uncertainty of the measurement which is about 10%. Decreasing the ASB concentration the curves clearly split up showing a 20 – 30% difference in the drag force in between the cases with the smallest and largest shear rate. Thus, the drag force on an object in a hydrogel rich sample is increasing with shear rate, similarly to viscous liquids or colloids, but here the magnitude of change is small.

## 7.4 Summary

Our measurements on the flow rate of a mixture of hydrogel beads and airsoft (plastic) beads during silo discharge show that adding hard grains to hydrogel beads strongly changes the discharge behaviour up to a concentration of about 30%. Increasing the ASB concentration further has a smaller effect, but the general trend is clear: while ASB rich samples discharge with a constant flow rate (independent of the fill height of the silo), the flow rate of HGS rich samples decreases with decreasing fill height.

Complementary measurements on the resistance of the material against shearing or drag force on an object moved horizontally in the sample both show increasing resistance or force with increasing hard grain (ASB) concentration. Thus, the general trends of the three tests are coherent: with increasing ASB concentration we get stronger resistance against shearing, larger drag force and smaller flow rate in the silo. However, comparing the data more carefully we find a mismatch: changes in the shear resistance and drag force are minor at low ASB concentration and become stronger in ASB rich samples, while the tendency is opposite for the silo discharge rate curves, where a small amount of added ASB had a strong influence on the discharge behavior in ASB poor samples, while in ASB rich samples the flow rate changes less with concentration. This difference clearly shows that in addition to the role of the effective (rate dependent) friction of the sample, there are other factors having a significant contribution to the evolution of the flow rate as a function of mixture concentration. Probably, the microscopic details of the flow dynamics, especially the nature of dynamic evolution of the force chains and dynamic arch formation above the orifice change with the concentration of low friction soft grains.

## 7.5 Appendix

Since the HGS are inherently wet, our mixtures contain a small amount of water, involving capillary bridges at particle contacts. In order to keep control of the water content of our samples, in the preparation process we soaked the excess water from the sample by a towel. For the pure ASB sample an additional series of measurements were done to test the effect of added water on the shear resistance of the sample. The resulting data (see Fig. 7.7 show, that adding water to 6.94 kg of ASB first slightly increases the measured shear resistance, but above 20 grams of added water the curve saturates and no more increase in the shear resistance is observed. The water content of our samples is similar to the ASB sample with 30 g of added water (denoted by a vertical dashed line in Fig. 7.7). This measurement shows that the data presented above are not especially sensitive to the actual water content.

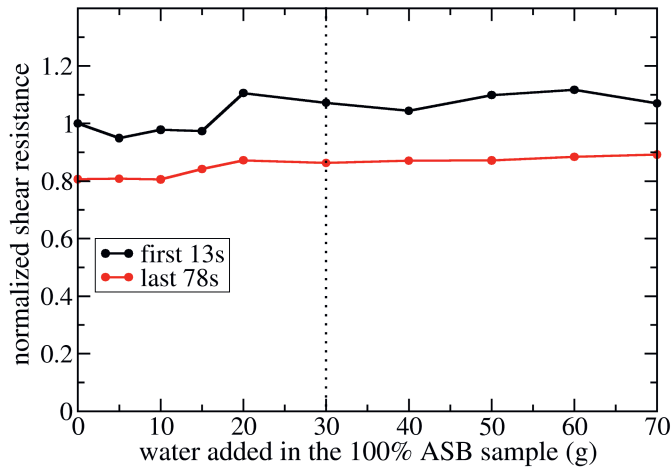


**Figure 7.7:** Shear resistance as a function of added water for 7 kg of 100% ASB sample. Data are normalized by the mass of the sample and by the value of the first-13s curve at 0g water. The black dotted line indicates the sample with similar moisture content to our mixtures. This sample was used for obtaining the data points in Figs. 7.3 and 7.4 for the 100% ASB sample.

---

## BIBLIOGRAPHY

- [1] Huber-Burnand, P. “Ueber das Ausfliessen und den Druck des Sandes”. In: *Annals of Physics* **92** (1829), 316–328.
- [2] Tighe, B. P. and Sperl, M. “Pressure and motion of dry sand: translation of Hagen’s paper from 1852”. In: *Granular Matter* **9** (2007), 141–144.
- [3] Beverloo, W. A., Leniger, H. A., and Van de Velde, J. “The flow of granular solids through orifices”. In: *Chemical Engineering Science* **15** (1961), 260–269.
- [4] Nedderman, R. M. et al. “The Flow of Granular Materials I: Discharge Rates from Hoppers”. In: *Chemical Engineering Science* **37** (1982), 1597.
- [5] Pongó, T. et al. “Flow in an hourglass: particle friction and stiffness matter”. In: *New Journal of Physics* **28** (2021), 023001.
- [6] Hong, X. et al. “Clogging of soft particles in two-dimensional hoppers”. In: *Physical Review E* **96** (2017), 062605.
- [7] Tao, R., Wilson, M., and Weeks, E. “Soft particle clogging in two-dimensional hoppers”. In: *Physical Review E* **104** (2021), 044909.
- [8] Cheng, Y. et al. “Hopper flows of deformable particles”. In: *Soft Matter* **18** (2022), 8071–8086.
- [9] Qu, B. and Luo, Y. “Chitosan-based hydrogel beads: Preparations, modifications and applications in food and agriculture sectors – A review”. In: *International Journal of Biological Macromolecules* **152** (2020), 437–448.
- [10] Li, N. and Bai, R. “Copper adsorption on chitosan–cellulose hydrogel beads: behaviors and mechanisms”. In: *Separation and Purification Technology* **42** (2005), 237–247.



- 
- [11] Jain, S. et al. “Design and Development of Hydrogel Beads for Targeted Drug Delivery to the Colon”. In: *AAPS PharmSciTech.* **8** (2007), 56.
- [12] Daly, A. C. et al. “Hydrogel microparticles for biomedical applications”. In: *Nature Reviews Materials* **5** (2020), 20–43.
- [13] Campbell, C. S. “Granular shear flows at the elastic limit”. In: *Journal of fluid mechanics* **465** (2002), 261–291.
- [14] Chialvo, S., Sun, J., and Sundaresan, S. “Bridging the rheology of granular flows in three regimes”. In: *Physical Review E* **85** (2012), 021305.
- [15] Favier de Coulomb, A. et al. “Rheology of granular flows across the transition from soft to rigid particles”. In: *Physical Review Fluids* **2** (2017), 102301(R).
- [16] Brodu, N., Dijkstra, J., and Behringer, R. “Spanning the scales of granular materials through microscopic force imaging”. In: *Nature Communications* **6** (2015), 6361.
- [17] Dijkstra, J., Brodu, N., and Behringer, R. “Refractive Index Matched Scanning and Detection of Soft Particles”. In: *Review of Scientific Instruments* **88** (2017), 051807.
- [18] Wang, J. et al. “Characterization of shear zones in soft granular beds by means of a novel magnetic resonance imaging technique”. In: *Granular Matter* **24** (2022), 103.
- [19] Ashour, A. et al. “Silo outflow of soft frictionless spheres”. In: *Physical Review Fluids* **2** (2017), 123302.
- [20] Harth, K. et al. “Intermittent flow and transient congestions of soft spheres passing narrow orifices”. In: *Soft Matter* **16** (2020), 8013.
- [21] Stannarius, R. et al. “Packing and flow profiles of soft grains in 3D silos reconstructed with X-ray computed tomography”. In: *Granular Matter* **21** (2019), 56.
- [22] Stannarius, R. et al. “High-speed x-ray tomography of silo discharge”. In: *New Journal of Physics* **21** (2019), 113054.
- [23] Wang, J. et al. “Silo discharge of mixtures of soft and rigid grains”. In: *Soft Matter* **17** (2021), 4282.
- [24] Alborzi, S., Abrahamyan, D., and Hashmi, S. “Soft particles facilitate flow of rigid particles in a 2D hopper”. In: *Soft Matter* **18** (2022), 4127.
- [25] Alborzi, S., Clark, B., and Hashmi, S. “Mixing particle softness in a two-dimensional hopper: Particle rigidity and friction enable variable arch geometry to cause clogging”. In: *Physical Review E* **107** (2023), 024901.

## Bibliography

---

- [26] Dijksman, J. A. et al. “From frictional to viscous behavior: Three-dimensional imaging and rheology of gravitational suspensions”. In: *Physical Review E* **82** (2010), 060301.
- [27] Dijksman, J. A. and Van Hecke, M. “Granular flows in split-bottom geometries”. In: *Soft Matter* **6** (2010), 2901–2907.
- [28] Wegner, S. et al. “Effects of grain shape on packing and dilatancy of sheared granular materials”. In: *Soft Matter* **10** (2014), 5157–5167.
- [29] Unger, T. “Refraction of Shear Zones in Granular Materials”. In: *Physical Review Letters* **98** (2007), 018301.
- [30] Workamp, M. and Dijksman, J. A. “Contact tribology also affects the slow flow behavior of granular emulsions”. In: *Journal of Rheology* **63** (2019), 275–283.



# General discussion

## 8.1 Introduction

This thesis is devoted to the research of the influence of the particle properties such as shape, friction and elasticity on granular flow.

The effects of particle shape were investigated in chapters 2, 3, 4 and 5. Special attention was given to simple shapes like rods or ellipsoids since a good understanding of the flow of such granulates is the foundation to understand more complex systems as a further step forward.

Specifically, in chapters 2 and 3, we studied the influence of aspect ratio of the rod-like or ellipsoidal particles on the discharge rate of the granulate from a silo and investigated the reason for the observed behaviour. We found that there is a surge of flow rate at the end of the discharge process of rods in a narrow 3D silo for a certain range of orifice sizes, while for spherical particles the flow rate is always constant. Next, we discovered that the aspect ratio of ellipsoids affects the average flow rate in the 3D silo in a non-monotonic way. A granulate with slightly anisotropic shapes flows at a higher rate than spherical particles or grains with more anisotropic shapes.

Chapters 4 and 5 switched the focus from the flow rate to other characteristics of the elongated particles during a silo discharge process or in a shear flow. In chapter 4, the particles with low symmetry (sharpened pegs and corn seeds) were found to point down with their heavier end more frequently if the plane in which they are rotating due to the shear flow is different from a horizontal plane. In chapter 5, we found that a conveyor belt placed below the orifice of the 2D silo, which changes the boundary condition for silo discharge and thereby reduces the flow rate, increases the size of the

stagnant zone and the amplitude of the relative velocity fluctuations as the belt speed decreases, leading to an intermittent flow. The packing fraction and the orientational order of the elongated particles are influenced by the conveyor belt locally at the outlet region, they are increased or decreased, respectively.

The effects of friction and elasticity of mixed ensembles on granular flow were investigated in chapters 6 and 7 in a 2D and a 3D silo, respectively. For a pure ensemble of soft particles with a low friction coefficient, the silo flow rate and the bottom pressure are filling height-dependent. For a pure ensemble of hard frictional grains, constant flow rate and saturation of the bottom pressure with increasing filling height are observed. Remarkably, in the 2D silo, in the low-friction soft grain system the classical granular behaviour with a constant flow rate is already recovered by adding a small proportion (10%) of hard frictional grains. In the 3D silo the change is less abrupt: the strongly filling height dependent flow rate disappears around 30% hard frictional grains added.

In this chapter, we reflect on the previous chapters and discuss the findings in a broader and coherent view. Some preliminary results of ongoing work, concerning the effects of the size and shape of grains forming the shear flow on the orientational features of elongated grains, will be presented as well.

## **8.2 Shape effects on granular flow**

### **8.2.1 Effects on silo flow rate**

Granular materials discharge through the orifice at the bottom of a silo typically at a constant rate [1, 2], not depending on the fill height. The flow rate is determined by the orifice size and some other geometrical parameters [2–7] as well as the internal friction of the granulate. Moreover, the shape and roughness can influence the internal friction. Nevertheless, the role of shape in changing the flow rate is not as straightforward as that of roughness (increasing roughness causes decreasing flow rate). Increasing shape anisometry can increase the effective friction (defined as the ratio of shear stress to normal stress experienced by the granulate) of the granulate [8, 9], but decrease the average angle of the particles with respect to the flow direction [10–13]. The irregular rotation caused by the shear stress leads to hindering the motion of neighboring particles. Therefore, in our work in chapters 2 and 3 we investigated the role of simple shapes of non-spherical grains such as rods or ellipsoids on the flow rate evolution during the discharge process (chapter 2) or on the average flow rate (chapter 3) when the flow rate is constant. In the latter work, we kept the other parameters (surface friction, density, volume, elasticity etc.) identical while only altering the shape of the particles, which had not been done before in experiments. The previous works related to the latter issue

are mostly done with numerical simulations, and reported contradictory observations about the flow rate as a function of grain shape [14–17].

We characterized the rods and ellipsoids with their aspect ratio and analyzed the features of flow rate related to this property. In a 3D silo, for a certain range of orifice sizes, the flow rate during the discharge process of elongated particles is not constant but shows a surge at the end. When the flow rate is constant during the discharge of elongated particles, the average flow rate changes with the aspect ratio in a non-monotonic way. It has two maxima around aspect ratios of 0.6 (lentil-like shape) and 1.5 (rice-like shape), which is not far away from the shape of spheres for which the aspect ratio is 1.0.

### **Effect of grain shape on the evolution of flow rate**

When looking for the cause of the surge of flow rate at the end of the discharge process for a certain range of orifice sizes in chapter 2, we first need to verify that it is not because we have entered the accelerating flow regime (expected for large orifice size), when the particles in the silo will move downward with almost free fall. By using even larger orifices, we find that the flow rate becomes constant again, which excludes the above described possibility. In order to get more insight into the surging flow, we compared the results to discrete element method (DEM) simulations to investigate the velocity field and packing fraction field in the silo in detail. Once the orifice size compared to the silo diameter is large enough, for elongated grains the surge in flow rate is observed at the end of the discharge process. The fields for spherical particles are quite homogeneous, while those for elongated particles have strong gradients. Compared to the case of elongated particles with a smaller orifice size where no surge is observed, the stagnant zone at the silo bottom with a relatively large orifice is suppressed. However, the stagnant zone is recovered if we use a wider silo where no surge occurs, and the flow rate becomes constant again. Actually, the suppressed stagnant zone results in an increase in the packing fraction and in the flow velocity near the end of the discharge process, which altogether causes the increased flow rate at the end.

As a next step, we could formulate a function to describe the correlation between the geometric parameters and the occurrence of the flow regime of increasing flow rate and even predict more points in the flow regime diagram shown in Fig. 2.8. By the nature of this question, the final form of this function could be a Heaviside's function which would be able to depict the diagram with certain parametric conditions. Another point which could be worth studying would be the start point of the surge in flow rate evolution as a function of fill height. As we see in Fig. 2.2, these start points seem to have a correlation with the aspect ratio of the elongated grains. The more elongated

the grains become, the more earlier the start point appears, which might be caused by stronger entanglement of the more elongated grains (we see a “rat hole” formed in the silo center for the very elongated particles in the work of Ashour et al. [18]).

### **Effect of grain shape on the average flow rate**

Since we know from our study in chapter 2 that there will be a flow rate surge near the end of discharge process for elongated particles for a certain range of orifice sizes, we try to avoid this range of orifice sizes when studying the aspect ratio dependence of the discharge rate for ellipsoids in chapter 3. We find that the discharge rate changes non-monotonically with aspect ratio of ellipsoids (aspect ratio  $< 1.0$ : lentil-like shapes; aspect ratio  $> 1.0$ : rice-like shapes). Interestingly, the shapes slightly different from spheres (around aspect ratios of 0.6 and 1.5) have the largest flow rates, among which the lentil shape has a 15% increase compared to spheres. Since the flow rate is a result of velocity and density (packing fraction), we investigated the packing fraction and average grain velocity passing through the outlet to explain the non-monotonic trend in flow rate. We find that the packing fraction also shows a non-monotonic trend as a function of aspect ratio as the flow rate curve does but with a smaller increase than the flow rate, which is consistent with the observations of previous works [19, 20]. Thus, packing density effects could not fully account for the observations in terms of flow rate. In addition, the average velocity curves as a function of aspect ratio also show a non-monotonic trend. By analyzing the evolution of average grain velocity and acceleration along the distance from the orifice, we see that the grains with non-spherical shapes start to accelerate at a higher position than spheres, but the acceleration is slightly smaller than that of spheres as they get closer to the orifice. Combining the position where the grains start to accelerate and the acceleration rate, it becomes optimal for the lentils with an aspect ratio of 0.6 which pass through the orifice at the largest velocity.

For a potential future study, the explanation of why non-spherical grains started to accelerate at a higher position could be valuable. Considering the free-fall arch/dome theory [6, 21, 22], the shape of this dome might change with particle shape. In case this happens, we could be able to build a correlation between the dome shape and the start height of acceleration, which would require more microscopic analysis. Another natural question would be whether our observation of non-monotonic trend in average flow rate as a function of grain aspect ratio is still true for other modified conditions such as denser initial packing fraction or a silo with a conical orifice. So far, we have verified the non-monotonic trend for these cases too in the corresponding complementary experiments.

### 8.2.2 Characteristics of elongated grains in granular flow

As previous studies with numerical simulations [10, 11, 23–26] and experiments [10–12, 27, 28] on elongated particles in granular flow have shown, the elongated particles get orientationally ordered under shearing, and their average angle decreases with the extent of elongation. The elongated particles can rotate or tumble in shear or silo flow. In real life, asymmetry is quite common. However, shape asymmetry is not well investigated in such shear or silo flows, even though some works involved asymmetrical elongated particles [7, 29–31]. Therefore, in chapter 4 we studied the role of asymmetry in shear induced ordering of elongated particles. In addition, industrial practices usually involve conveyor belts below a silo to draw the granular materials out. In order to study this scenario, we used a 2D silo equipped with a conveyor belt below it, and investigated the discharge process at different belt speeds in chapter 5.

#### Influence of shape asymmetry on granular flow

In chapter 4, when the asymmetrical particles (corn seeds and pegs with one end sharpened) rotate in a plane which is not horizontal in shear flow, the orientational distribution becomes asymmetric. After the quantitative analysis, we find that the particles spend more time with the sharper (lighter) end pointing up, which can be explained by an energy argument. To achieve a lower energy state, these asymmetrical particles tend to have their heavier ends at a lower position. In detail, the corn seeds (wedge shape) and the one-end-sharpened pegs in shear flow in a split-bottom shear cell prefer to point up with their sharp ends. Nevertheless, the situation in the clog configuration in a silo is more complicated. Near the dome, the corn seeds intend to point down with their sharper ends, while they prefer to point up with their sharper ends in the regions away from the dome. Thus, it indicates that the sharper-end-down configuration enhances the formation of the clog dome for corn seeds. For the one-end-sharpened pegs, a slight asymmetry in orientation distribution was only observed in the orifice region. It can be caused by the fact that more elongated particles need larger shear deformation to reach a stationary state. Moreover, clog formation does not seem to be influenced by the particle asymmetry for the sharpened pegs.

Therefore, it would be useful to make the more elongated particles experience larger deformation by adopting a taller silo in a future study, in order to verify our assumption. Obviously, the size of the silo will be limited by the size of the x-ray tomograph. In case we could not manage to use a taller silo, rods with smaller size but the same aspect ratio could be used in the original silo since it is a matter of aspect ratio [32], where those grains could rotate more in the same distance and then reach a stationary state for the measurements. Additionally, future simulations could give us



more details of the particle rotation and the process of clog formation, so that we would be able to understand how the asymmetry in the grain shape leads to the asymmetry in orientational distribution and the preferred direction of grains in the clog dome.

### **Elongated particles in flow-rate-controlled silo flow**

Another interesting configuration is, when we want to ensure slow silo discharge by a combination of a large orifice (to avoid clogging) and a conveyor belt below the silo outlet to limit the flow speed. We have investigated the flow properties of such a system using particles with elliptic shape in a 2D silo with a conveyor belt in chapter 5. For grains with elliptic shape, we observed a bigger stagnant zone, lower flow rate, significantly larger relative velocity fluctuations, and a resulting intermittent flow as the conveyor belt runs at a low speed, compared to the case of free flow. The presence of the conveyor belt destroys the orientational order of the elongated particles in the outlet region, but does not impact on the order higher up in the rest of the silo. The conveyor's influence on packing is limited to the outlet region as well, where the packing fraction is increased due to the presence of the conveyor belt.

Besides, there is a transition of the average orientation of elongated particles passing through the outlet as the orifice size increases in the case with a conveyor belt, in contrast to the constant average grain alignment for the free flow case. This alteration in the average grain alignment for the belt controlled case can be attributed to the flow expansion below the orifice as a result of the trapezoid shape below the orifice line and the gap between the silo bottom wall and the belt. Concerning the orientational order parameter at the outlet, we see that its value for the belt controlled flow is globally lower than that of the free flow case, and the order parameter curves have a dip at the middle of the outlet compared to the convex shape in the free flow case. The particles' average orientation is vertical for both free flow and belt controlled flow at the middle of the orifice. However, the arrest in the system because of the intrinsic intermittency of the belt controlled flow makes the grains tend to turn (left or right with equal probability), leading to reduced order parameter at the middle. Thus, the concavity can be regarded as an indicator of the degree of flow intermittency developed within the system.

As we can see in the last row in Fig. 5.7, the normalized curves of the vertical velocity for the flow-rate-controlled cases especially with low belt speeds are not as smooth as the ones for free-flow case, which is a consequence of intermittent flow. Their smoothness could be improved by doing more measurements and then averaging the curves if it becomes necessary in future studies e.g. for the calculation of shear rate. As a next step in a potential future research, it would be interesting to see how the particle aspect ratio influences the orientation distribution and ordering in such a scenario with a conveyor belt, since we have done these experiments with only one

## 8.2. Shape effects on granular flow

aspect ratio and have seen in many other scenarios (e.g. chapter 2 and 3) that the aspect ratio does have an influence [10, 11, 14].

### Elongated particles with different neighboring grains in shear flow

The investigations presented above in chapters 4 and 5 involved elongated particles in a silo or a shear cell with the same type of particles as neighbors. What if we change the shape or size of the neighboring particles? The following part will present some preliminary results of our work inspired by the study of Jeffery's orbits [33], where the author studied the motion of particles of ellipsoidal shape immersed in a viscous fluid as an extension to the work of Einstein [34] on the influence of spherical

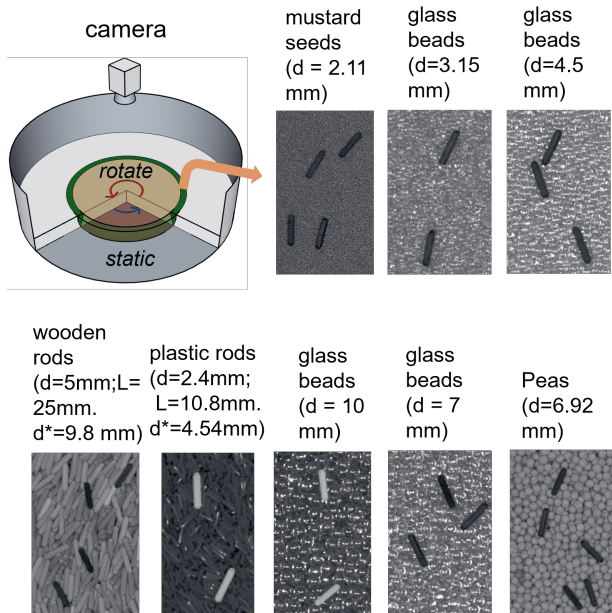


**Figure 8.1:** Experimental setup and materials. The green zone represents the shear zone induced by the split-bottom shear cell.  $d$  is the diameter of the grain's cross section in radial direction. The equivalent diameter  $d^*$  is defined as the diameter of a sphere with the same volume as the grain of interest.

particles on the properties of the suspension in bulk. We put the elongated particles on top of the shear flow in a split-bottom shear cell into which we feed different types

of grains (Mustard seed:  $d = 2.11 \text{ mm}$ , glass bead:  $d = 3.15, 4.5, 7, 10 \text{ mm}$ , pea:  $d = 6.92 \text{ mm}$ , plastic rod:  $d = 2.4 \text{ mm}, L = 10.8 \text{ mm}, d^* = 4.54 \text{ mm}$ , wooden rod:  $d = 5 \text{ mm}, L = 25 \text{ mm}, d^* = 9.8 \text{ mm}$ .  $d, L, d^*$  represent diameter, length and equivalent diameter respectively). Thus, we could observe the influence of neighboring particles on the characteristics of the elongated particles placed on the top of the shear flow within the shear zone, such as the average angle, order parameter, angular velocity and its fluctuation as a function of the angle of the elongated particle with respect to the streamline direction. The experimental setup and materials are displayed in Fig. 8.1.

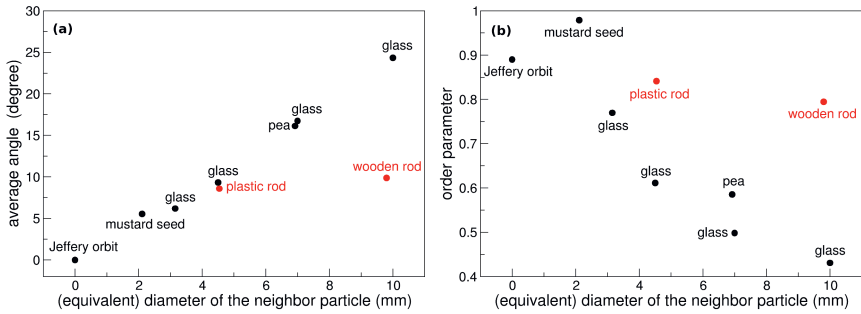


**Figure 8.2:** Average angle with respect to the streamline direction and the order parameter as a function of the diameter of the neighboring grains.

In Fig. 8.2, we can see that the average angle of the elongated particles with respect to the streamline direction increases with the diameter of neighboring grains, while the order parameter decreases with increasing diameter of neighboring grains. The correlation of increasing average angle and decreasing order parameter is coherent with previous observations of elongated particles in shear flow [10, 11]. As for the angular velocity and its fluctuation further investigations are in progress.

### 8.3 Influences of friction and elasticity of mixed ensembles on granular flow

The role of friction and elasticity have been studied for pure granular ensembles either in a silo or in a shear cell in many previous works. Luding [35] studied the effect of friction on the shear band induced by a slit-bottom Couette ring shear cell. Pongó et al. [36] found a correlation between the flow rate and the local pressure above the orifice for soft low-friction grains during a silo discharge, where the flow rate is fill height-dependent. Namely, for soft low-friction grains the local pressure above the

orifice changes much more during a discharge process than it does for hard low-friction grains. Moreover, the flow rate is more sensitive to the local pressure than it is for hard low-friction grains. Thus, the hard grains always keep a constant flow rate with any friction coefficient except for the frictionless case. The clogging behavior also changes with the change of friction and elasticity. For soft low-friction grains, the clogging probability becomes height-dependent [37, 38], and the critical orifice size below which clogging occurs is much smaller [39–42]. Since the previous studies focused on pure ensembles, the characteristics of mixtures of soft low-friction and hard frictional grains in different mixing ratios is interesting to study. We studied the flow rate and clogging of the mixtures in a 2D silo in chapter 6, and the transition from liquid-like behavior of pure soft low-friction grains to typical granular behavior of pure hard frictional grains in a 3D silo in chapter 7.

In chapter 6, we tested two mixing ratios of soft low-friction (hydrogel beads) to hard frictional (airsoft beads) grains, with 5% and 10% hard frictional grains in the mixtures, and compared them to the behavior of the pure soft low-friction system (0%). We find that 10% hard frictional grains in the mixtures can already restore the constant flow rate, which is independent of fill height of the granulate in the 2D silo. Nevertheless, the flow rates of different mixtures approach each other as the fill height is low, because the soft particles deform much less under low pressure, leading to approaching the mechanical properties of hard low-friction grains. Focusing on the influence of hard frictional grains in the vicinity of the orifice on flow rate, at high fill levels the flow rate decreases with the number of the hard frictional grains if the number of hard frictional grains in this region is larger than three, while it does not show any trend with the number of hard frictional grains at low fill levels. This is due to much smaller deformation of soft particles under low pressure at low fill levels, as explained above. Regarding the clogging behavior, the mixture can form non-permanent clogs, which spontaneously resolve due to the reorganization in packing structure after clogs occur. When there are no hard frictional grains in the first two layers of the clog arch, there is little difference in the probability distribution of clog duration between the ensemble of pure soft low-friction grains and the ensemble with 5% hard frictional grains.

As the transition from height dependence to height independence of the flow rate is drastic with increasing the concentration of hard frictional spheres in the mixture up to 10%, it would be interesting to use smaller steps for changing the concentration, aiming to demonstrate a more detailed transition process in a future work. By using Particle Tracking Velocimetry (PTV), we could analyse the velocity profiles of the grains passing through the orifice, the transition of which with increasing the concentration of hard frictional spheres would be an intriguing topic to work on as well.

Since a small amount of hard frictional grains in the mixture in a 2D silo are

able to cause such a drastic change in the collective behavior of flow rate (restoring the constant flow rate), it made us curious about the effect in the scenario in a 3D silo. In chapter 7, we filled a 3D silo with 11 samples with the concentration of hard frictional particles spanning from 0% to 100%, respectively. For the first 30% hard frictional grains added into the sample, the height dependence of the flow rate decreases significantly, while it approaches the height-independent scenario at a slower speed with further increasing concentration of hard frictional grains in the sample. In order to understand this transition, we performed some complementary measurements on the effective friction and the drag force on an object moving horizontally in the sample as a function of the concentration of the hard frictional particles. We find that the effective friction and the drag force both increase with the concentration of hard frictional grains. However, they increase less at low concentration of hard frictional grains, and more at high concentration, which is opposite to the trend of the height dependence of flow rate as a function of the concentration of hard frictional grains. This indicates that there are other factors to investigate which contribute to the relatively large change in the height dependence of flow rate at low concentration of hard frictional grains. To investigate this unsolved issue, we could perform measurements of surface friction coefficients of hydrogel-hydrogel, hydrogel-airsoft and airsoft-airsoft contact surfaces as a further step. Once having this information, we could use some help from simulation to explain the observation.

## 8.4 Conclusions and outlook

We investigated the effects of particle shape with special focus on elongated shapes, particle friction and elasticity on granular flow. The typical constant flow rate of granular materials discharged from a silo can be altered qualitatively by the shape (increasing flow rate during discharge with elongated particles) and the combination of friction and elasticity (soft low-friction grains give us a height-dependent flow rate during discharge). The average flow rate changes non-monotonically with the aspect ratio of ellipsoids, caused by the non-monotonic change in packing fraction and final outflow velocity (as a result of the combination of the starting height and the growth rate of acceleration of the grains). The characteristics of the flow field of elongated particles brings us a new aspect to analyze, namely the orientation-related issues such as the average angle, order parameter, angular velocity, etc. The shape asymmetry and the boundary condition change can both shift the states of the elongated particles in granular flow.

The last part of Section 8.2.2 showed some preliminary results of the influence of the shape or size of the neighboring particles on the average angle and order parameter

#### 8.4. Conclusions and outlook

---

of the elongated particles within the shear zone. As for the angular velocity and its fluctuation, further work is in progress to complete the preliminary findings. Moreover, the effects of non-spherical shapes (for instance, elongated shapes) together with different particle friction and elasticity can be an interesting topic for future studies as well. Since we have a set of model particles with the same volume but different aspect ratios, we could expand our research into more aspects of the behaviors of granular materials in terms of mixing, segregation, clogging and avalanches on the slope of a pile, in order to study the shape effect in more areas.



---

## BIBLIOGRAPHY

- [1] Fowler, R. and Glastonbury, J. “The flow of granular solids through orifices”. In: *Chemical Engineering Science* **10** (1959), 150.
- [2] Beverloo, W., Leniger, H., and van de Velde, J. “The flow of granular solids through orifices”. In: *Chemical Engineering Science* **15** (1961), 260–269.
- [3] Nedderman, R. M. et al. “The Flow of Granular Materials I: Discharge Rates from Hoppers”. In: *Chemical Engineering Science* **37** (1982), 1597.
- [4] Hilton, J. and Cleary, P. “Granular flow during hopper discharge”. In: *Physical Review E* **84** (2011), 011307.
- [5] Janda, A., Zuriguel, I., and Maza, D. “Flow Rate of Particles through Apertures Obtained from Self-Similar Density and Velocity Profiles”. In: *Physical Review Letters* **108** (2012), 248001.
- [6] Rubio-Largo, S. M. et al. “Disentangling the Free-Fall Arch Paradox in Silo Discharge”. In: *Physical Review Letters* **114** (2015), 238002.
- [7] Calderón, C. et al. “Correlations between flow rate parameters and the shape of the grains in a silo discharge”. In: *Powder Technology* **320** (2017), 43.
- [8] Nagy, D. et al. “Flow and rheology of frictional elongated grains”. In: *New Journal of Physics* **22** (2020), 073008.
- [9] Hidalgo, R. C. et al. “Rheological response of nonspherical granular flows down an incline”. In: *Physical Review Fluids* **3** (2018), 074301.
- [10] Börzsönyi, T. et al. “Orientational Order and Alignment of Elongated Particles Induced by Shear”. In: *Physical Review Letters* **108** (2012), 228302.



- 
- [11] Börzsönyi, T. et al. “Shear-induced alignment and dynamics of elongated granular particles”. In: *Physical Review E* **86** (2012), 051304.
- [12] Börzsönyi, T. and Stannarius, R. “Granular materials composed of shape-anisotropic grains”. In: *Soft Matter* **9** (2013), 7401–7418.
- [13] Botton, M. et al. “Quasistatic rheology and microstructural description of sheared granular materials composed of platy particles”. In: *Physical Review E* **87** (2013), 032206.
- [14] Liu, S. D. et al. “Flow characteristics and discharge rate of ellipsoidal particles in a flat bottom hopper”. In: *Powder Technology* **253** (2014), 70.
- [15] Li, J. et al. “Flow of sphero-disc particles in rectangular hoppers—a DEM and experimental comparison in 3D”. In: *Chemical Engineering Science* **59** (2004), 5917–5929.
- [16] Hesse, R., Krull, F., and Antonyuk, S. “Prediction of random packing density and flowability for non-spherical particles by deep convolutional neural networks and Discrete Element Method simulations”. In: *Powder Technology* **393** (2021), 559–581.
- [17] Langston, P. A. et al. “Distinct element modelling of non-spherical frictionless particle flow”. In: *Chemical Engineering Science* **59** (2004), 425–435.
- [18] Ashour, A. et al. “Outflow and clogging of shape-anisotropic grains in hoppers with small apertures”. In: *Soft Matter* **13** (2017), 402.
- [19] Donev, A. et al. “Improving the Density of Jammed Disordered Packings Using Ellipsoids”. In: *Science* **303** (2004), 990.
- [20] Gan, J., Zhou, Z., and Yu, A. “Structure analysis on the packing of ellipsoids under one-dimensional vibration and periodic boundary conditions”. In: *Powder Technology* **335** (2018), 327–333.
- [21] Hagen, G. “Bericht über die zur Bekanntmachung geeigneten Verhandlungen der Königlich Preussischen Akademie der Wissenschaften zu Berlin”. In: *Königlich Preussische Akademie der Wissenschaften zu Berlin* (1852), 35–42.
- [22] Tighe, B. P. and Sperl, M. “Pressure and motion of dry sand: translation of Hagen’s paper from 1852”. In: *Granular Matter* **9** (2007), 141–144.
- [23] Anki-Reddy, K., Kumaran, V., and Talbot, J. “Orientational ordering in sheared inelastic dumbbells”. In: *Physical Review E* **80** (2009), 031304.
- [24] Campbell, C. “Elastic granular flows of ellipsoidal particles”. In: *Physics of Fluids* **23** (2011), 013306.

- [25] Guo, Y. et al. “A numerical study of granular shear flows of rod-like particles using the discrete element method”. In: *Journal of Fluid Mechanics* **713** (2012), 1–26.
- [26] Nadler, B., Guillard, F., and Einav, I. “Kinematic Model of Transient Shape-Induced Anisotropy in Dense Granular Flow”. In: *Physical Review Letters* **120** (2018), 198003.
- [27] Wegner, S. et al. “Alignment and dynamics of elongated cylinders under shear”. In: *Soft Matter* **8** (2012), 10950.
- [28] Guillard, F., Marks, B., and Einav, I. “Dynamic X-ray radiography reveals particle size and shape orientation fields during granular flow”. In: *Scientific Reports* **7** (2017), 8155.
- [29] Tao, H. et al. “Discrete element method modeling of non-spherical granular flow in rectangular hopper”. In: *Chemical Engineering and Processing: Process Intensification* **49** (2010), 151.
- [30] González-Montellano, C. et al. “Validation and experimental calibration of 3D discrete element models for the simulation of the discharge flow in silos”. In: *Chemical Engineering Science* **66** (2011), 5116–5126.
- [31] Escudero, F. et al. “Silo discharge: influence of the particle shape on the velocity profiles”. In: *EPJ Web of Conferences* **249** (2021), 03029.
- [32] Marschall, T. A., Van Hoesen, D., and Teitel, S. “Shear-driven flow of athermal, frictionless, spherocylinder suspensions in two dimensions: Particle rotations and orientational ordering”. In: *Physical Review E* **101** (2020), 032901.
- [33] Jeffery, G. B. “The motion of ellipsoidal particles immersed in a viscous fluid”. In: *Proceedings of the Royal Society of London. Series A, Containing papers of a mathematical and physical character* **102** (1922), 161–179.
- [34] Einstein, A. “Eine neue bestimmung der moleküldimensionen”. PhD thesis. ETH Zurich, 1905.
- [35] Luding, S. “The effect of friction on wide shear bands”. In: *Particulate Science and Technology* **26** (2007), 33–42.
- [36] Pongó, T. et al. “Flow in an hourglass: particle friction and stiffness matter”. In: *New Journal of Physics* **28** (2021), 023001.
- [37] Hong, X. et al. “Clogging of soft particles in two-dimensional hoppers”. In: *Physical Review E* **96** (2017), 062605.
- [38] Tao, R., Wilson, M., and Weeks, E. “Soft particle clogging in two-dimensional hoppers”. In: *Physical Review E* **104** (2021), 044909.

- [39] Hong, X., Kohne, M., and Weeks, E. R. “Clogging of soft particles in 2D hoppers”. In: *Physical Review E* **96** (2017), 062605.
- [40] To, K. “Jamming transition in two-dimensional hoppers and silos”. In: *Physical Review E* **71** (2005), 060301.
- [41] Zuriguel, I. et al. “Jamming during the discharge of granular matter from a silo”. In: *Physical Review E* **71** (2005), 051303.
- [42] Thomas, C. C. and Durian, D. J. “Fraction of clogging configurations sampled by granular hopper flow”. In: *Physical Review Letters* **114** (2015), 178001.

---

## SUMMARY

In this thesis, we focus on the complex behavior of granular flow in a silo or a shear cell, such as the flow process, orientation-related issues (non-spherical particles), and clogging if the aperture of the silo is small, with special emphasis on the role of particle shape, surface friction or elasticity.

Chapter 2 is devoted to the study of a narrow silo filled with rods. We find that there is a certain range of the orifice size for which the flow rate is not constant, with a surge at the end of the discharge process. Yet, the flow rate is constant for small and large orifices. The change from the constant flow rate regime to the regime with surge at the end is characterized by a change in the flow field. For the case of constant flow rate there is a larger stagnant zone near the silo wall, while the stagnant zone shrinks in the cases of increasing flow rate. The shrunk stagnant zone leads to an increase in the packing fraction and the flow velocity near the end of the discharge process, which causes the increased flow rate at the end.

In chapter 3, we focus on the constant flow rate regime and investigate how the average flow rate changes with aspect ratio of ellipsoids in silo flow. The average flow rate changes with the aspect ratio of ellipsoids non-monotonically. There are two maxima around the aspect ratios of 0.6 (lentil-like) and 1.5 (rice-like). Our results reveal two contributing factors (with similar strength) to the non-monotonic nature of the flow rate: both the packing fraction and the particle velocity through the orifice are non-monotonic functions of the grain shape. Thus, particles with slightly non-spherical shapes not only form a better packing in the silo but also flow faster through the orifice than spheres. We also show that the resistance of the granulate against shearing increases with aspect ratio for both elongated and flat particles, thus change in the effective friction of the granulate due to changing particle shape does not coincide with

the trend in the flow rate.

Chapter 4 focuses on grain orientations of low symmetry particles (sharpened pegs and wedge shaped corn seeds) in silo flow and shear flow. There is a new type of gravity effect on grain orientation: if the particles rotate in a plane which is not exactly horizontal, they spend more time in the configuration with their thicker (heavier) end down, indicated by the asymmetry in the orientation distributions. This can be explained by the energy argument.

In chapter 5, we performed experiments of ellipses discharged from a 2D silo with a conveyor belt below the orifice. The conveyor belt placed below the silo outlet, decreases the flow rate and increases the size of the stagnant zone. The relative velocity fluctuation in the silo is strongly increased with decreasing belt speed. Altogether, this leads to an intermittent flow as the conveyor belt runs at a low speed. It is interesting to observe that this intermittency correlates with a strong reduction of the orientational order of the particles at the orifice region. Moreover, we observe that the average orientation of the grains passing through the outlet is modified when they are extracted with the belt, which becomes more evident for large orifices.

Chapter 6 concentrates on the study of mixtures of soft low-friction and hard frictional grains in a 2D silo. Adding a small proportion of hard frictional grains to a granulate of soft low-friction grains can change the collective features of the sample significantly in terms of height dependence of flow rate and bottom pressure conditions. The number of hard frictional particles in the vicinity of the orifice influences the clogging behavior and it also affects the flow rate at large fill height.

Chapter 7 as a follow up work of chapter 6 extends the study of the mixtures of soft low-friction and hard frictional grains from a 2D scenario to a 3D one. The height dependence of flow rate considerably reduces as the concentration of hard frictional grains in the sample grows to 30%, whereas further increasing concentration leads to smaller change. The complementary effective friction and drag force measurements also show increasing trends with the concentration of hard frictional grains in the sample, but cannot account for the considerable change in height dependence of flow rate at low concentration of hard frictional grains, indicating the necessity for the investigation of other factors.

Lastly, chapter 8 discusses the work in the previous chapters and their coherence in a broader sense. Some ongoing and possible future topics focusing on further aspects of granular flow are presented as well.

---

# LIST OF PUBLICATIONS

## This thesis

- Chapter 2  
**Tivadar Pongó\***, **Bo Fan\***, **Dariel Hernández-Delfin**, **János Török**, **Ralf Stannarius**, **Raúl Cruz Hidalgo** and **Tamás Börzsönyi** “The role of the particle aspect ratio in the discharge of a narrow silo” *New J. Phys.* **24**, 103036 (2022)  
\*shared first authorship.
- Chapter 3  
**Bo Fan**, **Tivadar Pongó**, **Raúl Cruz Hidalgo** and **Tamás Börzsönyi** “Effect of particle shape on the flow of an hourglass” *submitted* (2023)
- Chapter 4  
**Viktor Nagy**, **Bo Fan**, **Ellák Somfai**, **Ralf Stannarius** and **Tamás Börzsönyi** “Flow of asymmetric elongated particles” *submitted* (2023)
- Chapter 5  
**Bo Fan**, **Iker Zuriguel**, **Joshua Dijkstra**, **Jasper van der Gucht** and **Tamás Börzsönyi** “Elongated particles discharged with a conveyor belt in a two-dimensional silo” *submitted* (2023)
- Chapter 6  
**Wang, J.\***, **Fan, B.\***, **Pongó, T.\***, **Harth, K.**, **Trittel, T.**, **Stannarius, R.**, **Illig, M.**, **Börzsönyi, T.**, **Cruz Hidalgo, R.** “Silo discharge of mixtures of soft and rigid grains” *Soft Matter* **17**, 4282–4295 (2021) \*shared first authorship.

- Chapter 7

**Bo Fan, Joshua Dijkstra, Jasper van der Gucht and Tamás Börzsönyi**  
“Granular flow of mixtures of soft and hard spheres” *in preparation* (2023)

### **Other work**

- **Jing Wang, Bo Fan, Tivadar Pongó, Tamás Börzsönyi, Raúl Cruz Hidalgo and Ralf Stannarius** “Force on a sphere suspended in flowing granulate” *submitted* (2023)

---

## ACKNOWLEDGEMENTS

It has been a four-year PhD journey to come to this point. Going back to the beginning of this story, I was searching for a PhD position at the end of my master internship, during which I became more and more determined to pursue a career in the scientific research sector since I felt the excitement, self-development and joy of discovery through the scientific exploration. Fortunately, I got into to the current research project on granular physics. During my PhD, I have received a lot of support from the people along the journey. Thus, I would like to thank you in the following.

Tamás, thank you for all the guidance and the opportunity to do research in this project on granular physics. I learned a lot from our daily interactions in terms of research, scientific writing, etc. It will be great treasure for my future career. I also thank you for the atmosphere you created, so that efficient, honest and helpful conversations became natural.

Jasper, thank you for the guidance and being my promotor in Wageningen University. It has been always helpful to discuss the progresses in my research on a periodical basis with you, which has become nice chances for me to demonstrate and rethink my works.

Joshua, thank you for the guidance and being one of my supervisors. Your devotion to work is impressive. You can always bring me enlightened ideas and thinking. Being the coordinator of our research network, you have done a great job in the management. I really enjoyed the network activities. They are definitely precious memories to me.

I am grateful for having been hosted by the Complex Fluids group in Wigner Research Centre for Physics (Wigner RCP) in Budapest, Hungary and also as a PhD candidate in the laboratory of Physical Chemistry and Soft Matter (PCC) in Wageningen University in Wageningen, the Netherlands. Thank you for answering my questions about programming and other IT related matters, Ellák. I really appreciated it. I



improved and learned a lot by studying your codes. Thank you for the engineering help, Viktor. Thank you for the company and the fun trip together to Balaton lake, Ameer. Thank you for your help and joyful moments at the lunch breaks and after work during my time at PCC, Chandan and Zohreh. Jose, Rihanna, Akankshya, Leonardo, thank you for the fun moments, too. I should like to extend my thanks to all the people I met there for the help and support. Moreover, without the training and activities in the CALIPER research network, the graduation would not be possible. Thank you all members in this network. It has been a pleasure and honor to be part of it. Thank you for the host and the work we did together, Jing and Tivadar. Thank you for the instruction and help during my research visits to Otto-von-Guericke-University Magdeburg, Germany and University of Navarra, Spain, Prof. Ralf Stannarius and Prof. Iker Zuriguel. Thank you for the work, Raúl and other collaborators to whom I apologize for not mentioning the names here. Thank you for the company during my visit to University of Navarra, Ahmed. It was a lovely trip to Foz dos Arbayun. Thank you for that, Lars.

Last but not least, thank you, pa, ma and sister. You are always there to support and hold me no matter what. It is the source of my sense of safety. Sometimes, there is argument as no life is perfect. But I know that it is because we care for each other and out of love. *May we all be blessed. Though far apart, under the shared moonlight we are all connected.*

---

## ABOUT THE AUTHOR

Bo Fan was born on October 20, 1994 in Shaanxi, China. After obtaining his high school diploma from Baoji High School in Baoji, China, he went on to study Energy and Power Engineering in Xi'an Jiaotong University in Xi'an, China and concluded the program with a bachelor thesis investigating experimentally the temperature distribution in hypergolic ignition of ionic liquids under the supervision of Prof. Chenglong Tang in 2017. Afterwards, he went to pursue a master degree in Computational Mechanics in Ecole Centrale de Nantes, France and finished with an internship under the supervision of Dr. Michel Pons in the Laboratoire d'informatique pour la mécanique et les sciences de l'ingénieur (currently LISN) of CNRS in University Paris-Saclay, France, on the topic of simulation and optimization of cold distribution networks. After obtaining the Master Degree at Ecole Centrale de Nantes in 2019, he started his PhD research with a Marie Skłodowska-Curie Actions (MSCA) fellowship in Wigner Research Centre for Physics in Budapest, Hungary and as a PhD candidate in the Laboratory of Physical Chemistry and Soft Matter in Wageningen University & Research in Wageningen, the Netherlands, studying the effects of grain shape, surface friction and grain elasticity on granular flows under the supervision of Dr. Tamás Börzsönyi, Dr. Joshua A. Dijksman and Prof. Jasper van de Gucht.



---

# OVERVIEW OF COMPLETED TRAINING ACTIVITIES

## Discipline specific activities

CALIPER Training School 1	University of Graz	2020
CALIPER Training School 2	Wageningen University & Research	2020
VLAG Rheology Course	Wageningen University & Research	2020
Soft Matter	Wigner Research Centre for Physics	2020
Institute Seminars	Wigner Research Centre for Physics	2020-2023
CALIPER Training School 3	Grenoble University and ESPCI Paris	2021
CALIPER Training School 4	PMMH ESPCI Paris	2022
Powders and Grains	AEMMG	2021
Secondment in University of Navarra	University of Navarra	2021
APS March meeting*	American Physical Society	2021
DPG Meeting*	German Physical Society	2022
SoftComp Conference*	Forschungszentrum Juelich GmbH	2022

\* oral presentation

## General courses

CALIPER Training School 1	University of Graz	2020
CALIPER Training School 2	Wageningen University & Research	2020
CALIPER Training School 3	Grenoble University and ESPCI Paris	2021
CALIPER Training School 4	PMMH ESPCI Paris	2022
Labview Training	Wageningen University & Research	2020
Work safety training	Wigner Research Centre for Physics	2020
Career development	Wageningen University & Research	2020
Project and Time Management	Wageningen University & Research	2021
Writing grant proposals	Wageningen University & Research	2023

## Optionals

Preparation of research proposal	Wigner Research Centre for Physics	2020
Weekly group meeting	Wageningen University & Research	2019-2023
Organization of network meeting	Wigner Research Centre for Physics	2021

The research described in this thesis was financially supported by the European Union's Horizon 2020 research and innovation programme under the Marie Skłodowska Curie grant agreement No. 812638.

Cover design by Bo Fan  
Printed by ProefschriftMaken



